Computational derivation of conditions for upscalability of bioclogging in pore network models

Lopez Pena, Luis

DOI
10.4233/uuid:ef832c33-4b4c-4327-b500-1ef070f16611

Publication date
2019

Document Version
Final published version

Citation (APA)
Lopez Pena, L. (2019). *Computational derivation of conditions for upscalability of bioclogging in pore network models*. [Dissertation (TU Delft), Delft University of Technology].
https://doi.org/10.4233/uuid:ef832c33-4b4c-4327-b500-1ef070f16611

Important note
To cite this publication, please use the final published version (if applicable).
Please check the document version above.

COMPUTATIONAL DERIVATION OF CONDITIONS FOR UPSCALABILITY OF BIOCLOGGING IN PORE NETWORK MODELS

COMPUTATIONAL DERIVATION OF CONDITIONS FOR UPSCALABILITY OF BIOCLOGGING IN PORE NETWORK MODELS

Proefschrift

ter verkrijging van de graad van doctor
aan de Technische Universiteit Delft,
op gezag van de Rector Magnificus Prof.dr.ir. T.H.J.J. van der Hagen
voorzitter van het College voor Promoties,
in het openbaar te verdedigen op
donderdag 2 mei 2019 om 10:00 uur

door

Luis Antonio LOPEZ PEÑA

Master of Science in Materials Science and Engineering,
Universidad Nacional Autónoma de México (UNAM) , Distrito Federal, México.
geboren te Distrito Federal, Mexico.

Dit proefschrift is goedgekeurd door de

promotor: prof. dr. ir. C. Vuik
promotor: dr. ir. F.J. Vermolen
copromotor: dr. B.J. Meulenbroek

Samenstelling promotiecommissie:

Rector Magnificus,	voorzitter
Prof. dr. ir. C. Vuik	Technische Universiteit Delft, promotor
Dr. ir. F.J. Vermolen	Technische Universiteit Delft, promotor
Dr. B.J. Meulenbroek,	Technische Universiteit Delft, copromotor
Onafhankelijke leden:	
Prof. dr. rer. nat. habil. F.A. Radu,	Universiteit Bergen, Noorwegen
Prof. dr. ir. S. M. Hassanizadeh,	Universiteit Utrecht
Prof. dr. J. Bruining	Technische Universiteit Delft
Prof. dr. ir. P.L.J. Zitha,	Technische Universiteit Delft

Keywords: Biofilm growth, pore network model, Upscaling bioclogging, porosity-permeability relation, Damköhler number

Front & Back: ProefschriftMaken || www.proefschriftmaken.nl

This research was funded by the Mexican Institute of Petroleum (IMP) through the Programa de Capacitación de Talento, Reclutamiento, Evaluación y Selección de Recursos Humanos (PCTRES). This project was supervised by ScD.dr.ir. L. Sheremetov, IMP, Mexico.

ISBN 978-94-6384-035-4

Printed by ProefschriftMaken || www.proefschriftmaken.nl

CONTENTS

SUMMARY

During the primary oil recovery, wells are drilled into the reservoir, and due to natural driving forces, the oil flows to the surface through these production wells. Unfortunately, the production of oil in this first stage is typically between only five and ten percent of the oil in place in the reservoir. In the secondary oil recovery some wells (used in the previous stage for production) are converted into injection wells and water or gas are injected into the reservoir to displace the oil to the surface. However, even after primary and secondary oil recovery about 60% of the oil-in-place remains in the reservoir.

Microbial Enhanced Oil Recovery (MEOR) is a tertiary enhanced oil recovery technique used to extract the remaining oil after the secondary recovery. MEOR technique was proposed since the 1920's however it was until 1940's that it was considered seriously. In MEOR, bacteria and the resulting bioproducts are used to increase the mobilization of oil in the reservoir. Bacterial growth can produce gases that increase the pressure of the reservoir and decrease the viscosity of oil. Biosurfactants decrease the oil viscosity which may lead to an increase of the mobility of oil. Furthermore, bacteria can selectively plug the high permeability zones which changes the direction of water flow to the areas where the oil is still trapped. Selective plugging by bacteria is a process that is used simultaneously with a waterflooding operation. Among all the effects of biofilm growth, selective plugging and interfacial tension reduction are thought to have the greatest impact on oil recovery. The applicability of selective plugging to divert the flow of water has been shown in laboratory experiments. However, on the field scale the applicability of MEOR techniques is still under investigation since the MEOR techniques in pilot fields have produced different outcomes.

In this study, we present a new 2D microscopic pore network biofilm growth model that takes into account that nutrients might not be able to penetrate the biofilm completely. This phenomenon occurs if the consumption of nutrients is faster than the diffusion of them. We incorporate in the model a characteristic volume related to the penetration depth of the nutrients within the biofilm. This inclusion allows a more accurate description of the biofilm growth in porous media. In addition, we model the continuous spreading of the biofilm through the whole network, which is a phenomenon that has been observed experimentally. Our numerical experiments show that the nutrients spread fast throughout the whole network during the early stages of the process. Since the nutrients are present in the whole network, the biofilm grows and spreads to the neighbouring tubes. For a longer period of time the biofilm grows uniformly through the network, however after this, the depletion of nutrients is observed and the biofilm grows preferentially near the inlet of the network causing the complete blockage of the network. Our model describes the transition between uniform biofilm growth and heterogeneous biofilm growth.

Furthermore, we determine under which conditions this microscopic model of biofilm growth can be used for the description of the biofilm growth on a larger scale. For this

reason, we study the influence of parameters like the number of nodes in the network, the size of the domain of computation and the inlet concentration of nutrients on the relation between the porosity and permeability. We obtained the following results. If the biofilm growth is heterogeneous, then the relation between permeability and porosity is not unique and hence upscaling is not possible. However, with certain inlet concentrations it is possible to obtain uniform biofilm growth; in this case upscaling is possible. We use the Damkhöler number to determine the upscalability of the biofilm growth process. The simulation shows that there is a transition region between uniform growth and heterogeneous growth. This transition occurs within the same range of Damköhler number for all the cases studied. (different number of nodes, size of the domain of computation and different concentration of nutrients). If the Damköhler number is lower than the transition value, then biofilm growth is uniform for the entire process and therefore upscaling is possible.

Thereafter, we extend our 2D model to a 3D biofilm growth model. The porous medium is represented as a 3D cubic network. We study the influence of the number of nodes in the z direction on the porosity-permeability relation and on the criteria for upscalability that were obtained in 2D. In addition, we incorporate a log-normal distribution for the radii of the tubes in the network. For the heterogeneous biofilm growth regime, we obtained that as the number of nodes in the z direction increases the amount of biomass needed to block the network converges to a limit value. We obtained that the transition between homogeneous and heterogeneous biofilm growth for the 3D cases occurs approximately within the same range of Damköhler numbers as in the 2D cases. Furthermore, we investigate the influence of the log-normal radius distribution on the biofilm growth. It was observed that if the variance of the radius is large then the amount of biomass needed to block the network decreases. However, also in this case the transition between the homogeneous and the heterogeneous regime takes place in the same Damköhler number regime as in Chapter 3.

Additionally, we use a 2D network model to study the influence of biofilm growth on the flow diversion of water. We model two regions having different permeability. We use a log-normal distribution for the radii of the tubes. The average radius was larger for the high permeability zone than in the low permeability zone. Since we are interested in the production of oil from the low permeability zones which is hard to accomplish, we computed the outflow of water from the low permeability region during the biofilm growth process. We obtained that the flux from the low permeability region increased 60% during a certain period. However, the flux through the low permeability region starts to decrease due to the accumulation of biofilm. Therefore it is suggested that the injection of nutrients has to be stopped in time to prevent clogging of the network. The increase of the outflow from the low permeability region may indicate a successful flow diversion and hence an increase of the efficiency of waterflood.

Finally, we applied the porosity-permeability relation obtained via the random biofilm growth to two poroelasticity problems. We study the applicability of this microscopic relation on a macro-scale problem. In the first problem, a high pressure is imposed in the inlet of the porous medium package. This high pressure causes a movement of the grains to towards the outlet and consequently a change in the local porosity of the medium. In the second problem, the package is squeezed in the middle on the top and bottom edges

of the domain. The network inspired relations were obtained using a quadrangular network, a triangular structured network and a triangular unstructured network in 2D and a cubic network in 3D. We compared the results obtained with the network inspired relations to the results obtained via the Kozeny-Carman equation which is often used in this kind of problems. For the set of parameters chosen, we noticed that the permeability computed with the network-inspired relations are higher than the one obtained with Kozeny-Carman. Furthermore, we observe that the porosity is very similar for the cases studied. A possible explanation for this behaviour can be that the relation, between the velocity field and the change of the displacements in time is not strong enough to lead to significant changes in the porosity profile. The network inspired porosity-permeability relation could be used as an alternative to the Kozeny-Carman equation.

SAMENVATTING

Tijdens de primaire oliewinning worden sommige putten in het reservoir geboord en vanwege natuurlijke aandrijfkrachten stroomt de olie via de productieputten naar de oppervlakte. Helaas is de productie van olie tijdens deze eerste winning slechts tussen de vijf en de tien procent van de totale hoeveelheid aanwezige olie. In de secundaire oliewinning worden sommige boorputten (die in de vorige fase zijn gebruikt voor productie) omgezet in injectieputten en wordt water of gas in de boorput geïnjecteerd om de olie naar het oppervlak te verplaatsen. Echter, zelfs na de primaire en secundaire oliewinning blijft ongeveer 60

Microbieel versterkte oliewinning (EN: MEOR- Microbial Enhanced Oil Recovery) is een tertiaire oliewinningstechniek die wordt gebruikt om de resterende olie na het secundaire herstel te extraheren. MEOR werd voorgesteld in de jaren '20, maar pas vanaf de 40'er jaren serieus is beschouwd. In MEOR worden bacteriën en de daaruit voortkomende bioproducten gebruikt om de mobilisatie van olie in het reservoir te vergroten. Bacteriële groei kan gassen produceren die de druk op het reservoir verhogen en de viscositeit van de olie verlagen. Biosurfactanten verlagen de viscositeit van de olie, wat kan leiden tot een toename van de mobiliteit van olie. Bovendien kunnen bacteriën selectief zones met hoge permeabiliteit dichtstoppen, wat ervoor zorgt dat de richting van de waterstroom verandert naar gebieden waar de olie nog steeds gevangen zit. Selectieve verstopping door bacteriën is een proces dat tegelijkertijd met een overstromingsoperatie wordt ingezet. Van alle effecten van biofilmgroei wordt gedacht dat selectieve verstopping en reductie van grensvlakspanning de grootste impact hebben op oliewinning. De toepasbaarheid van selectieve verstopping om de stroming van water te veranderen is aangetoond in laboratoriumexperimenten. De toepasbaarheid van de MEOR-technieken op de veldschaal wordt echter nog onderzocht, omdat de MEOR-technieken in proefvelden verschillende resultaten hebben opgeleverd. In hoofdstuk 1 geven we een probleembeschrijving van MEOR.

In deze studie presenteren we een nieuw 2D microscopisch porienetwerk biofilm groeimodel, dat rekening houdt met het feit dat voedingsstoffen mogelijk niet volledig in de biofilm door kunnen dringen. Dit fenomeen treedt op wanneer de consumptie van voedingsstoffen sneller is dan de diffusie ervan. In het model nemen we een karakteristiek volume op, dat is gerelateerd aan de penetratiediepte van de voedingsstoffen in de biofilm. Dit maakt een meer nauwkeurige beschrijving van de biofilmgroei in poreuze media mogelijk. Daarnaast modelleren we de continue verspreiding van de biofilm door het hele netwerk, een fenomeen dat experimenteel is waargenomen. Onze numerieke experimenten tonen aan dat de voedingsstoffen zich tijdens de vroege stadia van het proces snel door het hele netwerk verspreiden. Doordat de voedingsstoffen in het hele netwerk aanwezig zijn, groeit de biofilm en verspreidt deze zich naar de naburige buizen. Gedurende een langere periode groeit de biofilm gelijkmatig in het netwerk, maar hierna wordt de uitputting van voedingsstoffen waargenomen en groeit de biofilm bij

voorkeur dicht bij de ingang van het netwerk, wat een volledige blokkering van het netwerk veroorzaakt. Ons model beschrijft de overgang tussen gelijkmatige biofilmgroei en een heterogene biofilmgroei.

Voorts bepalen we onder welke omstandigheden dit microscopische model van biofilmgroei kan worden gebruikt voor de beschrijving van de biofilmgroei op grotere schaal. Om deze reden bestuderen we de invloed van parameters zoals het aantal knooppunten in het netwerk, de grootte van het berekeningsdomein en de inlaatconcentratie van voedingsstoffen op de relatie tussen de porositeit en de permeabiliteit. We hebben de volgende resultaten verkregen. Als de biofilmgroei heterogeen is, dan is de relatie tussen permeabiliteit en porositeit niet uniek en is opschaling dus niet mogelijk. Met bepaalde inlaatconcentraties is het echter mogelijk om een uniforme biofilmgroei te verkrijgen; in dat geval is opschaling mogelijk. We gebruiken het Damkhöler-getal om de opschaalbaarheid van het biofilmgroeiproces te bepalen. De simulatie laat zien dat er een overgangsgebied bestaat tussen uniforme groei en heterogene groei. Deze overgang vindt in alle bestudeerde gevallen plaats binnen hetzelfde bereik van het Damköhler-getal (verschillend aantal knooppunten, grootte van het rekengebied en verschillende concentraties van voedingsstoffen). Als het Damköhler-getal lager is dan de overgangswaarde, dan is de biofilmgroei in het gehele proces uniform en is opschaling daarom mogelijk.

Daarna, breiden we ons 2D-model uit naar een 3D-biofilmgroeimodel. Het poreuze medium wordt weergegeven als een 3D kubiek netwerk. We bestuderen de invloed van het aantal knooppunten in de z-richting op de porositeit-permeabiliteitsrelatie en op de criteria voor opschaalbaarheid die werden verkregen in 2D. Daarnaast nemen we een lognormale verdeling voor de straal van de buizen in het netwerk op. Voor het heterogene biofilmgroeistelsel verkregen we dat naarmate het aantal knooppunten in de z-richting toeneemt, de hoeveelheid biomassa die nodig is om het netwerk te blokkeren convergeert naar een grenswaarde. We hebben vastgesteld dat de overgang tussen homogene en heterogene biofilmgroei voor de 3D-gevallen ongeveer binnen hetzelfde bereik van het Damköhler-getal voorkomt als in de 2D-gevallen. Verder onderzoeken we de invloed van de lognormale straalverdeling op de biofilmgroei Het is waargenomen dat als de afwijking van de straal groot is, de hoeveelheid biomassa die nodig is om het netwerk te blokkeren afneemt. Echter, ook in dit geval vindt de overgang tussen het homogene en het heterogene stelsel plaats in hetzelfde Damköhler-getal stelsel als in hoofdstuk 3.

Bovendien, gebruiken we een 2D-netwerkmodel om de invloed van biofilmgroei op verandering van de waterstroom te bestuderen. We modelleren twee gebieden met een verschillende permeabiliteit. We gebruiken een lognormale verdeling voor de straal van de buizen. De gemiddelde straal was groter voor de zone met een hoge permeabiliteit dan in de zone met een lage permeabiliteit. Omdat we geïnteresseerd zijn in de productie van olie uit de lage permeabiliteitszones, wat erg moeilijk is, berekenden we de uitstroom van water uit het gebied met lage permeabiliteit tijdens het groeiproces van de biofilms. We verkregen dat de flux uit het gebied met lage permeabiliteit in een bepaalde periode 60

Tenslotte, hebben we de via de willekeurige biofilmgroei verkregen porositeit-permeabiliteitsrelatie toegepast op twee poro-elasticiteitsproblemen. We bestuderen de toepasbaarheid van deze microscopische relatie op een macro-schaal pro-

bleem. Bij het eerste probleem wordt een hoge druk opgelegd in de inlaat van het poreuze mediumpakket. Deze hoge druk veroorzaakt een beweging van de korrels naar de uitlaat en daarmee een verandering in de lokale porositeit van het medium. Bij het tweede probleem wordt het pakket in het midden aan de boven- en onderrand van het domein dichtgedrukt. De op netwerken geïnspireerde relaties werden verkregen met behulp van een vierhoekig netwerk, een driehoekig gestructureerd netwerk en een driehoekig ongestructureerd netwerk in 2D en een kubisch netwerk in 3D. We hebben de verkregen resultaten vergeleken met de op het netwerk geïnspireerde relaties met de resultaten verkregen via de Kozeny-Carman-vergelijking, die vaak bij dit soort problemen wordt gebruikt. Voor de gekozen set van parameter zagen we dat de permeabiliteit berekend met de op het netwerk geïnspireerde relaties hoger is dan die verkregen met Kozeny-Carman. Verder zien we dat de porositeit voor de onderzochte gevallen erg vergelijkbaar is. Een mogelijke verklaring hiervoor kan zijn dat de relatie tussen het snelheidsveld en de verandering van de verplaatsingen in de tijd niet sterk genoeg is om tot significante veranderingen in het porositeitsprofiel te leiden. De door het netwerk geïnspireerde porositeit-permeabiliteitsrelatie zou kunnen worden gebruikt als een alternatief voor de Kozeny-Carman-vergelijking.

1

INTRODUCTION

The energy resources of the world still rely heavily on oil production [1]. In the primary recovery stage the oil is extracted from the reservoir by drilling a well and by natural pressure part of the oil, mainly (dissolved) gas, comes out to the surface. In this stage only 5-10% of the oil-in-place is obtained. In the secondary recovery stage some production wells are converted into injection wells and water or gas is injected into the reservoir to physically displace the oil to the surface. However, after primary and secondary oil recovery 60% of the total oil-in-place is still trapped in the reservoir.

The mobilization of oil is mainly determined by two factors: the capillary number and the mobility ratio [2]. The capillary number is defined as, $N_c = v\mu/\sigma$, in which v is the Darcy velocity $[m/s]$, μ is the viscosity and σ is the interfacial tension. This number represents the effects of the viscous forces and the surface tension between two immiscible fluids. One way to improve oil recovery is by increasing the capillary number which is usually done by decreasing the interfacial tension σ via the injection of surfactants or the application of heat. The mobility ratio is defined as $M = \lambda_{ing}/\lambda_{ed}$, here λ_{ing} is the mobility of the displacing fluid and λ_{ed} is the mobility of the displaced fluid [2]. If the mobility ratio is larger than one, the displacing fluid flows easier than the displaced fluid, which causes fingering of the displacing fluid. Consequently, the displacing fluid by-passes the oil residual regions. Another way to improve oil recovery is by decreasing the mobility ratio such that the fingering effect is reduced. For this reason, enhanced oil recovery (EOR) methods aiming at decreasing the mobility ratio and increasing the capillary number are often used after secondary oil recovery.

EOR methods can be subdivided into the following categories: thermal methods, chemical methods, miscible methods, foam methods and microbial enhanced oil recovery (MEOR) methods. In thermal processes, oil recovery is carried out by the reduction of the viscosity caused by high temperatures. The main methods used in thermal processes are steam injection and in-situ combustion. In chemical flooding, a chemical substance is added to the displacing water to stimulate oil mobility by reducing the interfacial tension. The most common chemical substances used are polymers, surfactants and alkaline solutions [2]. In miscible flooding a displacing fluid that is miscible

with the oil in the reservoir is used. In this case, interfacial tension is reduced to nearly zero. In foam flooding a surfactant is injected into the reservoir together with a gas such as CO_2 or N_2 to produce foam in-situ. Foam is used to improve gas sweep efficiency.

Microbial Enhanced Oil Recovery (MEOR) is a technique in which the growth of bacteria and the resulting by-products are used to increase residual oil production as a tertiary oil recovery method. There are two main approaches for MEOR. In the ex-situ method the desired by-products are produced outside of the field and then they are injected into the well. In this approach, the microbes are isolated in the laboratory and subsequently injected into the well to enhance the production of oil from the reservoir [1]. In the second approach, the in-situ methods use the indigenous microorganisms to obtain a large portion of the trapped oil. In this MEOR technique bacterial population growth is supported by the injection of nutrients into the reservoir [3].

Microbes enhance oil displacement via various processes: interfacial tension reduction, a decrease of the viscosity of oil [4], rock wettability change and an increase of the waterflood sweep efficiency caused by selective plugging [5]. The interfacial tension reduction is caused by microorganisms that produce amphiphilic compounds and biosurfactants [5]. In the process of wettability alteration, the microorganisms form a biofilm that grows around the rock of the porous medium changing the wettability. Depending on the biofilm characteristics the reservoir's wettability might change to a more water-wet or more oil-wet condition [5]. During selective plugging, bacteria grow and adhere within a self-produced matrix of extra-cellular polymeric substances (EPS) to the walls of the pores of high permeability zones. The adhering bacteria and the self-produced matrix are referred to as biofilm. Biofilm growth plugs the pores in high-permeability zones diverting the water-flood from these thief zones towards oil-rich areas. Among these mechanisms interfacial tension reduction and selective plugging are thought to have the greatest impact on recovery [3, 4]

The oil recovery via MEOR at field scale has had different outcomes [3, 6]. However, the applicability of MEOR techniques to increase oil extraction has been demonstrated in laboratory experiments [6–8]. Raiders et al. [9] show that biofilm accumulates in high permeability zones, diverting the water flood towards oil trapped zones. This suggests that MEOR can be a successful tertiary oil recovery technique.

1.1. MEOR MODELLING

The success of MEOR techniques depends on a good understanding of microbial activity in porous media, both quantitatively and qualitatively. For this reason, it is vital to develop mathematical and numerical models to predict the bacterial population growth, nutrients transport and the effects of selective plugging on porosity and permeability in order to develop a proper field strategy [3]. Several numerical models have been proposed to describe biofilm growth in porous media [10–17]. However, usually in macroscopic models [18] it is assumed that the biofilm grows uniformly through the domain of computation and the microscopic heterogeneity produced by biofilm growth is not taken into account. Therefore pore-scale models have been used to provide a constitutive equation for macro-scale models [17]. Among pore-scale models, Pore Network Models (PNM) have been extensively used to describe flow and transport in porous media. In this thesis, we are going to use a network model to describe the biofilm growth in

a porous medium.

In general, MEOR methods are difficult to model due to the different scales involved in the process [19]. It might be impractical to use all the data obtained at the micro-scale to describe MEOR at the macro-scale. For this reason effective parameters and constitutive equations are used to replace the microscopic details of the system [19, 20]. In general the effective parameters are obtained via an up-scaling process. There exist different up-scaling processes: averaging volume methods, homogenization and statistical procedures. In the homogenization process it is assumed that there exists spatial periodicity in the medium. Furthermore, this medium is subjected to periodic boundary conditions and it is supposed that the period is very small compared to the size of the studied domain [21]. Van Duijn et al. [20] obtained effective equations for two-phase flow in porous media when the medium consists of alternating layers with two different permeabilities. They found a good agreement between the effective solution and the average solution that takes into account the details of the microstructure. In the statistical methods the effective variables are considered as random functions in space. The probability distribution of the effective permeability is obtained via stochastic differential equations [22]. In Cliffe et al. [23] the permeability is described as a log-normal random distribution field. They computed the expectation of the pressure given the random distribution for the permeability using a Quasi-Monte Carlo method.

In the existing biofilm pore network models from the previous paragraph there are some important phenomena that are not taken into account that are vital for a proper understanding of biofilm growth in porous media. Firstly, the biofilm growth rate is commonly assumed to be proportional to the volume of biomass. Nevertheless, the nutrients might not be available in the entire volume of the biofilm. This phenomenon occurs if the consumption of nutrients is faster than the diffusion rate within the biofilm so that the (diffusion) penetration of the nutrients into the biofilm proceeds at a slower rate than the other processes [24, 25]. Secondly, it is usually assumed that microbial activity takes place only in the interior of the tubes and that there is no spreading of biomass between neighbouring tubes [15–17, 26, 27]. However, experiments show that the biomass or biofilm grows continuously, extending through the whole medium [28]. Finally, the up-scaling of the micro-scale biofilm growth requires an equivalent permeability as a constant permeability that represents a heterogeneous medium. However, in general, it is impossible to obtain a one-to-one mapping between the real heterogeneous medium and the homogeneous up-scaled medium. Therefore the equivalence, that is the one-to-one mapping, is defined in a limited sense [22].

The goal of this thesis is to obtain a better description of selective plugging caused by biofilm growth in porous media in order to provide a new insight into the applicability of MEOR techniques and to optimize MEOR techniques. For this purpose, we develop a new micro-scale biofilm growth model that takes into account the likelihood of a non-homogeneous distribution of nutrients within the biofilm and it describes the spreading of the biofilm through the whole network. Then we discuss the effects of biofilm growth on porosity and permeability and we set the conditions for up-scalability of these results to the macro-scale. Further, we present a model of the kinetics of the flow diversion caused by selective plugging. Finally, a network-inspired porosity-permeability relation obtained via the random biofilm growth model was used to describe two poroelasticity

problems.

REFERENCES

[1] J. Patel, S. Borgohain, M. Kumar, V. Rangarajan, P. Somasundaran, and R. Sen, *Recent developments in microbial enhanced oil recovery,* Renewable and Sustainable Energy Reviews **52**, 1539 (2015).

[2] S. Thomas, *Enhanced oil recovery-an overview,* Oil & Gas Science and Technology-Revue de l'IFP **63**, 9 (2008).

[3] R. Sen, *Biotechnology in petroleum recovery: the microbial eor,* Progress in energy and combustion Science **34**, 714 (2008).

[4] I. Lazar, I. Petrisor, and T. Yen, *Microbial enhanced oil recovery (meor),* Petroleum Science and Technology **25**, 1353 (2007).

[5] R. T. Armstrong and D. Wildenschild, *Investigating the pore-scale mechanisms of microbial enhanced oil recovery,* Journal of Petroleum Science and Engineering **94**, 155 (2012).

[6] Q. Li, C. Kang, H. Wang, C. Liu, and C. Zhang, *Application of microbial enhanced oil recovery technique to daqing oilfield,* Biochemical Engineering Journal **11**, 197 (2002).

[7] K. Behlulgil, T. Mehmetoglu, and S. Donmez, *Application of microbial enhanced oil recovery technique to a turkish heavy oil,* Applied microbiology and biotechnology **36**, 833 (1992).

[8] M. M. Yakimov, M. M. Amro, M. Bock, K. Boseker, H. L. Fredrickson, D. G. Kessel, and K. N. Timmis, *The potential of bacillus licheniformis strains for in situ enhanced oil recovery,* Journal of Petroleum Science and Engineering **18**, 147 (1997).

[9] R. A. Raiders, R. M. Knapp, and M. J. McInerney, *Microbial selective plugging and enhanced oil recovery,* Journal of industrial microbiology **4**, 215 (1989).

[10] W. Van Wijngaarden, F. Vermolen, G. Van Meurs, and C. Vuik, *A mathematical model and analytical solution for the fixation of bacteria in biogrout,* Transport in porous media **92**, 847 (2012).

[11] C. Picioreanu, J.-U. Kreft, and M. C. Van Loosdrecht, *Particle-based multidimensional multispecies biofilm model,* Applied and environmental microbiology **70**, 3024 (2004).

[12] T. Pintelon, D. Graf von der Schulenburg, and M. Johns, *Towards optimum permeability reduction in porous media using biofilm growth simulations,* Biotechnology and Bioengineering **103**, 767 (2009).

[13] D. G. von der Schulenburg, T. Pintelon, C. Picioreanu, M. Van Loosdrecht, and M. Johns, *Three-dimensional simulations of biofilm growth in porous media,* AIChE Journal **55**, 494 (2009).

[14] C. Ezeuko, A. Sen, A. Grigoryan, and I. Gates, *Pore-network modeling of biofilm evolution in porous media,* Biotechnology and bioengineering **108**, 2413 (2011).

[15] M. Thullner, J. Zeyer, and W. Kinzelbach, *Influence of microbial growth on hydraulic properties of pore networks,* Transport in porous media **49**, 99 (2002).

[16] B. J. Suchomel, B. M. Chen, and M. B. Allen, *Macroscale properties of porous media from a network model of biofilm processes,* Transport in porous media **31**, 39 (1998).

[17] B. Chen-Charpentier, *Numerical simulation of biofilm growth in porous media,* Journal of computational and applied mathematics **103**, 55 (1999).

[18] S. W. Taylor and P. R. Jaffé, *Biofilm growth and the related changes in the physical properties of a porous medium: 3. dispersivity and model verification,* Water resources research **26**, 2171 (1990).

[19] L. Orgogozo, F. Golfier, M. Buès, and M. Quintard, *Upscaling of transport processes in porous media with biofilms in non-equilibrium conditions,* Advances in Water Resources **33**, 585 (2010).

[20] C. J. van Duijn, H. Eichel, R. Helmig, and I. S. Pop, *Effective equations for two-phase flow in porous media: the effect of trapping on the microscale,* Transport in porous media **69**, 411 (2007).

[21] C. Farmer, *Upscaling: a review,* International journal for numerical methods in fluids **40**, 63 (2002).

[22] P. Renard and G. De Marsily, *Calculating equivalent permeability: a review,* Advances in water resources **20**, 253 (1997).

[23] K. A. Cliffe, M. B. Giles, R. Scheichl, and A. L. Teckentrup, *Multilevel monte carlo methods and applications to elliptic pdes with random coefficients,* Computing and Visualization in Science **14**, 3 (2011).

[24] H. Horn and S. Lackner, *Modeling of biofilm systems: a review,* in *Productive Biofilms* (Springer, 2014) pp. 53–76.

[25] P. S. Stewart, *Diffusion in biofilms,* Journal of bacteriology **185**, 1485 (2003).

[26] C.-Z. Qin and S. M. Hassanizadeh, *Pore-network modeling of solute transport and biofilm growth in porous media,* Transport in Porous Media **110**, 345 (2015).

[27] R. Rosenzweig, A. Furman, C. Dosoretz, and U. Shavit, *Modeling biofilm dynamics and hydraulic properties in variably saturated soils using a channel network model,* Water Resources Research **50**, 5678 (2014).

[28] M. Peszynska, A. Trykozko, G. Iltis, S. Schlueter, and D. Wildenschild, *Biofilm growth in porous media: Experiments, computational modeling at the porescale, and upscaling,* Advances in water resources **95**, 288 (2016).

2

A NETWORK MODEL FOR THE BIOFILM GROWTH IN POROUS MEDIA AND ITS EFFECTS ON PERMEABILITY AND POROSITY GROWTH MODEL

An accurate description of the effects of biomass growth in porous media at pore scale is needed for a better understanding of MEOR at the field scale. The pore network models of biofilm growth often ignore the possibility of spreading of biomass through the network even though this phenomenon has been reported in laboratory experiments, e.g. in experiments with biomass growth in glass beds. In addition, biofilm growth models usually assume that the biofilm growth rate is proportional to the biofilm volume. This assumption is only justified only if the nutrients are homogeneously distributed within the biofilm volume which could be an oversimplification.

In this chapter we present a novel approach for the biofilm growth in porous media. We assume that there are two kinds of biofilm growth: biofilm growth in the interior of the tube and biofilm growth in the extremes of the tubes. The biofilm growth in the extremes of the tube leads to the spreading of biomass to the neighbouring tubes. This mechanism allows spreading of biomass through the whole network. In addition we propose the existence of a characteristic volume which measures the penetration of nutrients within the biofilm.

In Section 2.1 we are going to describe the state of the art of biofilm growth models at pore-scale. Then in the mathematical model Section 2.2, we are going to describe the equations that model the transport of nutrients and the biofilm growth in the pore network. Subsequently in the numerical method section 2.3 the numerical scheme used to solve these equations is presented. After this, in the simulation results Section 2.4 we

discuss the effects of biofilm growth on the permeability and the porosity of the network. Additionally, in this section we compare the full model with two different biofilm growth models in order to interpret the results obtained with the full biofilm growth model. Finally, we draw some conclusions in Section 2.5.

2

2.1. INTRODUCTION

The production of oil from the reservoir is initially accomplished by the internal pressure of the reservoir. However, when the primary production declines some external forces have to be applied, hence waterflooding or gas injection techniques are implemented to extract oil from the reservoir. These injection schemes are called the secondary oil recovery production. Nevertheless, even after primary and secondary recovery two-thirds of the oil are still trapped in the ground ([1]). The tertiary oil recovery extraction aims to increase the mobility of the remaining oil. One of the tertiary (or enhanced) oil recovery techniques is the Microbial Enhanced Oil Recovery (MEOR) which uses the growth of bacteria and the resulting by-products in order to increase the oil production. Microbial growth may enhance oil displacement by increasing the efficiency of the waterflooding process, by reducing interfacial tension and by changing the rock wettability ([2, 3]). ([4]).

Since it is hard to quantify the relation between the successful application of MEOR and parameters like the individual reservoir characteristics and the microbial activity, the development of computational models is of vital importance. These models are used to predict the bacterial growth and the in-situ regeneration of bioproducts in order to develop a proper field strategy ([4]). The influence of biofilm growth on porous media characteristics such as permeability and porosity has been modelled in several studies ([5–11]). The mathematical description is based on a theoretical framework and phenomenological relations obtained from experimental results ([5, 7, 9–12]). Biofilm growth models include Darcy continuum models ([13, 14]), bacterially-based models ([10]), Lattice Boltzmann based simulations ([15, 16]) and Pore Network Models (PNM) ([5, 7, 9, 17–19]). Usually, in biofilm growth models the porous medium consists of three components: the grains, the biofilm which grows on the walls of the solid grains and the liquid in the pore space. The grains are assumed to be impermeable to the liquid and the nutrients, therefore hydrodynamic model equations are written only for the liquid and biofilm ([15]).

[20] showed experimentally the effect of the accumulation of biofilm on the porosity, permeability and friction factor of the porous media. The porosity of the media decreased between 50% and 96% due to the accumulation of biofilm, while permeability decreased between 92% and 98%. [21] obtained an analytic expression to describe changes in the porous media as a result of biofilm growth in the continuum scale. However, in [21] it is assumed that biofilm growth proceeds uniformly through the network which is an oversimplification according to laboratory experiments, ([22]). [6] model the biofilm growth using a macroscopic approach. This model does not assume any specific pattern for biofilm accumulation, instead it is based on macroscopic estimates of average biomass concentrations. [23] proposed a mathematical model for bioclogging that takes into account the nonuniform microbial distribution of colonies which ranges from micro-colonies to biofilm. However assuming uniform biofilm thickness in their model

gives an overestimation of the bioclogging process ([24]). Therefore, pore network models and pore-scale models are needed to describe the growth of biomass and its effects on the macroscopic properties of the media properly ([25]).

In PNMs, the porous medium is modelled by cylindrical interconnected tubes in which water or any fluid can flow. The biofilm development is stimulated by the injection of nutrients into the network. Transport of nutrients takes place within an aqueous phase and is described by a convection-diffusion-reaction equation. The reaction term models the consumption of nutrients caused by bacterial population growth. The bacterial population will determine the development of biofilm in the pores of the medium. This biofilm will grow and will change the radii of the pores, leading to porosity and permeability reduction and hence to a modification in the flow pattern dynamics of the fluid that carries the nutrients through the network ([5, 18, 19]). [8] studied the effects of biofilm growth on porosity under starvation conditions. They show a good agreement with experimental results and show the existence of a critical shear stress. [26] used a pore network model to describe two-phase flow in porous media. They took into account the influence of the nodes of the network on the effective resistance of the fluids. They used a coordination number distribution which allows a maximum coordination number of 26. Additionally, they assigned a variety of cross-sectional shapes including circular, rectangular and triangular. They claimed that the inclusion of the volume of the nodes of the network affects the relation between the relative permeability and the saturation of the fluids. Despite the relevance of their work, in their model, they did not include the development of biofilm in the porous medium. In this study, as an approximation, we disregard the volume of the nodes to avoid additional complications in the model. [27] studied the effect of topology in the relative permeability of the networks. They found that the relative permeability curves obtained with stochastic networks are in good agreement with the ones obtained from imaged rock networks. The bacteria and Extracellular Polymeric Substance (EPS) in porous media are often lumped together and are represented as a continuous uniform layer of biomass attached on the surface of the solid grains of the porous media ([7, 18, 19]). This uniform layer of biomass is referred to as biofilm. Furthermore, the biofilm growth rate is usually assumed to be proportional to the volume of biomass. Nevertheless, the nutrients might not be available in the entire volume of the biofilm. This phenomenon occurs if the consumption of nutrients is faster than the diffusion rate within the biofilm so that the (diffusion) penetration of the nutrients into the biofilm proceeds at a slower rate than the other processes ([28, 29]). Hence, the hypothesis that the nutrients are distributed over the whole volume of biofilm is questionable. Therefore, we assume that biofilm growth occurs only in a limited volume where the concentration of nutrients is maximal.

Usually, in PNMs the microbial activity is assumed to exist only within the tubes and no spread of biomass between neighbouring tubes is described ([5, 9, 17–19]). However, experiments show that the biomass or biofilm continuously grows, extending through the whole medium [22]. To model the inter-pore transport, [7] consider a spreading potential among neighbouring tubes. The spreading of the biofilm is allowed once the biomass has completely saturated the host pore. [19] modelled the colony growth by assuming that a tube in the network was completely full or empty. Hence a binary switch mechanism is used to describe the spreading of biomass. The switch to completely filled

tubes is determined by the size of the tubes. However, they did not consider any exchange of biomass between neighbouring tubes. In our model, we describe the continuous spreading of the biofilm between adjacent tubes by computing the spreading of biomass from one pore to its neighbours, if there is a difference of volume of biomass between neighbouring tubes.

In this study, we present a new biofilm growth model which takes into account that nutrients cannot fully penetrate the biofilm since consumption of nutrients is faster than the diffusion rate through the biofilm. We take into account that the biofilm growth is limited within a thin penetration layer, in which bacteria are in direct contact with the nutrients. In our model, there are two types of biofilm development: growth in the interior of the tube and growth at the extremes of the tube. Biofilm growth in the extremes of the tube will lead to the spreading of the biofilm to the neighbouring tubes and through the whole network. The currently proposed biofilm growth model approach has several advantages over other models. Firstly, we incorporate the likely non-homogeneous distribution of the nutrients within the biofilm. Secondly, since biofilm growth takes place mainly in the boundary between water and biofilm, the internal biofilm growth will naturally stop if the tube is full of biofilm. Finally, the biofilm growth in the extremes of the tubes leads to spreading of biomass through the whole network. In this model there is no need to seed initially all the tubes in the network to observe the clogging of the network. This paper is focused on the presentation of biofilm growth model in a pore network. Future research might be the use of these results to obtain an alternate relation between porosity and permeability. The up-scaling of these results is beyond the scope of this paper.

2.2. MATHEMATICAL MODEL

We represent the porous medium as a 2D rectangular network composed of interconnected cylindrical tubes. The point where these tubes are connected is called a node of the network and is indexed as node n_i. The tube between the node n_i and n_j is indexed as the tube t_{ij} (see Figure 2.1). We assume that the radius is the same for all the tubes (which differs from previous studies because we want to express the spreading of the biofilm in a simple way, the modelling of this phenomenon is explained later) and the same length l. The number of tubes connected in each node is four for interior nodes, three for boundary nodes and two for the nodes in the corners of the network.

We assume the bacteria and the biofilm are lumped together and hence we refer to them as the single phase: biofilm. We assume that nutrients are injected through the network and transported within a fluid phase. For simplicity we chose water as the fluid in which the nutrients are transported. We define the thickness of the biofilm in the tube t_{ij} by $r_{b_{ij}}$, the radius available for water by $r_{w_{ij}}$ and the total radius of the tube by R (see Figure 2.1). The volumetric flow of the water phase q_{ij} in the tube t_{ij} is described by a modified form of the Poiseuille equation, ([30]),

$$q_{ij} = \frac{\pi}{8\mu l}[r_{w_{ij}}^4 + (R^4 - r_{w_{ij}}^4)\beta^{-1}]\Delta p, \tag{2.1}$$

where Δp is the pressure drop between neighbouring nodes, μ is the viscosity of water that flows in the bulk, l is the length of the tube and the dimensionless number β is

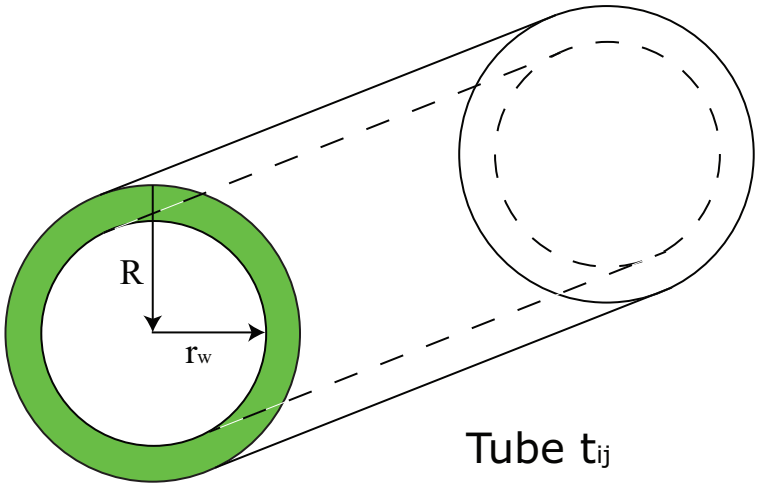

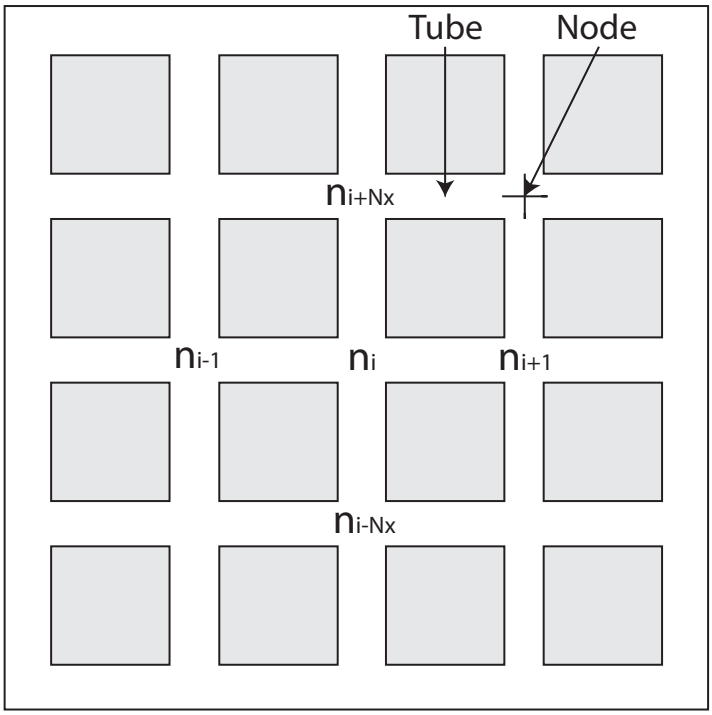

Figure 2.1: Pore network and biofilm thickness within a tube

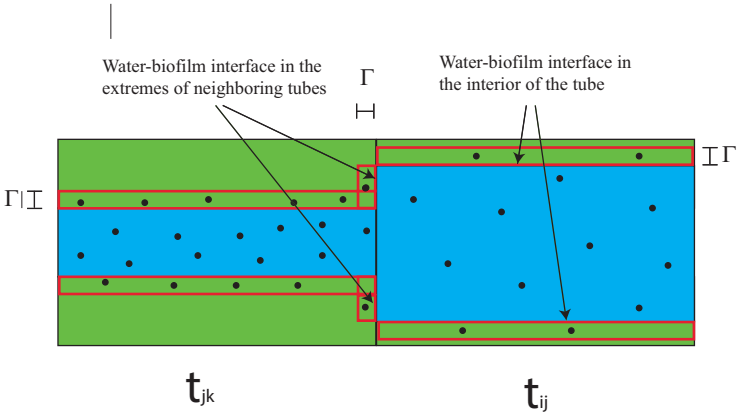

Figure 2.2: Biofilm growth in the interior and in the extremes of the tube

the ratio between the viscosity of water flowing through the biofilm and the viscosity of water flowing through the bulk. We use $\beta = 10^7$ which according to [30] is a good approximation for an impermeable biofilm. Despite the β term only a negligible addition in equation (2.1) we incorporate it to keep the description general. Mass conservation is imposed on each of the nodes. For the node n_i we have

$$\sum_{j \in S_i} q_{ij} = 0, \tag{2.2}$$

where,

$$S_i = \{j \mid n_j \text{ is adjacent to the node } n_i\}, \tag{2.3}$$

and further q_{ij} is the flux in the tubes connected to node n_i.

The balance of nutrients is described by an advection-diffusion-reaction equation. Denoting the concentration of nutrients by C, this gives

$$\frac{\partial C}{\partial t} + \mathbf{u} \cdot \nabla C - D\nabla^2 C = -\frac{\partial b^+}{\partial t}, \tag{2.4}$$

where $\mathbf{u}$ is the advection velocity related to the local flux $\mathbf{q}$ by $\mathbf{u} = \mathbf{q}/A$. Here A denotes the area of the cross-section of the tube and D is the diffusion coefficient of water. Further b^+ represents the concentration of biofilm that grows as a result of consumption of nutrients (no detachment term is taken into account in this equation). In general, the concentration of nutrients b is linked to the volume of biofilm, V_{bf} by

$$b = \frac{\rho}{V_T} V_{bf}, \tag{2.5}$$

where ρ and V_T, respectively, denote the mass density of biofilm and the total volume of the tube. We describe the overall growth rate of the biofilm in the following paragraphs.

In this model we assume that nutrients might not penetrate completely through the biofilm since the reaction is faster than the diffusion rate within the biofilm. Therefore

we propose that there exists a maximal distance (from the water biofilm interface) that the nutrients can travel within the biofilm. The maximal distance is called the penetration layer, Γ, and implicitly defines a maximal volume in which the nutrients can diffuse. This volume is called the penetration volume V_p and it is assumed to be constant during the whole process of biofilm growth. If the volume of biofilm is smaller than the penetration volume, the nutrients can penetrate the whole biofilm volume and hence the biofilm growth rate is proportional to the volume of biofilm. However, if the biofilm volume is much larger than the penetration volume, the nutrients react with the biofilm only within this penetration volume, which is adjacent to the water-biofilm interface. In this case, the biofilm growth rate is proportional to the area of the water biofilm interface. Further, since in general there are two regions in the tube where the biofilm encounters the nutrients, we model two kinds of biofilm growth: internal biofilm growth and biofilm growth at the extremes of the tube (see 2.2). Firstly, we describe the internal growth.

The biofilm growth rate in the interior of the tube t_{ij} is modelled as follows,

$$\frac{\partial V^i_{bf_{ij}}}{\partial t} = k_1 \frac{A^i_{wbf}}{A^i_T} V_T \frac{C_{ij}}{E_s + C_{ij}} f(V_{bf_{ij}}). \tag{2.6}$$

Here $V^i_{bf_{ij}}$ denotes the volume of interior biofilm in the tube t_{ij}. Further, $f(V_{bf_{ij}}) \geq 0$ is the positive part of a sigmoid function for $V_{bf_{ij}}$ that depends on the penetration volume V_p, k_1 is the specific biofilm growth rate, A^i_{wbf} is the internal interface water biofilm area, A^i_T is the external area of the tube, C_{ij} is the concentration of nutrients within the tube and E_s is a saturation constant. The positive part of the sigmoid-like function is defined as,

$$f(V_{bf}) = \frac{\frac{V_{bf}}{V_p}}{1 + \frac{V_{bf}}{V_p}}. \tag{2.7}$$

The dependence of biofilm growth rate (equation 2.6) on the concentration of nutrients is given by the Monod equation which models the limiting nutrient consumption by the biofilm. Next we explain the reason why we use the positive part of a sigmoid-like function: if the volume of biofilm is small, i.e. $V_{bf} << V_p$, then $A^i_{wbf} \sim A^i_T$ and $f(V_{bf}) \sim \frac{V_{bf}}{V_p}$. Therefore, the biofilm growth rate is proportional to the volume of biofilm, $\frac{\partial V^i_{bf_{ij}}}{\partial t} \sim \frac{C_{ij}}{E_s + C_{ij}} V_{bf}$. If the volume of biofilm is much larger than the penetration volume, $V_{bf} >> V_p$, then $f \sim 1$ and therefeore the biofilm growth is proportional to the area of the interface between water and biofilm, $\frac{\partial V^i_{bf_{ij}}}{\partial t} \sim \frac{C_{ij}}{E_s + C_{ij}} \frac{A^i_{wbf}}{A^i_T}$.

The biofilm growth rate is zero when there is no biofilm in the tube or when the tube is filled with biofilm, consequently, biofilm growth in the interior of the tube stops if there is no more space in the tube. Note that our approach is phenomenological. Further, the area A^i_{wbf} can be written in terms of the total volume of the tube V_T and the volume of biofilm V_{bf}, therefore equation (2.3) for the biofilm which grows in the interior of the tubes, is expressed as follows,

$$\frac{\partial V^i_{bf_{ij}}}{\partial t} = k_1 R \frac{C_{ij}}{E_s + Cij} \sqrt{\pi l (V_T - V_{bf_{ij}})} f(V_{b_{ij}}). \tag{2.8}$$

Note that the above relation for $V^i_{bf_{ij}}$ represents a continuous relation of biomass growth with the volume of biofilm.

Secondly, we describe the biofilm that grows in the extremes of the tube. Since the penetration volume in the extremes is very small compared to the whole volume of biofilm, the biofilm growth rate in the extremes of the tubes is proportional to the area of the interface between water and biofilm (see Figure 2.2). We assume binary interactions with the neighbouring tubes. The area of the interface between water and biofilm A^e_{wbf} between the tube t_{ij} and the tube t_{jk} can be written in terms of the difference between biofilm volumes of neighbouring tubes. The biofilm grows in the extreme of the tube with a larger volume of biofilm and it is given to the neighbouring tube which has a smaller volume of biofilm.

If we assume that the volume of biofilm $V_{bf_{jk}}$ in the neighbouring tube t_{jk} (connected to the node n_j) is larger than the volume of biofilm $V_{bf_{ij}}$ in the tube t_{ij}, then the biofilm growth in the extreme of the neighbouring tube t_{jk} is given by,

$$\frac{\partial V^e_{bf_{jk}}}{\partial t} = k_1 \frac{A^e_{wbf}}{A^e_T} V_T \frac{C_{jk}}{E_s + C_{jk}}. \tag{2.9}$$

Here $V^e_{bf_{jk}}$ represents the volume of biofilm at the extreme of the tube, A^e_{wbf} is the external interfacial water biofilm area and A^e_T is the cross-sectional area in the extreme of the tube. The ratio between the external interfacial water biofilm area and the cross-sectional area of the tube A^e_T is a measure of the biofilm growth in the extremes of the tube. This ratio is zero if the volume of biofilm is the same in both interacting tubes which means there is no biofilm growth in the extreme of the tube and hence no volume of biofilm is added to either of them. On the other hand, when this ratio is one, the biofilm grows at a maximal rate and the accumulated biofilm is added to the tube t_{ij}. Note that there is no biomass exchange between neighbouring tubes; the biomass is produced in the extreme of the tube and it is given to the neighbouring one, hence no loss term for the biomass growth is necessary to describe this phenomenon. In this way, this model for the biofilm growth allows the spreading of the biofilm through the whole network, which is consistent with experimental observations. The area A^e_{wbf} between the tube t_{ij} and the tube t_{jk} can be written in terms of the volume of the biofilm of the tubes. Hence equation (2.9) for the biofilm growth at the extreme of the tube t_{jk} changes into,

$$\frac{\partial V^e_{bf_{jk}}}{\partial t} = k_1 \frac{C_{jk}}{E_s + C_{jk}} (V_{bf_{jk}} - V_{bf_{ij}}). \tag{2.10}$$

We take into account all the neighbouring tubes whose volumes of biofilm are larger than the volume of biofilm in the tube t_{ij}. To this extent we introduce the following index set notation for the tube t_{ij} which connects nodes n_i and n_j. Consider the node n_j then we define the set of neighbouring nodes of it, except n_i by Λ_{ji} (see Figure 2.1). Therefore,

taking into account all neighbouring tubes, the equation for the biofilm growth in the tube t_{ij} due to biofilm growth in the extremes of the neighbouring tubes is written as,

$$\frac{\partial V^e_{bf_{ij}}}{\partial t} = k_1 \sum_{k\in\Lambda_{ji}} \frac{C_{jk}}{E_s + C_{jk}} (V_{bf_{jk}} - V_{bf_{ij}})_+ + k_1 \sum_{k\in\Lambda_{ij}} \frac{C_{ki}}{E_s + C_{ki}} (V_{bf_{ki}} - V_{bf_{ij}})_+, \tag{2.11}$$

in which we use the notation $(V_{bf_{ki}} - V_{bf_{ij}})_+ = \max(0, V_{bf_{ki}} - V_{bf_{ij}})$. Finally, using that $V_{bf_{ij}} = V^i_{bf_{ij}} + V^e_{bf_{ij}}$ we combine the internal growth of biofilm with the biofilm growth in the extremes of the neighbouring tubes and including a possible detachment of biofilm, which is proportional to the interfacial water-biofilm area, we obtain,

$$\begin{aligned}\frac{\partial V_{bf_{ij}}}{\partial t} &= k_1 R \frac{C_{ij}}{E_s + C_{ij}} \sqrt{\pi l (V_T - V_{bf_{ij}})} f(V_{bf_{ij}}) + k_1 \sum_{k\in\Lambda_{ji}} \frac{C_{jk}}{E_s + C_{jk}} (V_{bf_{jk}} - V_{bf_{ij}})_+ \\ &+ k_1 \sum_{k\in\Lambda_{ij}} \frac{C_{ki}}{E_s + C_{ki}} (V_{bf_{ki}} - V_{bf_{ij}})_+ - k_2 R \sqrt{\pi l (V_T - V_{bf_{ij}})} H(V_{bf_{ij}}).\end{aligned} \tag{2.12}$$

where k_2 is the detachment rate coefficient. Further, $H(V_{bf_{ij}})$ is defined as,

$$H(V_{bf_{ij}}) = \begin{cases} 0 & \text{if } V_{bf_{ij}} = 0 \\ 1 & \text{if } V_{bf_{ij}} \geq 0. \end{cases} \tag{2.13}$$

We include the function H because detachment occurs only when there is biofilm within the tube. In case there is no biofilm in the tube, $H = 0$, which means the detachment rate is zero. In equation (2.12) the first term is the interior biofilm growth, the second and third term describes the biofilm which grows in the extremes of the neighbouring tubes and the fourth term is a term for the detachment of the biofilm.

The reaction rate of the nutrients is given by,

$$\begin{aligned}\left[\frac{\partial b^+_{ij}}{\partial t}\right] = \frac{k_1}{Y} \frac{\rho}{V_T} \frac{C_{ij}}{E_s + C_{ij}} \Bigg[& R \sqrt{\pi l (V_T - V_{bf_{ij}})} f(V_{bf_{ij}}) \\ & + \sum_{k\in\Lambda_{ji}} (V_{bf_{ij}} - V_{bf_{jk}})_+ + \sum_{k\in\Lambda_{ij}} (V_{bf_{ij}} - V_{bf_{ki}})_+ \Bigg].\end{aligned} \tag{2.14}$$

In summary, we solve the following coupled mathematical problem: Find p, subject to

$$\begin{aligned} p(0, y) &= 1600 L_x, \\ p(L_x, y) &= 0, \\ \frac{\partial p}{\partial n}(x, 0) &= 0, \\ \frac{\partial p}{\partial n}(x, L_y) &= 0, \end{aligned} \tag{2.15}$$

such that,

$$\sum_{j \in S_i} q_{ij} = 0, \forall n_i, \tag{2.16}$$

where,

$$q_{ij} = \frac{\pi}{8\mu l}[r_{w_{ij}}^4 + (R_{ij}^4 - r_{w_{ij}}^4)\beta^{-1}](p_j - p_i). \tag{2.17}$$

Here L_x is the size of the network in the x direction and L_y the size in y direction. Next to this $r_{w_{ij}}$ decreases as a result of deposition of biofilm, which grows under the presence of nutrients. The balance of nutrients is given by,

$$\frac{\partial C}{\partial t} + \mathbf{u} \cdot \nabla C - D\nabla^2 C = -\frac{\partial b^+}{\partial t}, \tag{2.18}$$

subject to,

$$\begin{aligned} C(x, y, t_0) &= 0, \\ t_0 &= 0, \end{aligned} \tag{2.19}$$

$$\begin{aligned} C(0, y, t) &= 1, \\ \frac{\partial C}{\partial x}(L_x, y, t) &= 0, \\ \frac{\partial C}{\partial y}(x, 0, t) &= 0, \\ \frac{\partial C}{\partial y}(x, L_y, t) &= 0. \end{aligned} \tag{2.20}$$

The biofilm grows according to,

$$\begin{aligned} \frac{\partial V_{bf_{ij}}}{\partial t} &= k_1 R \frac{C_{ij}}{E_s + C_{ij}} \sqrt{\pi l (V_T - V_{bf_{ij}})} + k_1 \sum_{k \in \Lambda_{ji}} \frac{C_{jk}}{E_s + C_{jk}} (V_{bf_{jk}} - V_{bf_{ij}})_+ \\ &+ k_1 \sum_{k \in \Lambda_{ij}} \frac{C_{ki}}{E_s + C_{ki}} (V_{bf_{ki}} - V_{bf_{ij}})_+ - k_2 R \sqrt{\pi l (V_T - V_{bf_{ij}})} H(V_{bf_{ij}}). \end{aligned} \tag{2.21}$$

Subject to the initial condition

$$V_{bf_{ij}}(t = 0) = \begin{cases} \frac{b_0 V_T}{\rho} & \text{if the tube } t_{ij} \text{ is chosen} \\ 0 & elsewhere. \end{cases} \tag{2.22}$$

Our routine randomly chooses 4% of the tubes. Note that $b_{ij} = \frac{\rho V_{bf_{ij}}}{V_T}$. We have chosen $b_0 = 10^{-4}\,[kg/m^3]$ for the initial tubes that were seeded with biofilm. The consumption of nutrients is modelled by,

$$\left[\frac{\partial b_{ij}^{+}}{\partial t}\right] = \frac{k_1}{Y}\frac{\rho}{V_T}\frac{C_{ij}}{E_s + C_{ij}}\left[R\sqrt{\pi l(V_T - V_{bf_{ij}})}f(V_{bf_{ij}}) + \sum_{k\in\Lambda_{ji}}(V_{bf_{ij}} - V_{bf_{jk}})_+ + \sum_{k\in\Lambda_{ij}}(V_{bf_{ij}} - V_{bf_{ki}})_+\right]. \tag{2.23}$$

Further $C_{ij} = \frac{C_i + C_j}{2}$ links the concentration of nutrients in the nodes and the concentration in the tubes.

2.3. NUMERICAL METHOD

The numerical approach and the computational procedure used in this work are described in this section. When mass conservation, equation (2.1), is combined to equation (2.2) a linear system for the pressures at the nodes p_i arises. After solving this system, the flux q_{ij} in each of the tubes is computed.

The equation for the balance of nutrients is solved for the concentration C_i at each node n_i of the network (see Figure 2.4). To discretize the equation for the balance of nutrients, we write it in the following form,

$$\frac{C_i^{\tau+1} - C_i^{\tau}}{\Delta t} = J_{adv}^{\tau+1,\tau} + J_{diff}^{\tau+1,\tau} - R_{cons}^{\tau+1,\tau} \tag{2.24}$$

where the first-order upwind scheme for the advection term gives,

$$J_{adv}^{\tau+1,\tau} = \sum_{j\in\Omega_i}\frac{{q_{ij}}^{\tau}}{V_T}({C_j}^{\tau+1} - {C_i}^{\tau+1}), \tag{2.25}$$

where $\Omega_i = \{j \mid q_{ij} \text{ is directed towards the node } n_i\}$.

Further, the diffusion term of the equation (2.4) is discretized using a time-implicit method for the concentration. The area is used from the previous time step. We use a finite difference scheme in space. Therefore the discretization for the diffusion part, reads as,

$$J_{diff}^{\tau+1,\tau} = \frac{D}{l^2}\sum_{j\in S_i}({C_i}^{\tau+1} - {C_j}^{\tau+1})\frac{A_{w_{ij}}^{\tau}}{A_{ij}}, \tag{2.26}$$

where $A_{w_{ij}}^{\tau}$ is the area of the cross section of the bulk water in the tube t_{ij} and A_{ij} is the total area of cross section of the tube t_{ij}.

To write the reaction term in each node, we assume that at each node there is a perfect mixture of biofilm. Therewith we get,

$$R_{cons}^{\tau+1,\tau} = \frac{k_1}{Y}\frac{C_i^{\tau+1}}{E_s + C_i^{\tau}}\frac{\sum_{j\in S_i}G(V_{bf_{ij}}^{\tau})V_T}{\sum_{j\in S_i}V_T}. \tag{2.27}$$

where,

$$G(V^{\tau}_{bf_{ij}}) = \frac{\rho}{V_T}\left[R\sqrt{\pi l(V_T - V^{\tau}_{bf_{ij}})}f(V^{\tau}_{bf_{ij}}) + \sum_{k\in\Lambda_{ji}}(V^{\tau}_{bf_{ij}} - V^{\tau}_{bf_{jk}})_+ + \sum_{k\in\Lambda_{ij}}(V^{\tau}_{bf_{ij}} - V^{\tau}_{bf_{jk}})_+\right]. \tag{2.28}$$

The solution of the concentration of nutrients obtained from the advection-diffusion-reaction is used for the approximation of the biofilm volume.

The biofilm growth takes place within the tubes of the network. Here we use an explicit Euler time integration method to arrive at,

$$\begin{aligned}\left[\frac{{V_{bf_{ij}}}^{\tau+1} - {V_{bf_{ij}}}^{\tau}}{\Delta t}\right] &= k_1 R\left[\frac{{C_{ij}}^{\tau}}{E_s + {C_{ij}}^{\tau}}\right]\sqrt{\pi l(V_T - V^{\tau}_{bf_{ij}})}f(V^{\tau}_{bf_{ij}}) \\ &+ k_1\sum_{k\in\Lambda_{ji}}\left[\frac{C^{\tau}_{jk}}{E_s + C^{\tau}_{jk}}\right](V^{\tau}_{bf_{jk}} - V^{\tau}_{bf_{ij}})_+ + k_1\sum_{m\in\Lambda_{ij}}\left[\frac{C^{\tau}_{mi}}{E_s + C^{\tau}_{mi}}\right](V^{\tau}_{bf_{mi}} - V^{\tau}_{bf_{ij}})_+ \\ &- k_2 R\sqrt{\pi l(V_T - V^{\tau}_{bf_{ij}})}H(V^{\tau}_{bf_{ij}})\end{aligned} \tag{2.29}$$

The computational procedure used in this work is as follows. Firstly, the pressure is imposed in the left and right boundary of the network. Subsequently, the pressure in each node is computed from the linear system resulting from the mass conservation in each node. For solving this system, we consider Dirichlet boundary conditions in the left and right boundaries and homogeneous Neumann boundary condition for the upper and lower boundary. The pressures in each node are used to compute the flux in each tube by means of equation (2.1). After this step, we proceed to solve the advection-diffusion reaction equation for the nutrients and we compute the concentration of nutrients in each node as well as the volume of biofilm in the tubes. The thickness of the biofilm and the radius of the void space available for water is updated and the process starts again at the next time step (See Figure 2.3).

2.4. SIMULATION RESULTS

In this section we describe the numerical experiments and the results obtained for the biofilm growth in a pore network. Firstly, in order to validate the advection-diffusion part of our code, we compare our results with an analytic solution and with a Continuous Time Random Walk (CTRW) transport model [31]. Secondly, we studied the biofilm growth effects on the out-flux and porosity. For this study, the biofilm growth rate k_1 is fixed but three different detachment rates k_2 are used. Finally, we compare our results with the Kozeny-Carman relation and with two quasi-steady biofilm growth models.

Firstly, the evolution of the concentration of nutrients through the network is studied without the presence of biofilm. We disregard the reaction term in order to be able to compare the transport and diffusion of nutrients with an analytic solution in 1-D and with an existing model based on CTRW. The CTRW transport model can consider classical and non-classical Fickian dispersion. In this case we use Fickian diffusion for the

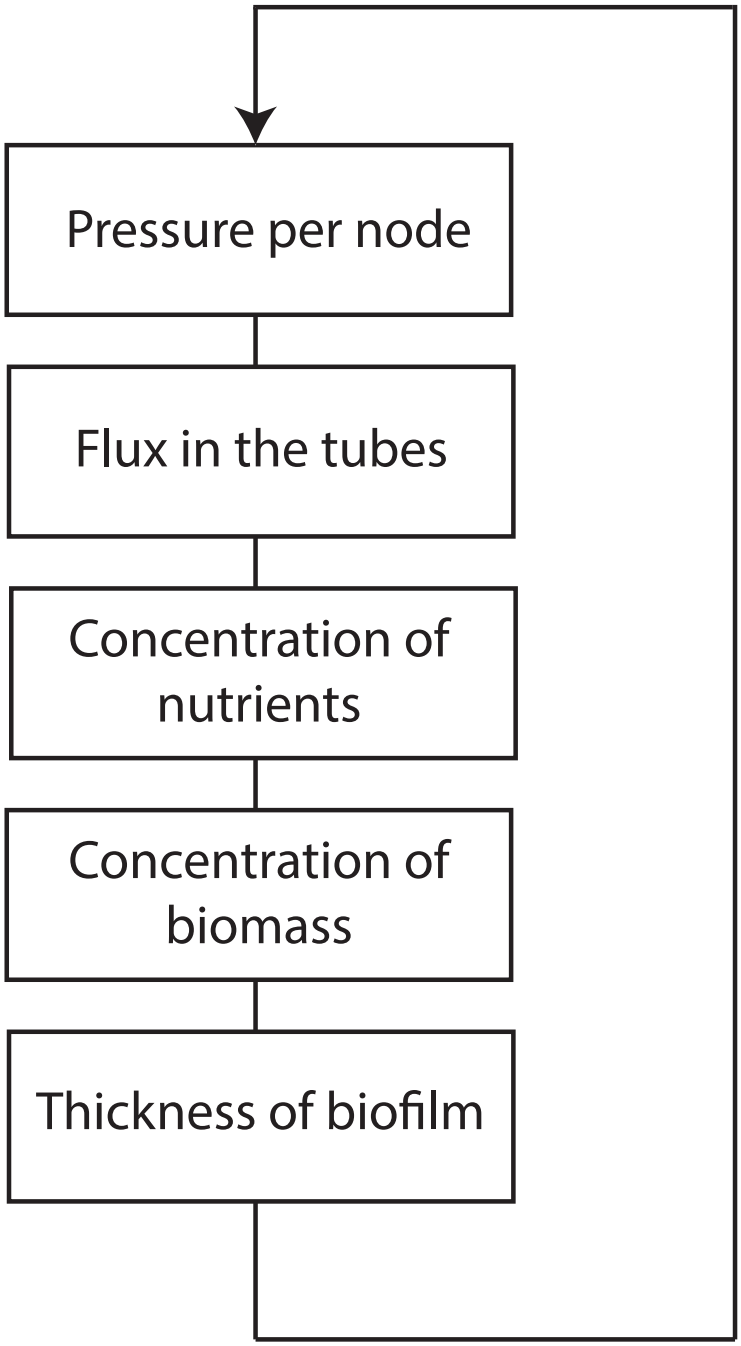

Figure 2.3: Full model algorithm that combines the transportation of nutrients and biofilm growth

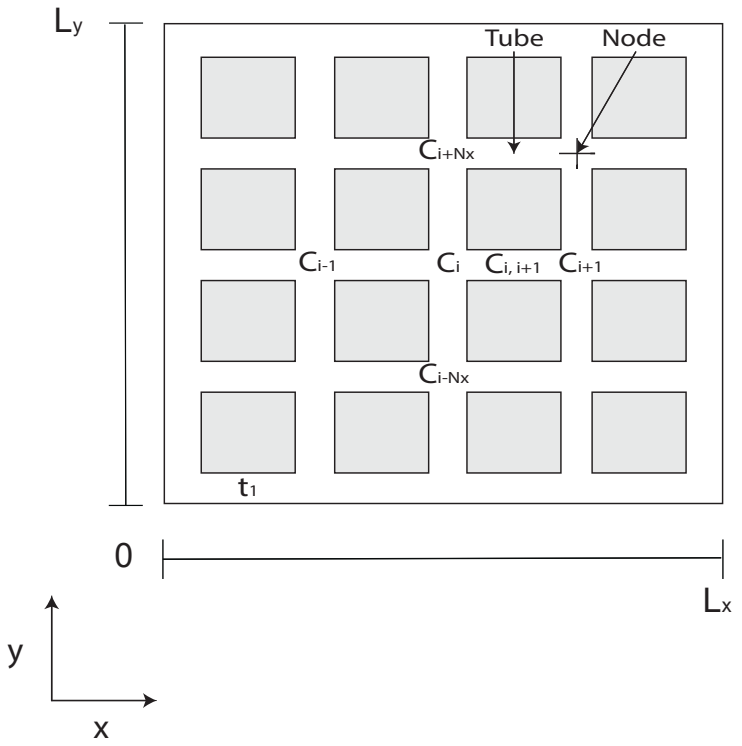

Figure 2.4: Network discretization and domain of computation

CTRW since in our model we are not considering other kinds of diffusion. We use a MATLAB toolbox developed by [31] to obtain the breakthrough curve with the CTRW model. The diffusion coefficient and the pore velocity used in the CTRW transport model are listed in Table 2.1.

We solve the advection-diffusion equation for the concentration of nutrients with our model using a mesh with 201×11 nodes, which means there are 201 nodes in x direction and 11 nodes in y direction. The number of tubes is determined implicitly by the number of nodes and by the topology of the network. Further, we assume that all the tubes in the network have the same radius. We use the volumetric flows through the pores from the network model for the solution of the concentration of nutrients. Under these conditions for the size of the mesh and the uniform size of the radii in all the tubes, we can compare the results with a model based on CTRW and with an analytic solution in one dimension, ([32]). The analytic solution of the advection-diffusion equation (equation 2.4 without reaction term) in 1-D is given by:

$$c(x,t) = \frac{C_{in}}{2}\left[erfc\left(\frac{x - v^* t}{\sqrt{4D^* t}}\right) + erfc\left(\frac{x + v^* t}{\sqrt{4D^* t}}\right) exp\left(\frac{v^* x}{D^*}\right)\right], \tag{2.30}$$

in which erfc is the complementary error function, v^* is the velocity and D^* is the diffu-

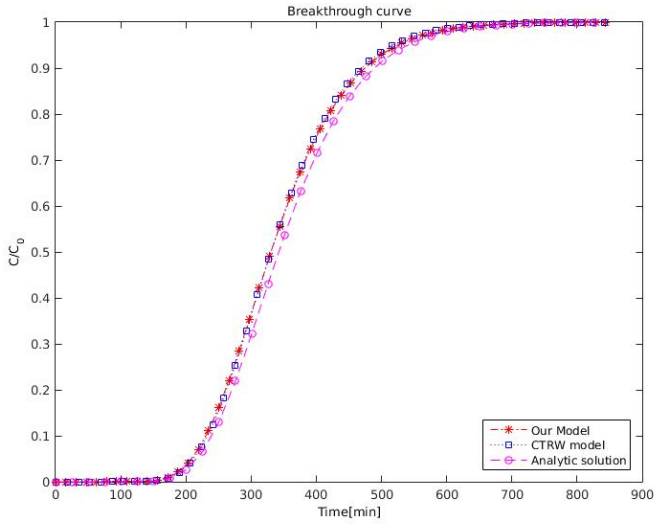

Figure 2.5: Comparison of the solution of the advection diffusion equation for our model CTRW model and an analytic solution

sion coefficient used in this first simulation.

Figure 2.5 shows the results for the normalised concentration of nutrients C/C_0 in one of the tubes that is located adjacent to to the outlet of the network for our model, a model based on CTRW and the analytic solution given by equation (2.30). We observe a good agreement between, the CTRW model, the analytic solution and our model, which indicates that our scheme produces consistent results. However we observe a small shift between our model, the CTRW and the analytic solution. The shift is attributed to the following cause: our model contains a Neumann boundary condition at the outflow boundary, whereas the analytic solution is valid in a domain with infinite size. Therefore the concentration calculated by our model is a little higher than the one computed the use of the analytic solution. This can be proved in more rigour using smoothness of the solution and the maximum principle. The complete set of parameters for this simulation is presented in Table 2.1.

The next step is to quantify the effects of biofilm growth on the porosity and permeability of the porous medium. Therefore, we solve the biofilm growth and the transport of nutrients as a coupled problem. Initially 4% of the tubes are seeded with an initial concentration of biomass $b_0 = 1 \times 10^{-4}$ $[kg/m^3]$. We performed three sets of simulations in which the biofilm growth rate is fixed, however three different values for the detachment rate factor are chosen, $k_2 = 10^{-6}$ $[1/s]$, $k_2 = 10^{-7}$ $[1/s]$ and $k_2 = 0$ $[1/s]$. For this set of simulations we used a network with 101 x 61 nodes and we considered a radius $R = 1.1937 \times 10^{-5}$ $[m]$ for all the tubes of the network. The complete set of parameters for this set of simulations is listed in Table 2.2.

For each pair of biofilm growth k_1 and detachment rate factor k_2, we performed ten

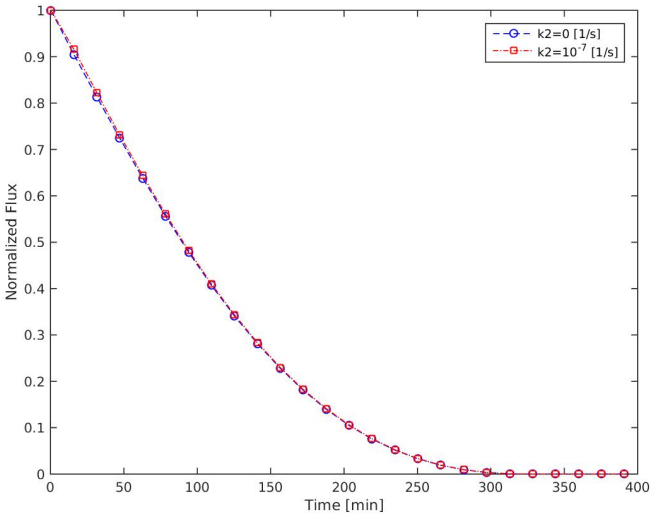

Figure 2.6: Average normalised flux for two different detachment rates $k_2 = 0[1/s]$ and $k_2 = 10^{-4}[1/s]$

Parameters for the simulations without growth of biofilm		
Name	Symbol	Value
Pore length	l	95×10^{-6} $[m]$
Network size in the x direction	L_x	0.019 $[m]$
Network size in the y direction	L_y	0.00095 $[m]$
Number of tubes in the network	N_a	4210
Mean pore radius	r_{mean}	3.5339×10^{-6} $[m]$ [7]
Global pressure gradient	ΔP	1.6 $[kPa/m]$
Viscosity of water	μ	$4.7 \times 10^{-}5$ $[Pa \cdot min]$
Density of water	ρ_w	1000 $[kg/m^3]$
Diffusion coefficient of water	D_w	3.9710×10^{-8} $[m^2/min]$ [33]
Inlet reservoir concentration	C_{in}	1 $[kg/m^3]$

Table 2.1

Parameters for the second series simulation		
Name	Symbol	Value
Mean pore radius	R	12.2×10^{-6} $[m]$ [7]
Pore length	l	95×10^{-6} $[m]$
Global pressure gradient	ΔP	1.6 $[kPa/m]$
Viscosity of water	μ	0.001/60 $[Pa \cdot min]$
Density of water	ρ_w	1000 $[kg/m^3]$
Density of biofilm	ρ_{bf}	20 $[kg/m^3]$ [34]
Yield coefficient	Y	0.34 [35]
Half saturation constant for biofilm	E_{sb}	2×10^{-3} $[kg/m^3]$ [35]
Inlet reservoir concentration	C_{in}	1 $[kg/m^3]$
Initial biomass concentration	b_0	1×10^{-6} $[kg/m^3]$
Biofilm / bulk water viscosity ratio	β	10^7 [30]

Table 2.2

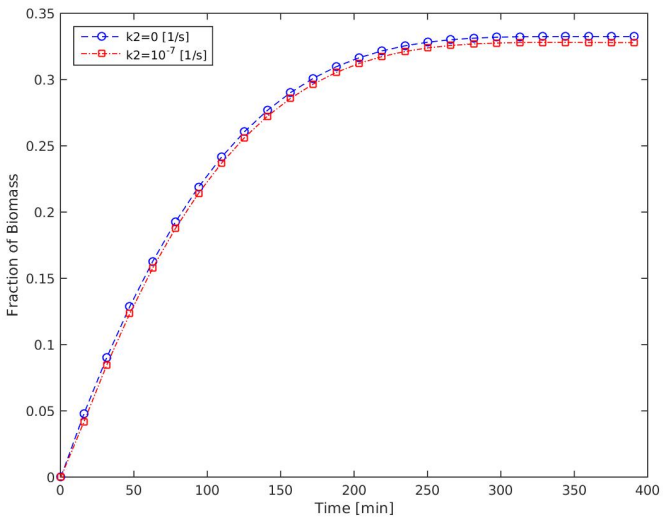

Figure 2.7: Average fraction of biomass for two different detachment rates $k_2 = 0[1/s]$ and $k_2 = 10^{-4}[1/s]$

simulations where we fixed all the parameters, except the initial distribution of tubes seeded with biofilm. The normalised flux Q_n is defined as, $Q_n = \frac{Q}{Q_0}$, where Q_0 is the initial flux in the network (i.e. before biofilm growth). We compute the average of the normalised flux and we observe that the 95% confidence interval is very close to the average value of the normalised flux, therefore the initial random biofilm distribution does not have a significant effect on the results.

The evolution of the average normalised flux through the network for the detachment rate $k_2 = 10^{-7}\,[1/s]$ and $k_2 = 0\,[1/s]$ is shown in Figure 2.6. For detachment rates $k_2 = 10^{-7}\,[1/s]$ and $k_2 = 0\,[1/s]$, we observe a decrease of the normalised flux due to the accumulation of biomass in the network. However, for $k_2 = 10^{-6}\,[1/s]$ the detachment of biofilm dominates over biofilm growth and the initial distribution of biomass is removed during the first stage. Therefore, in this case no biofilm develops in the medium and there will be no changes in the permeability and porosity of the network. This implies that $Q_n = 1$ at all times. If the biofilm detachment rate is smaller, the development of biofilm attached to the walls of the pores leads to a reduction in the radius available for the water flow and consequently biofilm growth leads to a reduction of the normalised flux of the network. We observe very similar behaviour for the detachment rate $k_2 = 10^{-7}\,[1/s]$ and $k_2 = 0\,[1/s]$.

In Figure 2.7 the average of the fraction of biofilm volume is presented for $k_2 = 10^{-7}\,[1/s]$ and $k_2 = 0\,[1/s]$. The fraction of volume of biofilm in the network is given by $V_{pbf} = \frac{\sum_{ij} V_{bf_{ij}}}{\sum_{ij} V_{T_{ij}}}$. The sum is taken over all the tubes in the network. Since we neglect the volume of the nodes, the volume of the tubes corresponds to the volume of the pore space. We observe that during the first minutes the volume of biofilm in the network increases monotonically for the two cases. Further, after approximately 300 min the biomass growth reaches a steady state. We observe that approximately 32% of the void space of the network is occupied by volume of biomass at the steady state for both cases.

Finally, in addition to the full model which considers the transport of nutrients and the biofilm growth as two coupled phenomena, two quasi-steady state models of biofilm growth are also considered in this work. In these models we set an amount of volume of biofilm in the network, then we compute the effect of the volume of biofilm in the radius available for water and finally we compute the flux through the network. Note that the transport-diffusion equation is not solved in these models.

In the first model we consider that initially biofilm is present in all the tubes of the network and that the biofilm grows at the same rate in all the tubes. Therefore we refer to this model as uniform biofilm growth.

In the second model we hypothesise that each tube in the network could either be completely filled with biofilm or completely empty. We vary the percentage of tubes filled with biofilm from 1% of the tubes to 100% of the tubes. In each stage, the tubes filled with biofilm are chosen randomly. We refer to this model as random biofilm growth. We perform 10 simulations and we determine the average flux in the outlet of the network. We found that the variance of the result was very small. We compare the results of the full biofilm growth model with the uniform growth, with the random growth and with the Kozeny-Carman relation. The Kozeny-Carman is a well-known equation that provides a relation between the porosity ϕ and the permeability K and it is given by the

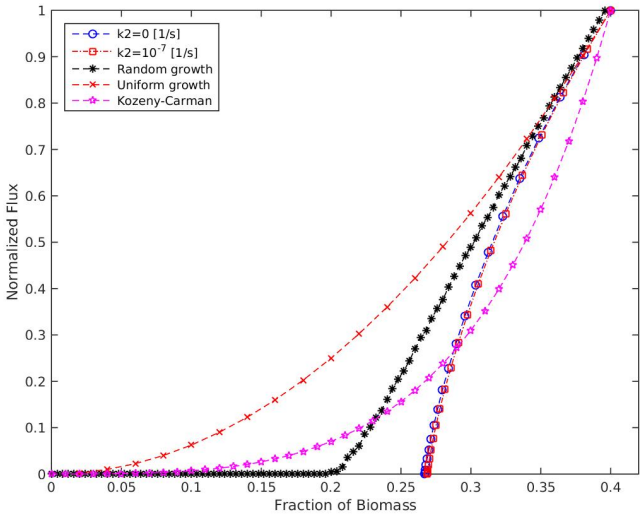

Figure 2.8: Compariosn of the normalised flux vs porosity for the full model, the random growth model, the uniform growth model and the Kozeny-Carman relation

following equation,

$$K = C_k \frac{\phi^3}{(1-\phi)^2}, \tag{2.31}$$

in which C_k is a parameter related to the specific internal surface area of the pores in a porous media.

In order to be able to compare the full model with the uniform growth model, with the random growth and with the Kozeny-Carman equation, we have to express the volume of biofilm in terms of porosity and the normalised flux in terms of the permeability. The relation between the fraction of biomass and porosity is given by the following equation,

$$V_{pbf} = 1 - \frac{\phi}{\phi_0}, \tag{2.32}$$

in which ϕ_0 is the initial porosity.

The relation between the normalised flux Q_n and the permeability is determined by the Darcy's Law,

$$K = \frac{QL\mu}{\Delta P A_n}. \tag{2.33}$$

If the pressure drop ΔP, the cross-sectional area of the network A_n, the length in the flux direction L and the viscosity μ are constant during the process of biofilm growth, we have that

$$\frac{K}{K_0} = \frac{Q}{Q_0}. \tag{2.34}$$

In which K_0 is the initial permeability. Then, using equation (2.31) and equation (2.34) we can write the normalised flux predicted by Kozeny-Carman as follows,

$$\frac{Q}{Q_0} = \frac{(1-\phi_0)^2\phi^3}{\phi_0^3(1-\phi)^2}. \tag{2.35}$$

Note that in order to derive equation (2.35) the parameter C_k has been taken constant. However, since the porous medium channels are changed by the non-uniform accumulation of biomass, the assumption of taking C_k constant is probably inappropriate. Hence, our results may deviate from the results predicted by the Kozeny-Carman model.

In Figure 2.8 the numerical results for the porosity ϕ versus the normalised flux are shown for the two different detachment rates studied in this work $k_2 = 10^{-7}\,[1/s]$ and $k_2 = 0\,[1/s]$, the two cases of quasi-steady-state biofilm growth models and the Kozeny-Carman relation (equation (2.35)).

The uniform growth model and the full model overlap from the initial porosity to 0.35 approximately where a sudden decrease in the normalised flux is described in the full-model for $k_2 = 0\,[1/s]$ and $k_2 = 10^{-7}\,[1/s]$. This is explained as follows: in the beginning in the full model, the biomass starts spreading through the network and since the thickness of the biomass in the tubes is still small, the influence of the biomass on the permeability is insignificant at this stage. However, since the nutrients are transported through the network and the biomass is spread continuously, uniform biofilm growth is stimulated in the network, causing a decrease in the permeability due to the accumulation of biomass. Afterwards, the nutrients are consumed by the bacteria and the biofilm starts growing and clogging the pores, therefore there is a reduction of the flux of the nutrients in the whole network. Hence, the nutrients are present preferentially near the inlet which causes a preferential growth of biofilm near the inlet and at the final stage causes the total decrease of the flux. The random growth model shows a linear decay of the normalised flux. For high porosity the slope of the decay of the normalised flux predicted by the random growth model is similar to the slope of the normalised flux predicted by the full model. The linear behaviour of the random growth model deviates from the full model for lower porosity. The random biofilm growth predicts a plugging of the network when the porosity is about 0.2. The porosity is approximately half the initial porosity, which is in accordance with the percolation threshold for a rectangular network, ([36]). The fact that the full model stays in accordance with the uniform growth model seems to indicate that at the beginning the time evolution of the flux is predominantly determined by the localized growth kinetics of the biofilm, rather than the kinetics of spreading over the network. Finally, the Kozeny-Carman relation shows a behaviour that is similar to the uniform biofilm growth, but the decrease of the normalised flux with the decrease in porosity is faster than the uniform growth.

2.5. CONCLUSIONS AND OUTLOOK

In this work, we simulate biofilm growth, in particular its effects on the porous medium characteristics such as porosity and permeability. We use a two-dimensional pore network model to represent the porous medium. We develop a new model for biofilm

growth, which predicts that the nutrients are not able to penetrate fully in the biofilm if the reaction term is dominant over the diffusion of nutrients within the biofilm. In addition, our model is able to simulate the spreading of the biofilm through the whole network which is a phenomenon that has been observed experimentally ([22]). The proposed model shows that at early stages biofilm growth is mostly uniform through the whole network, however eventually the biofilm will grow preferentially near the inlet of the network, plugging the pores at the inlet and causing a cease of the flux through the network. The modifications in porosity and permeability caused by biofilm growth might be beneficial for a Microbial enhanced oil recovery technique, especially in the first stage before the plugging of the network. Since we see that uniform growth provides a relatively good correspondence with the full model for high porosity, we conclude that the clogging of the porous medium in high permeability layers is feasible without blocking the inlet. For this reason, we propose to stop injection of nutrients in order to avoid plugging the medium. This behaviour is not described by the uniform growth model, the random growth nor the Kozeny-Carman relation.

Since we consider a 2D rectangular pore network model consisting of cylindrical tubes with the same radii, this model could be too simplified to describe a real reservoir field. Interesting further research is to find the representative elementary volume in order to upscale these results to the macroscale. In addition, future plans entail the study of the effects of biofilm growth in porosity and permeability in more complex topologies in 2D and 3D.

REFERENCES

[1] L. R. Brown, *Microbial enhanced oil recovery (meor),* Current opinion in Microbiology **13**, 316 (2010).

[2] R. T. Armstrong and D. Wildenschild, *Investigating the pore-scale mechanisms of microbial enhanced oil recovery,* Journal of Petroleum Science and Engineering **94**, 155 (2012).

[3] I. Lazar, I. Petrisor, and T. Yen, *Microbial enhanced oil recovery (meor),* Petroleum Science and Technology **25**, 1353 (2007).

[4] R. Sen, *Biotechnology in petroleum recovery: the microbial eor,* Progress in energy and combustion Science **34**, 714 (2008).

[5] B. Chen-Charpentier, *Numerical simulation of biofilm growth in porous media,* Journal of computational and applied mathematics **103**, 55 (1999).

[6] T. Clement, B. Hooker, and R. Skeen, *Macroscopic models for predicting changes in saturated porous media properties caused by microbial growth,* Groundwater **34**, 934 (1996).

[7] C. Ezeuko, A. Sen, A. Grigoryan, and I. Gates, *Pore-network modeling of biofilm evolution in porous media,* Biotechnology and bioengineering **108**, 2413 (2011).

[8] D.-S. Kim and H. S. Fogler, *Biomass evolution in porous media and its effects on permeability under starvation conditions,* Biotechnology and Bioengineering **69**, 47 (2000).

[9] C.-Z. Qin and S. M. Hassanizadeh, *Pore-network modeling of solute transport and biofilm growth in porous media,* Transport in Porous Media **110**, 345 (2015).

[10] C. Picioreanu, J.-U. Kreft, and M. C. Van Loosdrecht, *Particle-based multidimensional multispecies biofilm model,* Applied and environmental microbiology **70**, 3024 (2004).

[11] M. Thullner, *Comparison of bioclogging effects in saturated porous media within one-and two-dimensional flow systems,* Ecological Engineering **36**, 176 (2010).

[12] R. Samsó, J. García, P. Molle, and N. Forquet, *Modelling bioclogging in variably saturated porous media and the interactions between surface/subsurface flows: Application to constructed wetlands,* Journal of environmental management **165**, 271 (2016).

[13] Y. Tang, A. J. Valocchi, and C. J. Werth, *A hybrid pore-scale and continuum-scale model for solute diffusion, reaction, and biofilm development in porous media,* Water Resources Research **51**, 1846 (2015).

[14] W. Van Wijngaarden, F. Vermolen, G. Van Meurs, and C. Vuik, *A mathematical model and analytical solution for the fixation of bacteria in biogrout,* Transport in porous media **92**, 847 (2012).

[15] T. Pintelon, D. Graf von der Schulenburg, and M. Johns, *Towards optimum permeability reduction in porous media using biofilm growth simulations,* Biotechnology and Bioengineering **103**, 767 (2009).

[16] D. G. von der Schulenburg, T. Pintelon, C. Picioreanu, M. Van Loosdrecht, and M. Johns, *Three-dimensional simulations of biofilm growth in porous media,* AIChE Journal **55**, 494 (2009).

[17] R. Rosenzweig, A. Furman, C. Dosoretz, and U. Shavit, *Modeling biofilm dynamics and hydraulic properties in variably saturated soils using a channel network model,* Water Resources Research **50**, 5678 (2014).

[18] B. J. Suchomel, B. M. Chen, and M. B. Allen, *Macroscale properties of porous media from a network model of biofilm processes,* Transport in porous media **31**, 39 (1998).

[19] M. Thullner, J. Zeyer, and W. Kinzelbach, *Influence of microbial growth on hydraulic properties of pore networks,* Transport in porous media **49**, 99 (2002).

[20] A. B. Cunningham, W. G. Characklis, F. Abedeen, and D. Crawford, *Influence of biofilm accumulation on porous media hydrodynamics,* Environmental science & technology **25**, 1305 (1991).

[21] S. W. Taylor and P. R. Jaffé, *Biofilm growth and the related changes in the physical properties of a porous medium: 3. dispersivity and model verification,* Water resources research **26**, 2171 (1990).

[22] M. Peszynska, A. Trykozko, G. Iltis, S. Schlueter, and D. Wildenschild, *Biofilm growth in porous media: Experiments, computational modeling at the porescale, and upscaling,* Advances in water resources **95**, 288 (2016).

[23] K. Seki and T. Miyazaki, *A mathematical model for biological clogging of uniform porous media,* Water resources research **37**, 2995 (2001).

[24] S. Ye, Y. Zhang, and B. E. Sleep, *Distribution of biofilm thickness in porous media and implications for permeability models,* Hydrogeology journal **23**, 1695 (2015).

[25] Q. Xiong, T. G. Baychev, and A. P. Jivkov, *Review of pore network modelling of porous media: experimental characterisations, network constructions and applications to reactive transport,* Journal of contaminant hydrology **192**, 101 (2016).

[26] A. Raoof and S. Hassanizadeh, *A new formulation for pore-network modeling of two-phase flow,* Water Resources Research **48** (2012).

[27] J.-Y. Arns, V. Robins, A. P. Sheppard, R. M. Sok, W. V. Pinczewski, and M. A. Knackstedt, *Effect of network topology on relative permeability,* Transport in Porous media **55**, 21 (2004).

[28] H. Horn and S. Lackner, *Modeling of biofilm systems: a review,* in *Productive Biofilms* (Springer, 2014) pp. 53–76.

[29] P. S. Stewart, *Diffusion in biofilms,* Journal of bacteriology **185**, 1485 (2003).

[30] M. Thullner and P. Baveye, *Computational pore network modeling of the influence of biofilm permeability on bioclogging in porous media,* Biotechnology and Bioengineering **99**, 1337 (2008).

[31] A. Cortis and B. Berkowitz, *Computing "anomalous" contaminant transport in porous media: The ctrw matlab toolbox,* Groundwater **43**, 947 (2005).

[32] A. W. Warrick, *Soil water dynamics* (Oxford University Press, 2003).

[33] J. Lawrence, G. Wolfaardt, and D. Korber, *Determination of diffusion coefficients in biofilms by confocal laser microscopy,* Applied and environmental microbiology **60**, 1166 (1994).

[34] K. S. Ro and J. Neethling, *Biofilm density for biological fluidized beds,* Research journal of the water pollution control federation , 815 (1991).

[35] R. Bakke, M. G. Trulear, J. Robinson, and W. G. Characklis, *Activity of pseudomonas aeruginosa in biofilms: steady state,* Biotechnology and bioengineering **26**, 1418 (1984).

[36] H. Kesten, *The critical probability of bond percolation on the square lattice equals 1/2,* Communications in mathematical physics **74**, 41 (1980).

3

CONDITIONS FOR UPSCALABILITY OF BIOCLOGGING IN PORE NETWORK MODELS

In order to have a reliable description of MEOR processes at the field scale a proper up-scaling technique of the effects of biofilm growth on porosity and permeability on the micro-scale is needed. In some previous continuous biofilm growth models homogeneous biofilm growth is assumed and the effects of heterogeneous biofilm growth are neglected (Taylor et al. 1990). In general using the upscaling processes an equivalent permeability is obtained via average volume, homogenisation or statistical methods. However it is not clear whether the assumption of homogeneity is justified.

In this chapter, we obtain a homogeneous upscalable biofilm growth model and we determine the physical conditions when this model applies. We study the influence of physical parameters like the size of the network and the inlet concentration of nutrients on the permeability-porosity relation and we also study the influence of numerical parameters like the number of nodes on this relation.

In Section 3.1 we present the state of the art of biofilm growth models and up-scaling techniques. In Section 3.2 we mention the equations that describe the biofilm growth and transport of nutrients and we describe the numerical method to solve these equations. After this in Section 3.3 we present the conditions for uniform biofilm growth and hence up-scalability of bioclogging in pore network models. We use the Damköhler number to determine whether up-scalability is applicable. Finally we draw some conclusions in Section 3.4.

3.1. INTRODUCTION

In primary oil production a wellbore is drilled from the surface to the ground and oil is extracted from the reservoir by natural mechanisms such as the internal pressure of the reservoir. When the initial production declines secondary oil recovery techniques

such as waterflooding or gas injection are implemented. However, two-thirds of the oil is still trapped in the ground even after primary and secondary recovery [1]. Microbial Enhanced Oil Recovery (MEOR) is a tertiary oil recovery technique which aims at increasing the mobility of the remaining oil using the growth of bacteria and the resulting by-products. Bacterial growth enhances oil recovery by increasing the efficiency of the waterflooding process, by clogging highly permeable layers such that the flow through the oil-containing regions with low permeability is enhanced. Furthermore, bacterial growth reduces interfacial tension and changes the rock wettability [2, 3] which enhances oil mobility.

The development of computational models is of vital importance to design a proper field strategy for MEOR in oil reservoirs. These models describe bacterial growth and predict the changes in the characteristics of the porous media like the permeability and porosity [4]. Among bacterial growth models in porous media there are the Darcy continuum models [5, 6], bacterially-based models [7], Lattice Boltzmann based simulations [8, 9] and Pore Network Models (PNM) [10–16]. The secretion of extracellular polymeric substances (EPS) by bacterial population causes the formation and growth of biofilm on the walls of the porous media. In biofilm growth models it is usually assumed that the porous medium consists of three components: the grains, the biofilm and the fluid which contains the nutrients needed for the biofilm growth. The equations that describe biofilm growth are written only for the fluid and biofilm since the grains are assumed to be impermeable to the liquid and the nutrients [8].

Cunningham et al. [17] studied experimentally the effect of biofilm growth on the porosity, permeability and friction factor of the porous medium. They reported a decrease in the porosity between 50% and 96% and a decrease in permeability between 92% and 98% due to the accumulation of biofilm. In the continuum scale Taylor et al. [18] obtained an analytic expression that describes the relation between porosity and permeability. However, they assumed that the biofilm grows uniformly through the domain of computation which not always occurred according to laboratory experiments [19]. Therefore, micro-scale biofilm growth models such as Pore Network Models (PNM) and pore-scale models are used to describe a non-uniform biofilm growth [11, 20]. It is needed to state the conditions such that the biofilm grows uniformly.

In PNMs the porous medium is usually represented as a two or three-dimensional lattice of cylindrical interconnected tubes in which water or any fluid can flow [21]. The biofilm development is caused by the injection of nutrients into the network which are transported within an aqueous phase. The injection and consumption of nutrients are described by a convection-diffusion-reaction equation in which the reaction term models the consumption of nutrients caused by bacteria which results in biofilm growth. The biofilm grows and it adheres to the walls of the cylinders. Thereby the biofilm changes the radii of the pores, which consequently leads to porosity and permeability reduction [10, 14, 15].

Even though the bacterial population and the EPS are two different phases, they are usually lumped together and are represented as a continuous uniform layer of biomass attached to the walls of pores [11, 14, 15]. This uniform layer of biomass is referred to as biofilm.

Biofilm growth models at the micro-scale are needed to account for heterogeneities

in the biofilm growth, which are typically ignored in large-scale models. In PNMs the information obtained at micro-scale is averaged over the network to get a macroscopic description at the continuum scale [22]. The influence of network characteristics such as the coordination number on macroscopic transport phenomenon has been shown in [23]. They showed that the dispersivity decreases if the coordination number increases.

In general the purpose of upscaling is to get an effective description on a macro level when there exists a good description on a small scale level [24]. Hese et al. [24] use upscaling methods to obtain an effective one dimensional representation based on a system of two dimensional partial differential equations. Their study is focused on the scaling behaviour of Monod-type reaction kinetics. They showed that the upscaled description of Monod kinetics leads to a concentration dependent transition between a reaction and a diffusion limited regime. Wu et al. [25] computed the upscaled grid-block permeability from fine-scale solutions of the flow equation. They studied the upscaling of single phase flows through media with a periodic small amount of heterogeneity. They claim that their results are also useful for the understanding of the upscaling of random media. The equivalent permeability is a constant permeability that represents a heterogeneous medium. However, it is impossible to obtain a one-to-one mapping as a complete mapping between the real heterogeneous medium and the homogeneous upscaled medium. Therefore the equivalence, that is the one-to-one mapping, is defined in a limited sense [26]. Battiato and Tartakovsky [27] studied the transport of a solute in a porous medium which is subjected to a nonlinear heterogeneous reaction. This solute precipitates on the solid matrix to form a crystalline solid. They investigated the sufficient conditions under which the macroscopic advection-dispersion-reaction equations provide an accurate description of the pore-scale processes. Despite their relevant findings they did not consider any change on the morphology of the porous medium. In the present study we investigate under which conditions we can upscale a small-scale heterogeneous medium to a large-scale homogeneous medium, in which we can apply models for uniform growth.

In this work we study the effects of biofilm growth on the porosity and permeability of the network. We use the model for biofilm growth described in [28], which models incomplete transmigration of nutrients through the biofilm as a result of high bacterial consumption rate and a low diffusion rate of the nutrients. In particular we study the process of bioclogging which features inhibition of the flux through the network due to biofilm growth. We compute the amount of biomass per volume needed to block the network for different number of nodes in the network, different network sizes and different inlet concentrations of nutrients in the network. Furthermore, we describe the conditions for uniformity and upscalability of the pore network biofilm growth model.

As long as the medium, in this case the pore network model, is evolving in a spatially homogeneous manner, upscaling can be performed on the basis of computing an effective porosity and permeability. In the current paper, however, we are dealing with the injection of nutrients on the inlet boundary. The nutrients are being consumed by the bacteria in the porous medium and thereby, effectively, converted into biomass that clogs the network tubes. If the concentration of the nutrients at the inlet boundary is not sufficiently high, then, the nutrients will all be consumed and converted before they are able to reach the regions in the domain that are further away from the inlet. If this hap-

pens in the current network, then the network cannot be used for upscaling purposes in which one determines the effective permeability and porosity relation. The current paper will address this issue in terms of derivation of a relation between permeability and porosity. For upscalable conditions we will derive a tractable, functional relation between the effective porosity and permeability of the network, which can be used as an alternative relation to standard Kozeny-Carman relation. We will analyse the applicability of such a relation by varying the characteristics of the pore network. The current network provides a more computational approach to classical upscaling that is carried in more mathematical rigour.

The chapter is organised as follows. In Section 3.2 we describe the equations for the transport of nutrients and the model used for the biofilm growth. In Section 3.3 we describe the effects of biofilm growth on porosity and permeability when we vary the number of nodes in the network, the network size and the inlet concentration of nutrients. Finally, in Section 3.4 we present the discussion, draw the conclusions and present the outlook.

3.2. MATHEMATICAL MODEL

In this section we present the equations that describe the transport of nutrients and the biofilm growth in the porous medium. Firstly, the porous medium is represented as a 2D rectangular network composed of interconnected cylindrical tubes whose radii and length are the same.

We assume that the bacteria and biofilm are lumped together and hence we refer to them as a single phase: biofilm. The growth of biofilm is initiated by the nutrients which are injected into the network and transported within a fluid phase. The thickness of the biofilm in the tube t_{ij} is represented by $r_{b_{ij}}$, the radius available for water by $r_{w_{ij}}$ and the total radius of the tube by R (see Figure 3.1). The volumetric flow of the aqueous phase q_{ij} in the tube t_{ij} is described by a modified form of the Poiseuille equation [29],

$$q_{ij} = \frac{\pi}{8\mu l}[r_{w_{ij}}^4 + (R^4 - r_{w_{ij}}^4)\beta^{-1}]\Delta p, \tag{3.1}$$

where Δp is the pressure drop between neighbouring nodes, μ is the viscosity of water that flows in the bulk, l is the length of the tube and the dimensionless number β is the ratio between the viscosity of water flowing through the biofilm and the viscosity of water flowing through the bulk. We use $\beta = 10^7$ which according to [29] is a good approximation for an impermeable biofilm.

In each of the nodes mass conservation is required. Therefore, for the node n_i we have

$$\sum_{j \in S_i} q_{ij} = 0, \tag{3.2}$$

where $S_i = \{j \mid n_j \text{ is adjacent to the node } n_i\}$ and where q_{ij} is the flux through the tube that connects node n_j to node n_i.

The transport of nutrients is described by an advection-diffusion-reaction equation. The concentration of nutrients is denoted by C,

$$\frac{\partial C}{\partial t} + \mathbf{u}\cdot\nabla C - D\nabla^2 C = -\frac{\partial b^+}{\partial t}, \tag{3.3}$$

where D is the diffusion coefficient of nutrients through water and $\mathbf{u}$ is the advection velocity which is related to the local flux $\mathbf{q}$ by $\mathbf{u} = \mathbf{q}/A$, where A is the area of the cross-section of the tube. Additionally, b^+ is the concentration of the biofilm produced as a result of the consumption of nutrients (no detachment of biofilm is taken into account in this term). The concentration of biofilm b is related to the volume of biofilm by,

$$b = \frac{\rho}{V_T} V_{bf}, \tag{3.4}$$

where ρ denotes the mass density of biofilm V_T, the total volume of the tube and V_{bf} the volume of biofilm.

The numerical method is based on finite differences and Euler time integration methods. More details about the numerical procedure can be found in [28].

The equation for the transport of nutrients is solved for the concentration C_i at each node of the network. The advection part is solved using first order upwind scheme and a time-implicit method for the time integration. Hence, the discretization of the advection part reads as,

$$\left[\frac{\Delta C_i}{\Delta t}\right]_{adv} \approx \sum_{j\in\Omega_i} \frac{{q_{ij}}^{\tau}}{V_T}({C_j}^{\tau+1} - {C_i}^{\tau+1}), \tag{3.5}$$

where $\Omega_i = \{j \mid q_{ij} \text{ is directed towards the node } n_i\}$.

The diffusion part is discretized using a time implicit method for the concentration. However the area used is from the previous time step,

$$\left[\frac{\Delta C_i}{\Delta t}\right]_{diff} \approx \frac{D_w}{l^2} \sum_{j\in S_i} ({C_i}^{\tau+1} - {C_j}^{\tau+1}) \frac{A^{\tau}_{w_{ij}}}{A_{tot_{ij}}}. \tag{3.6}$$

The reaction rate is described in the following paragraphs. In this work we use the model for the biofilm growth reported in [28]. Since the reaction rate of nutrients is higher than the diffusion rate within the biofilm, it is assumed that nutrients interact with the biofilm only in a thin layer adjacent to the water biofilm interface, Γ_p. This layer defines implicitly a volume which is called the penetration volume of the nutrients $V_p \approx 2\pi R\Gamma_p l$, and it is assumed to be constant during the whole process of biofilm growth. In general in each of the tubes, there are two different water biofilm interfaces. Therefore, we consider two modes of biofilm growth: internal biofilm growth and biofilm growth at the extremes of the tube. The interior biofilm growth takes place within the tube and is described as follows. If the volume of biofilm is smaller than the penetration volume V_p, the nutrients are present in the whole biofilm volume and hence the biofilm growth rate is proportional to the volume of biofilm (see Figure 3.1 (c) (b)). However, if the biofilm volume is much larger than the penetration volume, the nutrients are consumed only within this volume and the biofilm growth rate is proportional to the area between water and biofilm interface (see Figure 3.1 (c))

The biofilm interior growth rate in the tube t_{ij} , $V^i_{bf_{ij}}$ can be written as,

$$\frac{\partial V^i_{bf_{ij}}}{\partial t} = k_1 \frac{A^i_{wbf}}{A^i_T} V_p \frac{C_{ij}}{E_s + C_{ij}} f(V_{bf_{ij}}). \tag{3.7}$$

In this equation, $f(V_{bf_{ij}}) \geq 0$ is a sigmoid-like function for $V_{bf_{ij}}$ that depends on the penetration volume V_p. Further, $A^i_{wbf} = 2\pi r_w l$ is the internal interfacial area between water and biofilm, C_{ij} is the concentration of nutrients within the tube, E_s is a saturation constant, k_1 is a growth rate constant and $A^i_T = 2\pi R l$ is the external area of the tube. The ratio between the interior interfacial water biofilm area A^i_{wbf} and the external area of the tube A^i_T is a measure of the biofilm growth within the tube. If this ratio is zero then there is no biofilm in the tube or the tube is full with biofilm. This means that if the tube is entirely filled with biofilm, then, interior growth stops since there is no more space in the tube. The sigmoid-like function is defined as,

$$f(V_{bf}) = \frac{\frac{V_{bf}}{V_p}}{1 + \frac{V_{bf}}{V_p}}. \tag{3.8}$$

If $\frac{V_{bf}}{V_p} < 1$, the sigmoid-like function f tends to $\frac{V_{bf}}{V_p}$ and since $A_{wbf} \sim A^i_T$ the biofilm growth rate $\frac{\partial V^i_{bf_{ij}}}{\partial t} \sim V_{bf}$. On the other hand, if the the ratio $\frac{V_{bf}}{V_p}$ is large, the sigmoid-like function $f \sim 1$ and then the biofilm growth rate $\frac{\partial V^i_{bf_{ij}}}{\partial t} \sim A_{wbf}$.

Note that the function $\tilde{f} = V_p f(V_{bf_{ij}})$ is an increasing function of V_p. This means that if V_p increases the biofilm growth rate increases.

We write the area A^i_{wbf} in terms of the total volume of the pore V_T and the volume of biofilm V_{bf}, which gives,

$$\frac{\partial V^i_{bf_{ij}}}{\partial t} = k_1 R \frac{V_p}{V_T} \frac{C_{ij}}{E_s + Cij} \sqrt{\pi l (V_T - V_{bf_{ij}})} f(V_{b_{ij}}). \tag{3.9}$$

If there is no initial biofilm in the tube, the interfacial area between water and biofilm area is zero, therefore there is no biofilm growth in the interior of the tube.

Note that equation (3.9) represents a continuous relation between the biomass growth rate and the volume of biofilm $V^i_{bf_{ij}}$.

Secondly, we describe the biofilm that grows in the extremes of the tube. Since the penetration layer in the extremes is very small compared to the whole volume of biofilm, the biofilm growth rate is approximately proportional to the interfacial area between water and biofilm in the extremes A^e_{wbf} (see Figure 3.2). We assume only interactions between nearest neighbouring tubes. The interfacial area between water and biofilm A^e_{wbf} between the tube t_{ij} and the tube t_{jk} can be written in terms of the difference between volumes of biofilm of these neighbouring tubes. If the volume of biofilm $V_{bf_{jk}}$ in the tube t_{jk} (connected to the node n_j) is larger than the volume of biofilm $V_{bf_{ij}}$ in the tube t_{ij}, then the biofilm grows in the extreme of the tube t_{jk} and it is given to the

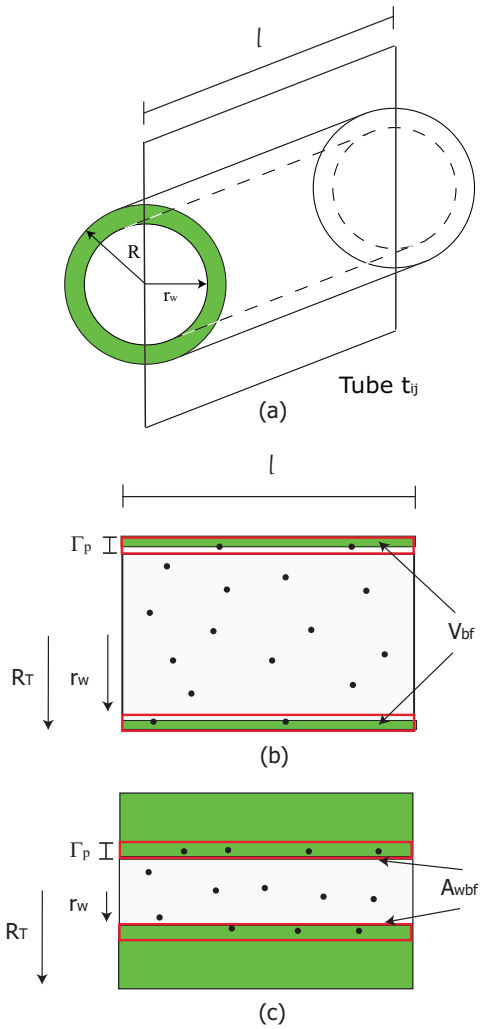

Figure 3.1: In Figure (a) a cylindrical tube t_{ij} is shown. Figure (b) and (c) show the side view of the tube t_{ij}. The volume of biofilm V_{bf} is shown in green and the penetration volume V_p is shown in red. In Figure (a) $V_{bf} < V_p$. In Figure (b) $V_{bf} > V_p$

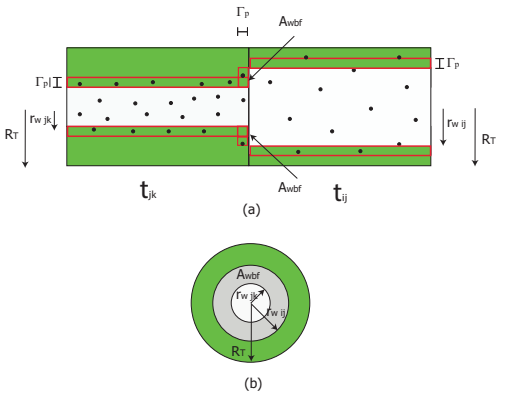

Figure 3.2: Biofilm growth in the interior and in the extremes of the tube. In Figure (a) the side view of two neighbouring tubes is shown. In Figure (b) the cross section of the boundary between the neighbouring tubes t_{jk} and t_{ij} is shown. The biofilm growth rate from t_{jk} to t_{ij} is proportional to A^e_{wbf}

neighbouring tube t_{ij}. The biofilm growth in the extreme of the neighbouring tube t_{jk} is given by

$$\frac{\partial V^e_{bf_{jk}}}{\partial t} = k_1 \frac{A^e_{wbf}}{A^e_T} V_T \frac{C_{jk}}{E_s + C_{jk}}. \tag{3.10}$$

Here, A^e_T is the cross-sectional area in the extreme of the tube. The ratio between the external interfacial water biofilm area A^e_{wbf} and the cross-sectional area of the tube A^e_T is a measure of the biofilm growth in the extremes of the tube. This ratio is zero if the volume of biofilm is the same in both interacting tubes which means there is no biofilm growth in the extreme of the tube and hence no volume of biofilm is added to either of them. On the other hand, when this ratio is one, the biofilm grows at a maximal rate and the accumulated biofilm is added to the tube t_{ij}. Note that there is no biomass exchange between neighbouring tubes; the biomass is produced in the extreme of the tube and it is given to the neighbouring one, hence no biomass is lost in the tube. In this way, this model for the biofilm growth allows the spreading of the biofilm through the whole network which is consistent with experimental observations. The area A^e_{wbf} between the tube t_{ij} and the tube t_{jk} can be written in terms of the volume of the biofilm of the tubes. Hence the equation for the biofilm growth at the extreme of the tube t_{jk} reads as

$$\frac{\partial V^e_{bf_{jk}}}{\partial t} = k_1 \frac{V_p}{V_T} \frac{C_{jk}}{E_s + C_{jk}} (V_{bf_{jk}} - V_{bf_{ij}}) \tag{3.11}$$

We take into account all the neighbouring tubes whose volumes of biofilm are larger than the volume of biofilm in the tube t_{ij}. To this extent we introduce the following index set notation for the tube t_{ij} which connects nodes n_i and n_j. Consider node n_j then we define the set of neighbouring nodes of it, except n_i by Λ_{ji}. Therefore, the equation for the biofilm growth in the tube t_{ij} due to biofilm growth in the extremes of the

neighbouring tubes is written as

$$\begin{aligned}\frac{\partial V^e_{bf_{ij}}}{\partial t} &= k_1 \frac{V_p}{V_T} \sum_{k\in\Lambda_{ji}} \frac{C_{jk}}{E_s + C_{jk}} (V_{bf_{jk}} - V_{bf_{ij}})_+ \\ &+ k_1 \frac{V_p}{V_T} \sum_{k\in\Lambda_{ij}} \frac{C_{ki}}{E_s + C_{ki}} (V_{bf_{ki}} - V_{bf_{ij}})_+,\end{aligned} \tag{3.12}$$

where $(V_{bf_{ki}} - V_{bf_{ij}})_+ = \max(0, V_{bf_{ki}} - V_{bf_{ij}})$.

We assume that the detachment of biomass is proportional to the area of the interface between water and biofilm, hence, detachment rate can be written in terms of the volume of biofilm as

$$\frac{\partial V_{bf_{ij}}}{\partial t}_{detach} = k_2 R \sqrt{\pi l (V_T - V_{bf_{ij}})}, \tag{3.13}$$

where k_2 is the detachment rate coefficient. Finally, when we take into account the interior growth, the growth in the neighbouring tubes and the detachment of biofilm, the equation for the biofilm growth in the tube t_{ij} can be written as

$$\begin{aligned}\frac{\partial V_{bf_{ij}}}{\partial t} &= k_1 R \frac{V_p}{V_T} \frac{C_{ij}}{E_s + C_{ij}} \sqrt{\pi l (V_T - V_{bf_{ij}})} f(V_{bf_{ij}}) + k_1 \frac{V_p}{V_T} \sum_{k\in\Lambda_{ji}} \frac{C_{jk}}{E_s + C_{jk}} (V_{bf_{jk}} - V_{bf_{ij}})_+ \\ &+ k_1 \frac{V_p}{V_T} \sum_{k\in\Lambda_{ij}} \frac{C_{ki}}{E_s + C_{ki}} (V_{bf_{ki}} - V_{bf_{ij}})_+ - k_2 R \sqrt{\pi l (V_T - V_{bf_{ij}})} H(V_{bf_{ij}}).\end{aligned} \tag{3.14}$$

Further, $H(V_{bf_{ij}})$ is defined as,

$$H(V_{bf_{ij}}) = \begin{cases} 0 & \text{if } V_{bf_{ij}} = 0 \\ 1 & \text{if } V_{bf_{ij}} \geq 0. \end{cases} \tag{3.15}$$

We include the function H because detachment occurs only when there is biofilm within the tube. In case there is no biofilm in the tube, $H = 0$, which means the detachment rate is zero. In equation (3.14) the first term is the interior biofilm growth, the second and third term describe the biofilm which grows in the extremes of the neighbouring tubes and the fourth term is a term for the detachment of the biofilm.

The nutrients consumption in the tube t_{ij} is the result of the interior biofilm growth and biofilm growth in the extremes of the tube.

$$\begin{aligned}&\left[\frac{\partial b^+_{ij}}{\partial t}\right] = \\ &\frac{k_1}{Y} \frac{\rho V_p}{{V_T}^2} \frac{C_{ij}}{E_s + C_{ij}} \left[R \sqrt{\pi l (V_T - V_{bf_{ij}})} f(V_{bf_{ij}}) \right. \\ &\left. + \sum_{k\in\Lambda_{ji}} (V_{bf_{ij}} - V_{bf_{jk}})_+ + \sum_{k\in\Lambda_{ij}} (V_{bf_{ij}} - V_{bf_{ki}})_+ \right].\end{aligned} \tag{3.16}$$

where Y is the yield coefficient and $\frac{\partial V^{+}_{bf_{ij}}}{\partial t}$ is given by,

The new thickness of the biofilm is computed and it is coupled back to the flux equation (3.1) and to the mass conservation equation (3.2).

3.3. RESULTS

In this section we describe the overall mechanism of biomass growth and its implications on network characteristics such as the porosity and permeability. In addition, in order to determine the conditions for upscalability to real reservoir dimensions, we study the influence of the numerical parameter such as the number of nodes and physical parameters such as the size of the network and the inlet concentration of nutrients on the dynamics of transport of nutrients and biofilm growth. At the end we mention the requirements in terms of the Damköhler number for up-scaling this microscopic model to a continuum-scale model.

Firstly, we present the results of the transport of nutrients and the biofilm growth process in the pore network. Initially, there is a biomass concentration $b_0 = 1 \times 10^{-4}$ $[kg/m^3]$ in 4% of tubes (Figure 3.3(a)). When the biomass gets into contact with the nutrients, biofilm starts growing and spreading to the neighbouring tubes (Figure 3.3 (b) and Figure 3.3 (c)). Due to a high injection rate, the nutrients are distributed over the whole network shortly after the beginning of the process. Therefore biofilm grows uniformly through the network and hence the nutrients are consumed (Figure 3.3 (d)). After several minutes depletion of nutrients near the outlet of the network is observed. This is because the consumption of nutrients by the bacteria near the inlet is very high, most nutrients are unable to reach the outlet. Hence, preferential biofilm growth is observed near the inlet (Figure 3.3 (e) and Figure 3.3 (d)) and the biofilm developed in this area causes the plugging of the network. This implies that a heterogeneous end-state is reached if the inlet concentration of nutrients is not large enough. The heterogeneous or preferential growth depends on parameters like the size of the network or the number of nodes in the network, therefore the relation among the fraction of biomass and permeability varies with these parameters and upscaling is not possible in this case. However if there is sufficient amount of nutrients, there is no depletion and the biofilm grows uniformly during the whole process. Therefore the relation between fraction of biomass does not depend on the size of the domain of computation or the number of nodes and the problem is upscalable. This scenario is not shown in the Figure 3.3.

3.3.1. VARIATION OF INPUT PARAMETERS

NUMBER OF NODES

In this first set of simulations we study the effect of the number of tubes in the network. The length in x and y direction and the initial porosity are constant for this simulations. We perform four simulations in which we use four different networks with different number of nodes (25 x 15, 50 x 30, 100 x 60 and 200 x 120). The length of the tubes decreases as the number of nodes increases. In order to keep the porosity constant throughout all four simulations, the radii of the tubes are adjusted in each of the simulations. Note that for each simulation the radius of the tubes is constant over the network. The inlet concentration for these simulations is $C_{in} = 1[kg/m^3]$. The value of

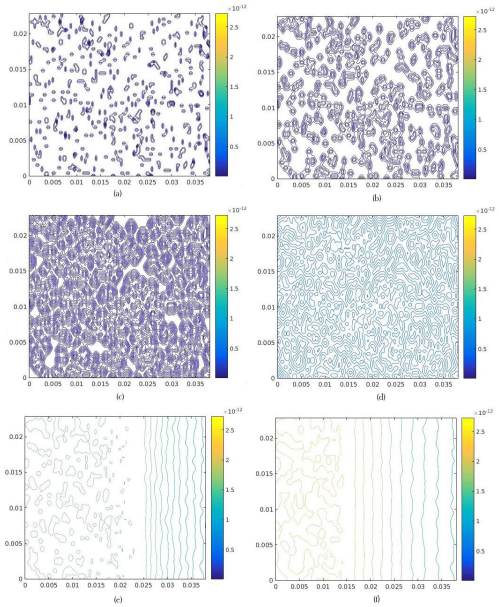

Figure 3.3: Contour plot of the biofilm growth for different times. Figure (a), $t = 0$ [min]; Figure (b), $t = 2$[min], Figure (c), $t = 4$ [min], Figure (d), $t = 35$ [min], Figure (e), $t = 120$ [min]; Figure (f), $t = 174$ [min]

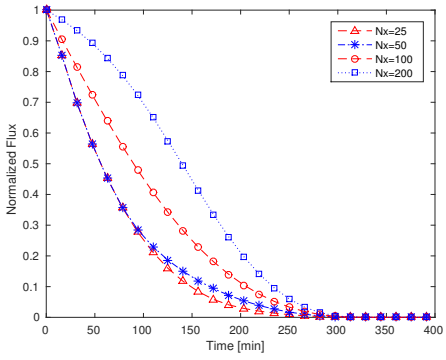

Figure 3.4: The normalised flux for different number of nodes for a rectangular network

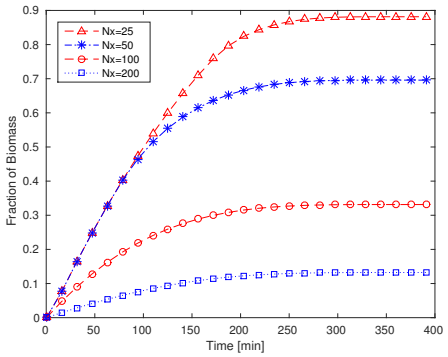

Figure 3.5: The fraction of biomass for different number of nodes for a rectangular network

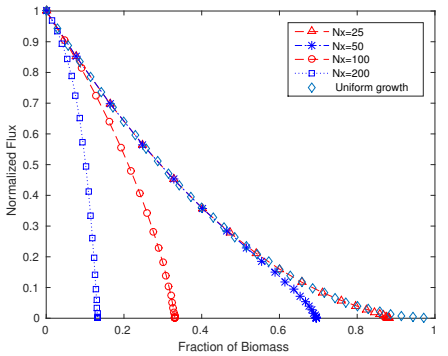

Figure 3.6: The fraction of biomass vs the normalised flux for different number of nodes for a rectangular network

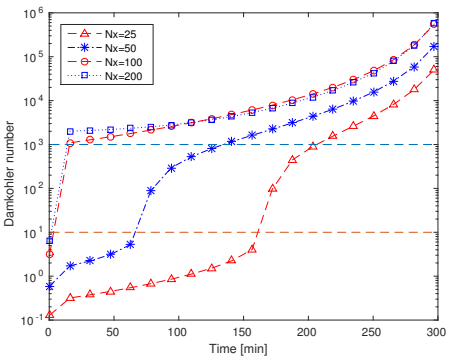

Figure 3.7: The Damköhler number for different number of nodes for a rectangular network

the radii and the length of the tubes for this set of simulations are shown in Table 3.1. The complete list of parameters is shown in Table 3.2. The normalised flux Q_n is defined as, $Q_n = \frac{Q}{Q_0}$, where Q_0 is the initial flux in the network (i.e. before biofilm growth). The evolution of the normalised flux through the network for the detachment rate $k_2 = 0\,[1/s]$ is shown in Figure 3.4. We observe that there are some deviations among the curves, however the network is plugged in all the cases around 300 minutes an even an S-shape is observed for very large number of tubes. The fraction of biofilm volume in the network is given by $S_b = \frac{\sum_{ij} V_{bf_{ij}}}{\sum_{ij} V_T}$, where $V_{bf_{ij}}$ is the volume of biofilm in the tube t_{ij} and V_T is the volume of the tube t_{ij}. In Figure 3.5 we present the results obtained for the evolution of the fraction of biofilm volume in the network for $k_2 = 0\,[1/s]$. At the beginning of the process the biofilm starts growing and spreading through the network, then, the biomass grows uniformly and in the final stage a preferential growth near the inlet causes the plugging of the network.

We observe that the fraction of biomass necessary to block the network $\tilde{S_b}$ decreases as the number of nodes increases. We can explain this by drawing an analogy with the minimum fraction of biomass needed to block one column of tubes in y direction. In order to keep the same initial porosity, if the number of nodes in the x and y direction doubles then the radii of the tubes and the length reduces approximately to the half. Therefore, the volume of biomass in one column of the tubes decreases by $1/4$ when the number of nodes in the y direction doubles. The sum of the volume of all the pores in the network decreases approximately by $1/2$ when the number of nodes increases. Therefore the fraction of biomass needed to block the network decreases by a factor of $1/2$. Note that in order to keep the same porosity, the total volume of the network, $V_{nt} = L_x \times L_y \times 2R$ decreases by $1/2$ when the number of nodes increases. Hence the fraction of biomass needed to block the network decreases when the number of nodes increases. In our simulations the preferential growth is taken over more than one column, however a similar argument to explain the decrease of $\tilde{S_b}$ is valid.

In Figure 3.6 we show the normalised flux versus the fraction of biomass. We observe that if the fraction of biomass remains small then the curves coincide for the four cases, however, as the fraction of biomass increases, the curves deviate from the uniform growth and exhibit a steeper descend as the number of nodes increases.

In order to determine when the preferential growth deviates from uniform growth, and therefore when upscalability is possible we study the effects of biofilm growth on the Damköhler number, which is defined as

$$Da = \frac{Reaction\ rate}{Advective\ transport\ rate}. \tag{3.17}$$

In this case, we compute the Damköhler number related to the advective rate because the transport of nutrients is mainly determined by this process since the Peclet number is larger than 10^1 from the beginning to 250 $[min]$ approximately.

The Damköhler number for the entire network, is obtained by dividing the average of the reaction rate by the average of the advective rate,

Number of nodes in the network	Radius of the tube	Length of the tube
25×15	4.5933×10^{-5} $[m]$	3.8×10^{-4} $[m]$
50×30	2.3563×10^{-5} $[m]$	1.9×10^{-4} $[m]$
100×60	1.1937×10^{-5} $[m]$	9.5000×10^{-5} $[m]$
200×120	6.0078×10^{-6} $[m]$	4.7500×10^{-5} $[m]$

Table 3.1: Network parameters values for the first set of simulations. All configurations have the same initial porosity

Name	Symbol	Value
Global pressure gradient	ΔP	$1.6\, L_x$ $[kPa/m]$
Viscosity of water	μ	$0.001/60$ $[Pa \cdot min]$
Density of water	ρ_w	1000 $[kg/m^3]$
Density of biofilm	ρ_{bf}	20 $[kg/m^3]$ [30]
Diffusion coefficient of water	D	9×10^{-8} $[m^2/min]$ [31]
Yield coefficient	Y	0.34 [32]
Half saturation constant for biofilm	E_{sb}	2×10^{-3} $[kg/m^3]$ [32]
Initial biomass concentration	b_0	1×10^{-6} $[kg/m^3]$
Biofilm / bulk water viscosity ratio	β	10^7 [29]

Table 3.2: Physical parameters for all the simulations

$$Da = \frac{\frac{k_1 \rho}{Y} \Sigma_{ij} \frac{1}{V_T} \frac{1}{C_{ij}+E_s} G(V_{bf_{ij}})}{\frac{\Sigma_{ij} u_{ij}}{L_x}}. \tag{3.18}$$

Here the sum is taken over all the tubes in the network. In Figure 3.7 the Damköhler number for a various number of nodes in the network is shown. We plot two horizontal lines that enclosed the Damköhler number at which a transition from uniform growth to preferential growth occurred. The transition from uniform growth to preferential growth occurs at different times for different number of nodes. However the Damköhler number of the transition ranges between the two horizontal lines for all the cases. For a Damköhler number less than 10^1 the biofilm grows uniformly for all the cases. Further, for Damköhler number greater than 10^3 there is no uniform growth and upscalability is not possible.

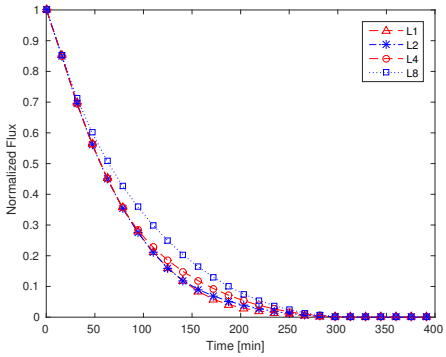

Figure 3.8: The normalised flux for different sizes of the domain of computation

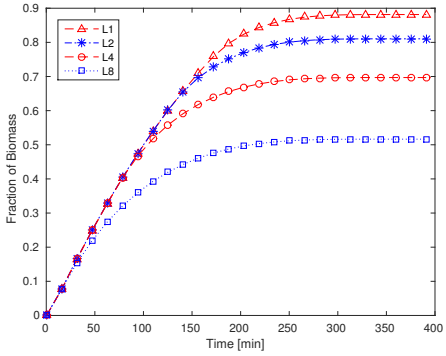

Figure 3.9: The fraction of biomass for different sizes for a rectangular network

SIZE OF THE NETWORK

In the second set of simulations we study the effect of the size of the network on the porosity and permeability. We perform four simulations with different sizes of the network. The ratio between the number of nodes in the x direction and the number of nodes in the y direction is constant. In order to keep the same initial porosity the radius increases slightly while we increase the size of the network. In Table 3.3 the size of the network and the radius for each network are shown. For each simulation the radius of the tubes is constant. In Figure 3.8, the normalised flux as a function of time for each simulation is shown. We observed that the network is plugged after 300 minutes for all the cases. In Figure 3.9 the fraction of biomass as a function of time is shown for various sizes of the computational domain. We observe that when the size of the computational domain is larger the fraction of biomass needed to block the network decreases, see Figure 3.10. Note that the total amount of biomass increases when the size of the network increases. The minimal amount of biomass required to block the network is the volume of all the tubes in one column. When we increase the size of the computational domain, the amount of tubes in one column is doubled while the total amount of tubes is four

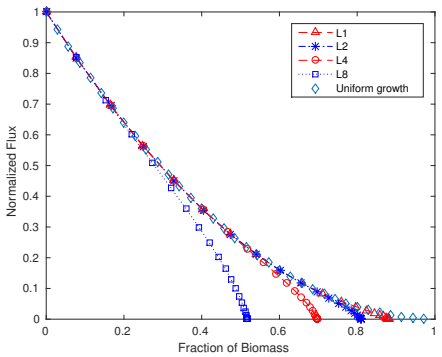

Figure 3.10: The fraction of biomass vs normalised flux for different sizes for a rectangular network

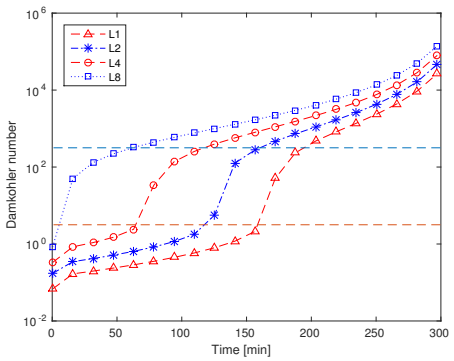

Figure 3.11: The Damköhler number for different sizes for a rectangular network

Network	Number of nodes in the network	Size of the network L_x	Size of the network L_y	Radius of the tube
L_1	25×15	9.5×10^{-3} $[m]$	5.7×10^{-3} $[m]$	4.5933×10^{-5} $[m]$
L_2	50×30	1.9×10^{-2} $[m]$	1.114×10^{-2} $[m]$	4.7126×10^{-5} $[m]$
L_4	100×60	3.8×10^{-2} $[m]$	2.28×10^{-2} $[m]$	4.7746×10^{-5} $[m]$
L_8	200×120	7.6×10^{-2} $[m]$	4.56×10^{-2} $[m]$	4.8063×10^{-6} $[m]$

Table 3.3: Network parameters values for the second set of simulations

times higher, hence the relative contribution to the volume from one column decreases when we increase the size of the network. The minimal amount of biomass to block the network tends to zero as the size of the network increases and it is lower than the percolation threshold for a rectangular network. On the other hand, there is a maximum of biofilm growth when there is uniform growth because in that case all the tubes have to be filled with biofilm in order to plug the network completely. A transition from uniform growth to preferential growth is observed as we increase the size of the network.

In Figure 3.11 the Damköhler number is shown for different sizes of the network. We observe that there is uniform growth and therefore upscalability when the Damköhler number is less than approximately 10^1. Above 10^3 there is a preferential growth and upscalability is not possible.

INLET CONCENTRATION OF NUTRIENTS

In the third set of simulations we study the effects of the inlet concentration on the biofilm growth. In this set of simulations the size of the network is 100×60 nodes and we use five different inlet concentrations, C_{in}, 1 $[kg/m^3]$, 5 $[kg/m^3]$, 10 $[kg/m^3]$, 25 $[kg/m^3]$, 50 $[kg/m^3]$. In Figure 3.12 the normalised flux is shown. We observe that the network is plugged at around 300 minutes for all the cases. In Figure 3.13 the evolution of the fraction of biomass is shown. It is shown that the biomass saturation value increases as the inlet concentration increases. When the concentration $C_{in} = 1$ the biomass saturation value is around $V_s = 0.70$ however if the inlet concentration is $C_{in} = 50$, then the fraction of biomass necessary to block the network is $V_s = 1$. Therefore when we increase the concentration, the nutrients can reach the region near the outlet of the network and no preferential growth is observed, hence the model predicts a uniform biofilm growth for concentrations larger than 25 $[kg/m^3]$, see Figure 3.14.

In Figure 3.15 the Damköhler number is shown for different inlet concentrations of the network. We observe that there is uniform growth and therefore upscalability when the Damköhler number is lower than 10^1. Further, we observe that when the inlet concentration $C_{in} = 25$ and $C_{in} = 50$ there is always uniform growth and hence upscalability.

3.3.2. UNIFORM BIOFILM GROWTH

In the uniform biofilm growth, the biomass grows at the same rate in all the tubes of the network. Using a similar process as the equivalent resistance in electric circuits, we can easily obtain a relation between the total flux in the network and the fraction of biomass. Since the radii are reduced in all the tubes at the same rate and assuming that initially the

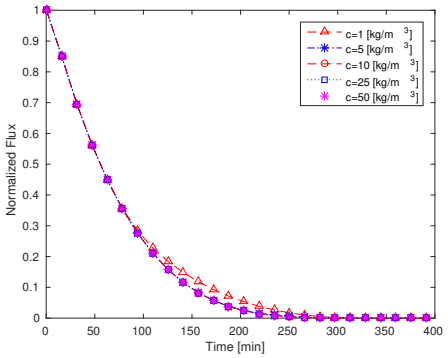

Figure 3.12: The normalised flux for different inlet concentration of nutrients, with network size L_4

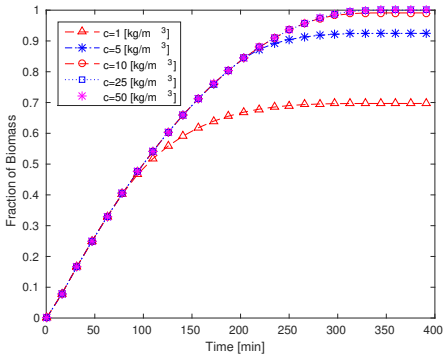

Figure 3.13: The fraction of biomass for different inlet concentration of nutrients, with network size L_4

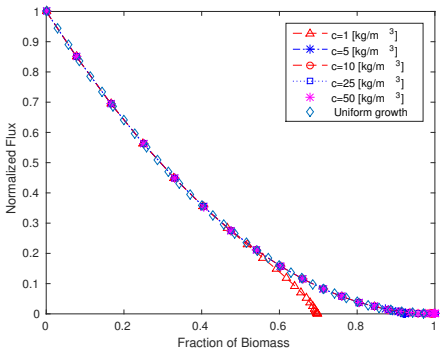

Figure 3.14: The fraction of biomass vs the normalised flux for different inlet concentration of nutrients, with network size L_4

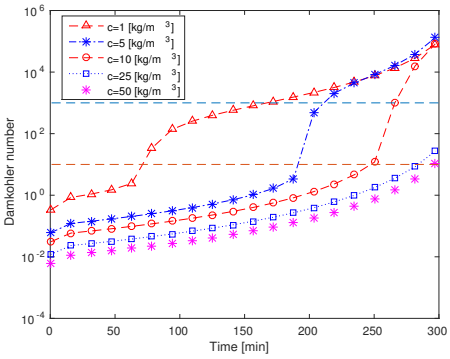

Figure 3.15: The Damköhler number for different inlet concentration of nutrients, with network size L_4

radii are equal in all the tubes of the network, it follows that during the whole uniform biofilm growth process the radius remains the same in all the tubes of the network. This implies that there is only flux in the horizontal tubes of the network. Hence the total flow in the network can be written as,

$$Q = \frac{N_y}{N_x}\frac{\pi}{8\mu l}[r_{w_{ij}}^4 + (R_{ij}^4 - r_{w_{ij}}^4)\beta^{-1}]\Delta P, \tag{3.19}$$

in which N_y is the number of tubes in the y direction and N_x is the number of tubes in x direction. This expression is equivalent to consider the whole network as a single tube.

If we disregard the second term in equation (3.19) and we express $r_{w_{ij}}^4$ as the fraction of volume of biomass, the normalised flux for uniform growth is given by,

$$Q_n = \frac{(1 - V_{pbf})^2}{(1 - V_{pbf_0})^2}. \tag{3.20}$$

In which V_{pbf_0} is the initial fraction of volume of biomass in the network. In terms of porosity, the normalised flux is given by the following equation,

$$Q_n = \left[\frac{\phi}{\phi_0}\right]^2, \tag{3.21}$$

where ϕ_0 is the initial porosity.

We use Darcy's Law to relate the permeability K with the flux Q,

$$K = QL\mu/\Delta PA. \tag{3.22}$$

If the pressure drop ΔP, the cross-sectional area of the network A, the length in the flux direction L and the viscosity μ are constant we have that $\frac{K}{K_0} = \frac{Q}{Q_0} = Q_n$. In which K_0 is the initial porosity and Q_0 is the initial flux. Therefore we can express equation (3.21) as,

$$\frac{K}{K_0} = \left[\frac{\phi}{\phi_0}\right]^2, \tag{3.23}$$

which relates the porosity and the permeability for the uniform biofilm growth.

3.4. DISCUSSION AND CONCLUSIONS

In this work we study the conditions for upscalability of bioclogging using a pore network model. We use a biofilm growth model that takes into account the spreading of the biofilm through the network and assumes that the consumption of nutrients is taken only in a small layer of biofilm adjacent to the water biofilm interface since the consumption of nutrients is faster than the diffusion of them through the biofilm in each tube. The biofilm growth requires the injection of nutrients through the network which are transported within a fluid phase. In general it is shown that initially the biofilm grows uniformly across the network but afterwards there is a preferential growth near the inlet of the network, due to depletion of nutrients in the back of the network. This causes the plugging of the network and blocks the nutrient inflow. The amount of nutrients needed to clog the network depends on factors like the size of the network, the number of nodes and the inlet concentration of nutrients. Therefore the analytical relation between the fraction of biomass and normalised flux may not be unique and upscalability is not always possible. However if the inlet concentration of nutrients is about 25 $[kg/m^3]$ there is no preferential growth and the biofilm grows uniformly through the network. This analytic relation does not depend on the size of the network, the number of nodes, or the inlet concentration, therefore upscalability is possible. In the case of uniform growth there is a unique relation between the fraction of biomass or porosity and the permeability of the network.

We use the Damköhler number to determine when the biofilm grows uniformly through the network and therefore when upscalability is possible. We found that if $Da < 10^1$ the biofilm grows uniformly through the network. However if the $Da > 10^3$ there is preferential growth and therefore no upscalability is possible. If $10^1 < Da < 10^3$ there is a transition between uniform and preferential growth.

We performed three sets of simulations to determine the conditions for upscalability of bioclogging. In the first set of simulations we vary the number of nodes in the network, we observe that at early stages the biofilm growth is mostly uniform for $N_x = 25$ and $N_x = 50$. However at the end of the process a heterogeneous biofilm growth in the network is observed. This phenomenon does not allow upscalability for the whole process. For $N_x = 100$ and $N_x = 200$ the preferential growth is more significant than in the previous case. For this set of simulations, it is shown that if the Damköhler number is lower than 10^1 approximately uniform growth is still observed in all the cases. However, if the Damköhler number is larger than 10^3 the biofilm growth model starts to deviate from uniform growth and upscaling is not possible. Note that increasing the number of nodes leads to a decrease in velocities and hence to a increase in the Damköhler, see equation (3.18).

In the second set of simulations we vary the size of the network. We observe that the fraction of biomass needed to block the network decreases when the size of the network increases. In this case, similar to the first one, there is no unique relation between

the fraction of biomass and the permeability of the network for the entire process. The Damköhler number predicts uniform growth below 10^1 approximately and preferential growth above 10^3. We see from equation (3.18) that if we increase the size of the network the Damköhler number also increases.

Finally for the third case of simulations we vary the inlet concentration of nutrients. We observe that for inlet concentrations $C_{in} = 25\ [kg/m^3]$ and $C_{in} = 50\ [kg/m^3]$, the fraction of biomass needed to block the network is approximately equal to one. For larger inlet concentration of nutrients there is no depletion and hence upscaling is possible since there is uniform biofilm growth. In this case if we increase the inlet concentration the Damköhler number decreases.

We performed three sets of simulations in which we vary the number of nodes in the network, the size of the network and the inlet concentration of nutrients. For the first two cases, upscalability is not possible since there is no unique relation between the amount of biofilm and the permeability of the network. However for the third case when we vary the inlet concentration of nutrients, we observe that for concentrations larger than 25 $[kg/m^3]$ the model describes uniform biofilm growth in the network, which allows upscalability of these results, since in uniform biofilm growth the relation between the fraction of biomass and the permeability does not depend on the volume of the network. In addition, we show that if the Damköhler number is less than approximately 10^1 the biofilm evolves similarly to uniform growth and that if it is above 10^3 preferential growth is observed, therefore we can use the Damköhler number to determine whether upscaling is possible. For the first two cases the Damköhler number is not always below this limit and therefore upscalability is not possible in these cases. However, for the third set of simulations we observe that the Damköhler number is below this limit for the entire process for an inlet concentration of $C_{in} = 25\ [kg/m^3]$ and $C_{in} = 50\ [kg/m^3]$. For the upscalable case, we obtain a relation between the permeability and the porosity, $K \sim \phi^2$. This formula can be seen as an alternative to the classical Kozeny-Carman equation in the case of gradually clogging of the network.

Interesting research may be the extension of this model to $3D$ networks with different topologies to determine the effects of biofilm growth on the relation between porosity and permeability. This relation could differ from $K \sim \phi^2$. In addition, it might be interesting to verify the relation between porosity and permeability, $K \sim \phi^2$, in laboratory scale and obtain an appropriate Damköhler number regime for uniform growth. Forthcoming research might be the extension of this model to two phase flow for studying the possibility of flow diversion for MEOR. Finally, this model can be used in other problems like pore-elasticity.

REFERENCES

[1] L. R. Brown, *Microbial enhanced oil recovery (meor),* Current opinion in Microbiology **13**, 316 (2010).

[2] R. T. Armstrong and D. Wildenschild, *Investigating the pore-scale mechanisms of microbial enhanced oil recovery,* Journal of Petroleum Science and Engineering **94**, 155 (2012).

[3] I. Lazar, I. Petrisor, and T. Yen, *Microbial enhanced oil recovery (meor),* Petroleum Science and Technology **25**, 1353 (2007).

[4] R. Sen, *Biotechnology in petroleum recovery: the microbial eor,* Progress in energy and combustion Science **34**, 714 (2008).

[5] Y. Tang, A. J. Valocchi, and C. J. Werth, *A hybrid pore-scale and continuum-scale model for solute diffusion, reaction, and biofilm development in porous media,* Water Resources Research **51**, 1846 (2015).

[6] W. Van Wijngaarden, F. Vermolen, G. Van Meurs, and C. Vuik, *A mathematical model and analytical solution for the fixation of bacteria in biogrout,* Transport in porous media **92**, 847 (2012).

[7] C. Picioreanu, J.-U. Kreft, and M. C. Van Loosdrecht, *Particle-based multidimensional multispecies biofilm model,* Applied and environmental microbiology **70**, 3024 (2004).

[8] T. Pintelon, D. Graf von der Schulenburg, and M. Johns, *Towards optimum permeability reduction in porous media using biofilm growth simulations,* Biotechnology and Bioengineering **103**, 767 (2009).

[9] D. G. von der Schulenburg, T. Pintelon, C. Picioreanu, M. Van Loosdrecht, and M. Johns, *Three-dimensional simulations of biofilm growth in porous media,* AIChE Journal **55**, 494 (2009).

[10] B. Chen-Charpentier, *Numerical simulation of biofilm growth in porous media,* Journal of computational and applied mathematics **103**, 55 (1999).

[11] C. Ezeuko, A. Sen, A. Grigoryan, and I. Gates, *Pore-network modeling of biofilm evolution in porous media,* Biotechnology and bioengineering **108**, 2413 (2011).

[12] C.-Z. Qin and S. M. Hassanizadeh, *Pore-network modeling of solute transport and biofilm growth in porous media,* Transport in Porous Media **110**, 345 (2015).

[13] R. Rosenzweig, A. Furman, C. Dosoretz, and U. Shavit, *Modeling biofilm dynamics and hydraulic properties in variably saturated soils using a channel network model,* Water Resources Research **50**, 5678 (2014).

[14] B. J. Suchomel, B. M. Chen, and M. B. Allen, *Macroscale properties of porous media from a network model of biofilm processes,* Transport in porous media **31**, 39 (1998).

[15] M. Thullner, J. Zeyer, and W. Kinzelbach, *Influence of microbial growth on hydraulic properties of pore networks,* Transport in porous media **49**, 99 (2002).

[16] M. Thullner, *Comparison of bioclogging effects in saturated porous media within one-and two-dimensional flow systems,* Ecological Engineering **36**, 176 (2010).

[17] A. B. Cunningham, W. G. Characklis, F. Abedeen, and D. Crawford, *Influence of biofilm accumulation on porous media hydrodynamics,* Environmental science & technology **25**, 1305 (1991).

[18] S. W. Taylor and P. R. Jaffé, *Biofilm growth and the related changes in the physical properties of a porous medium: 3. dispersivity and model verification,* Water resources research **26**, 2171 (1990).

[19] M. Peszynska, A. Trykozko, G. Iltis, S. Schlueter, and D. Wildenschild, *Biofilm growth in porous media: Experiments, computational modeling at the porescale, and upscaling,* Advances in water resources **95**, 288 (2016).

[20] Q. Xiong, T. G. Baychev, and A. P. Jivkov, *Review of pore network modelling of porous media: experimental characterisations, network constructions and applications to reactive transport,* Journal of contaminant hydrology **192**, 101 (2016).

[21] M. J. Blunt, *Flow in porous media—pore-network models and multiphase flow,* Current opinion in colloid & interface science **6**, 197 (2001).

[22] L. Li, C. A. Peters, and M. A. Celia, *Upscaling geochemical reaction rates using pore-scale network modeling,* Advances in water resources **29**, 1351 (2006).

[23] L. Vasilyev, A. Raoof, and J. M. Nordbotten, *Effect of mean network coordination number on dispersivity characteristics,* Transport in porous media **95**, 447 (2012).

[24] F. Heße, F. A. Radu, M. Thullner, and S. Attinger, *Upscaling of the advection–diffusion–reaction equation with monod reaction,* Advances in water resources **32**, 1336 (2009).

[25] X.-H. Wu, Y. Efendiev, and T. Y. Hou, *Analysis of upscaling absolute permeability,* Discrete and Continuous Dynamical Systems Series B **2**, 185 (2002).

[26] P. Renard and G. De Marsily, *Calculating equivalent permeability: a review,* Advances in water resources **20**, 253 (1997).

[27] I. Battiato and D. Tartakovsky, *Applicability regimes for macroscopic models of reactive transport in porous media,* Journal of contaminant hydrology **120**, 18 (2011).

[28] M. B. V. F. Lopez-Peña, LA, *A network model for the biofilm growth evolution in porous media and its effects on permeability and porosity,* (2018).

[29] M. Thullner and P. Baveye, *Computational pore network modeling of the influence of biofilm permeability on bioclogging in porous media,* Biotechnology and Bioengineering **99**, 1337 (2008).

[30] K. S. Ro and J. Neethling, *Biofilm density for biological fluidized beds,* Research journal of the water pollution control federation , 815 (1991).

[31] J. Lawrence, G. Wolfaardt, and D. Korber, *Determination of diffusion coefficients in biofilms by confocal laser microscopy,* Applied and environmental microbiology **60**, 1166 (1994).

[32] R. Bakke, M. G. Trulear, J. Robinson, and W. G. Characklis, *Activity of pseudomonas aeruginosa in biofilms: steady state,* Biotechnology and bioengineering **26**, 1418 (1984).

4

BIOFILM GROWTH MODEL IN A 3D CUBIC NETWORK

4.1. INTRODUCTION

In this chapter we study a three-dimensional biofilm growth pore network model. We investigate the influence of biofilm growth on the porosity-permeability relation. In this introduction, we will first give a short overview of the literature on 3D pore network models. Secondly we will address the problem in what aspects the 2D and 3D models are different and yield different results. Finally we will give an overview of the organisation of the chapter.

Biofilm growth has been modelled in 3D on the micro-scale [1]. They simulate the biofilm roughness, surface shape and porosity via a differential-discrete mathematical model [1]. According to their findings biofilm grows like a 'finger-like" or "mushroom" shape in a substrate-transport-limited regime. On the other hand, dense biofilm is found in systems where the biomass growth rate is the limiting factor. Despite the relevance of the biofilm morphology on the micro-scale, in this work we model the biofilm growth at the meso-scale. Therefore we assume that the biofilm is a uniform layer attached to the wall of the cylindrical pores.

[2] used a pore network model to describe the biofilm growth in a porous medium. They use a variable mass exchange coefficient which is a function of the biofilm volume fraction and the Damköhler number. They found that in the case of insufficient solute supply biofilm clogging occurs at the inlet of the network. In case of a higher water flow rate the biofilm accumulates away from the inlet. They also found that if the nutrient supply is sufficient the biofilm grows uniformly through the network.

In this chapter we extend the previous 2D model to three dimensions. We use a cubic network, which it could be seen as a set of 2D quadrangular networks (layers) joined by vertical tubes in the z direction. We describe the influence of bioflim growth on the porosity and the permeability of the network. Intuitively it seems to be easier to block a 2D network than a 3D network since in 3D it is easier to circumvent a blockage. This is

quantified by the percolation threshold.

The percolation threshold is associated with the existence of connecting paths between opposite sites in the network. To all tubes in the network we can associate a probability p of being full or empty. The percolation threshold is the critical value of the probability p such that a connecting path between opposite nodes in a network "always" exists... (with probability 99%). This means that above the percolation threshold a connecting path "always" exists. The percolation threshold for a 3D cubic network is approximately 0.2475. Meanwhile, the percolation threshold for a 2D quadrangular network is 0.5. This illustrates that it is easier to have a connecting path in 3D than in 2D.

In the 2D case we observed that we could replace the whole network by one effective tube in the uniform growth case. If we have uniform growth in the 3D case a similar argument might apply which could lead to similar permeability-porosity relations. In this case the Damköhler number could also be used to determine whether we are in the uniform (upscalable) regime.

In Section 4.2 we describe the mathematical model for the biofilm growth in 3D and the numerical method used. In Section 4.3 we present the results we obtained of the effects of biofilm growth on the porous medium characteristics. Finally we draw some conclusions in Section 4.4.

4.2. MATHEMATICAL MODEL AND NUMERICAL METHOD

In this section we present the equations used for the biofilm growth model in a porous medium in 3D. This model is an extension of the 2D model. We use a 3D cubic network to represent the porous medium in 3D (see Figure 4.1). The network is formed of interconnected cylindrical tubes. The number of neighbouring nodes for the interior nodes is 6. We assume that bacteria and biofilm form a single phase and we refer to them as a biofilm. Furthermore we assume that the nutrients are injected within a fluid to stimulate biofilm growth.

The volumetric flow of water within each tube is described by a modified Poiseuille equation [3],

$$q_{ij} = \frac{\pi}{8\mu l}[r_{w_{ij}}^4 + (R^4 - r_{w_{ij}}^4)\beta^{-1}]\Delta p. \tag{4.1}$$

Mass conservation is imposed in each node n_i,

$$\sum_{j \in S_i} q_{ij} = 0, \forall n_i. \tag{4.2}$$

This condition leads to an equation for the pressure in each node. The boundary conditions for the pressure are given by,

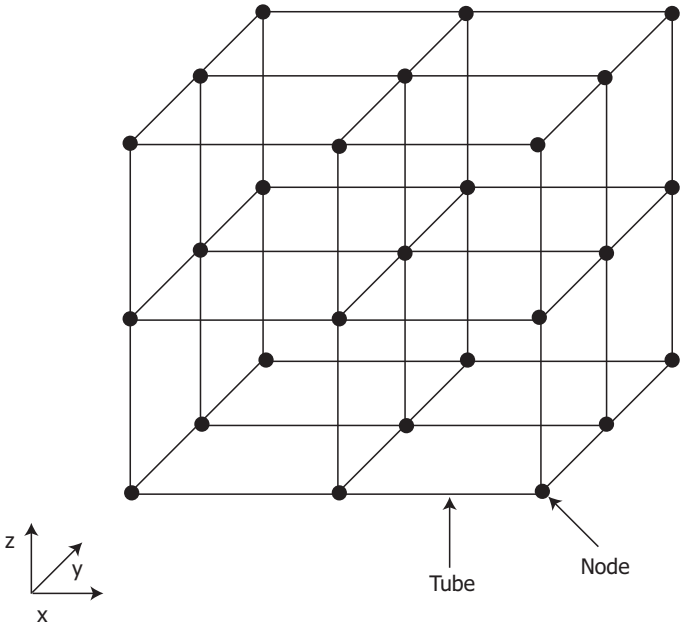

Figure 4.1: Cubic network used for the 3D simulations

$$
\begin{aligned}
p(0,y,z;t) &= 1600L_x,\\
p(L_x,y,z;t) &= 0,\\
\frac{\partial p}{\partial y}(x,0,z;t) &= 0,\\
\frac{\partial p}{\partial y}(x,L_y,z;t) &= 0,\\
\frac{\partial p}{\partial z}(x,y,0;t) &= 0,\\
\frac{\partial p}{\partial z}(x,y,L_z;t) &= 0.
\end{aligned}
\tag{4.3}
$$

The transport of nutrients is described by the advection-diffusion-reaction equation in 3D; the concentration of nutrients is denoted by C:

$$
\frac{\partial C}{\partial t} + \mathbf{u}\cdot\nabla C - D\nabla^2 C = -\frac{\partial b^+}{\partial t}. \tag{4.4}
$$

In this equation D is the diffusion coefficient of nutrients through water and $\mathbf{u}$ is the advection velocity which is related to the local flux $\mathbf{q}$ by $\mathbf{u} = \mathbf{q}/A$, where A is the area of the cross-section of the tube. Additionally, b^+ is the concentration of the biofilm

produced as a result of the consumption of nutrients (no detachment of biofilm is taken into account in this term).

The initial and boundary conditions for the concentration are:

$$\begin{aligned} C(x,y,z,t_0) &= 0, \\ t_0 &= 0, \end{aligned} \tag{4.5}$$

$$\begin{aligned} C(0,y,z,t) &= 1, \\ \frac{\partial C}{\partial x}(L_x,y,z,t) &= 0, \\ \frac{\partial C}{\partial y}(x,0,z,t) &= 0, \\ \frac{\partial C}{\partial y}(x,L_y,z,t) &= 0 \\ \frac{\partial C}{\partial z}(x,y,0,t) &= 0, \\ \frac{\partial C}{\partial z}(x,y,L_z,t) &= 0. \end{aligned} \tag{4.6}$$

The concentration of biofilm b is related to the volume of biofilm by

$$b = \frac{\rho}{V_T} V_{bf}. \tag{4.7}$$

In this model we assume that biofilm and nutrients can meet in the interior of the tube and in the extremes of the tube. For this reason there are two kinds of biofilm growth: biofilm growth in the interior of the tube and biofilm growth in the exterior of the tube. The biofilm growth in the interior of the tube is given by

$$\frac{\partial V^i_{bf_{ij}}}{\partial t} = k_1 \frac{A^i_{wbf}}{A^i_T} V_T \frac{C_{ij}}{E_s + C_{ij}} f(V_{bf_{ij}}). \tag{4.8}$$

The biofilm growth in the extreme of the neighbouring tube t_{jk} is given by

$$\frac{\partial V^e_{bf_{jk}}}{\partial t} = k_1 \frac{A^e_{wbf}}{A^e_T} V_T \frac{C_{jk}}{E_s + C_{jk}}. \tag{4.9}$$

Finally, taking into account the interior growth, the growth in the neighbouring tubes and the detachment of biofilm, the equation for the biofilm growth in the tube t_{ij} can be written as

$$\begin{aligned} \frac{\partial V_{bf_{ij}}}{\partial t} &= k_1 R \frac{C_{ij}}{E_s + C_{ij}} \sqrt{\pi l (V_T - V_{bf_{ij}})} f(V_{bf_{ij}}) + k_1 \sum_{k \in \Lambda_{ji}} \frac{C_{jk}}{E_s + C_{jk}} (V_{bf_{jk}} - V_{bf_{ij}})_+ \\ &+ k_1 \sum_{k \in \Lambda_{ij}} \frac{C_{ki}}{E_s + C_{ki}} (V_{bf_{ki}} - V_{bf_{ij}})_+ - k_2 R \sqrt{\pi l (V_T - V_{bf_{ij}})} H(V_{bf_{ij}}), \end{aligned} \tag{4.10}$$

where $H(V_{bf_{ij}})$ is defined as

$$H(V_{bf_{ij}}) = \begin{cases} 0 & \text{if } V_{bf_{ij}} = 0 \\ 1 & \text{if } V_{bf_{ij}} \geq 0. \end{cases} \tag{4.11}$$

The coupled system of equations 4.4 and 4.10 is solved via a finite difference scheme in space. To solve the equation 4.4 a time-implicit method for the concentration is used and a finite difference scheme in space. To solve equation 4.10 an explicit Euler time integration method was used. The details of the numerical approach to solve the transport of nutrients and the biofilm growth are shown in Section 2.3.

4.3. RESULTS

In this section we present the results obtained for the biofilm growth model in a 3D cubic network. The number of nodes in the x direction is $N_x = 50$ and the number of nodes in y direction is $N_y = 30$. The number of nodes in the z direction, N_z, was varied depending on the numerical experiment.

First we vary the number of nodes in the z direction to study the influence of the number of nodes on the porosity-permeability relation. The inlet concentration of nutrients was set constant and the radius is the same for all the tubes in the network.

Secondly we study the influence of the inlet concentration of nutrients on biofilm growth in the network. We set different inlet concentrations we set $N_z = 32$ [1]. Finally we study the biofilm growth evolution with a log-normal distribution for the radii of the network. In this case we vary the variance of the distribution; the inlet concentration and N_z were set constant.

4.3.1. CASE 1:A DIFFERENT NUMBER OF NODES IN THE z DIRECTION, EQUAL RADII AND EQUAL INLET CONCENTRATIONS

Firstly, we studied the effects of the number of nodes in the z direction on the dynamics of the system. For this purpose we performed five simulations with a different number of nodes in the z direction, $N_z = 3$, $N_z = 5$, $N_z = 9$, $N_z = 17$ and $N_z = 33$. We compare these results with the results of our 2D network model ($N_z = 1$).

In Figure 4.2 the normalised flux as a function of time is shown. We observe that the flow through the network ceases after approximately 300 minutes for all the cases.

In Figure 4.3 the evolution of the fraction of biomass in the network S_b is shown. If the network is blocked, then $\tilde{S_b}$ is around 0.7 for the 2D case. For the $3D$ cases this fraction is larger: if $N_z = 2$ then $\tilde{S_b}$ is around 0.8 and as the number of nodes in the z direction increases, this fraction converges to 0.85 approximately.

Figure 4.4 shows the relation between the normalised flux and the fraction of biomass, S_b, for the 2D case, the 3D cases and the case of uniform biofilm growth in 2D. Note that the uniform biofilm growth in 2D and 3D yield similar results because there is no flux in the z direction. The biofilm growth in the 2D case deviates from uniform growth at around $S_b = 0.5$. For the 3D cases the deviation from uniform growth occurs at around $S_b = 0.7$. We also observe this behaviour in Figure 4.5 where the average Damköhler

[1] Alfredo I also did this for various Nz, shall we mention this in the document?

number is plotted as a function of time. In Figure 4.5, it can be seen that there is a transition going on between Damköhler numbers of approximately $Da \approx 2$ and $Da \approx 10^2$. This transition marks the event between having uniform growth in the upscalable regime ($Da \leq 1$) and non-uniform growth ($Da \geq 10^2$) in the non-upscalable regime. It can be seen that the Damköhler values are of the same order of magnitude as in Figures 3.11 and 3.15. For the 2D case there is a transition between uniform growth and preferential growth between 70 and 100 minutes. For the 3D cases this transition is between 120 minutes and 160 minutes. This implies that in the 3D simulations the flow remains upscalable during a longer period, which may be attributed to the larger ability of the '3D-flow' to get around plugged sections and to the fact that there are more tubes to be filled so that the flow velocity stays larger during a larger period. A large flow velocity gives a lower Damköhler number.

In Figure 4.6, we show the normalised permeability versus the normalised porosity, which is an important relationship in porous media that is often modelled through Kozeny-Carman like relations. The figure that we propose here is an alternative to the Kozeny-Carman relation taking into account the gradual filling up of the pore. The results that we get are similar to the previous 2D results (see Figure 2.8), however, it can be seen that the permeability only becomes zero at a lower porosity. This effect becomes more pronounced if the number of nodes in the z-direction increases. This observation suggests that one needs more biomass to shut off the 3D-region than the 2D region. This may be caused by a combination of a larger number of tubes in 3D and a higher capability for flow diversion in 3D compared to 2D.

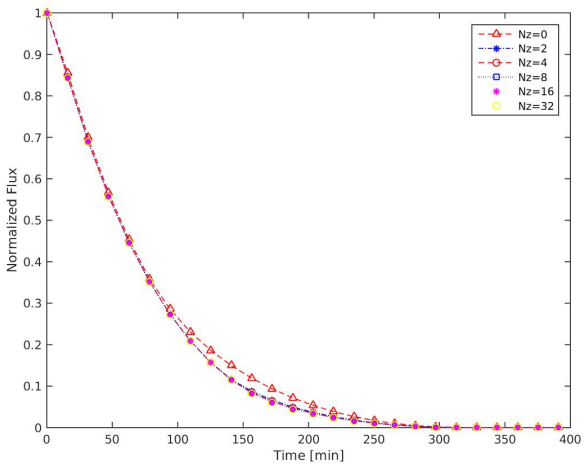

Figure 4.2: normalised flux vs time for different number of nodes in z direction

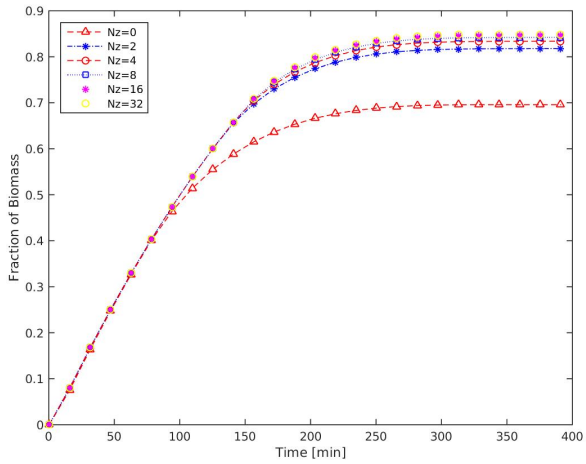

Figure 4.3: Fraction of biomass vs time for different number of nodes in z direction

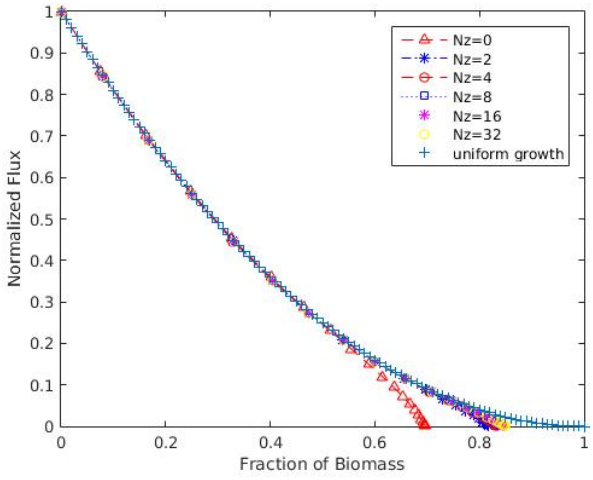

Figure 4.4: normalised flux vs Fraction of biomass for different number of nodes in z direction

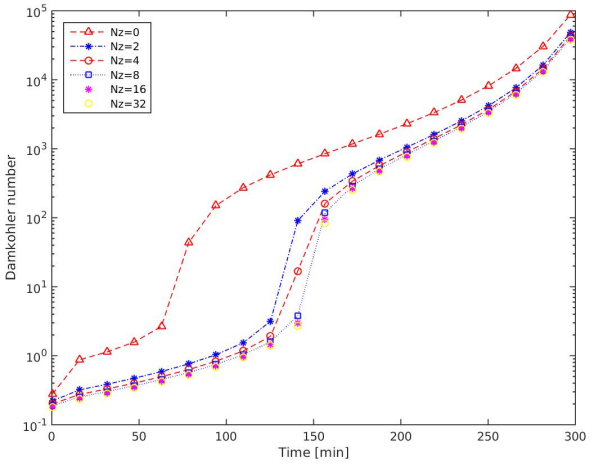

Figure 4.5: Damkohler number for different number of nodes in z direction

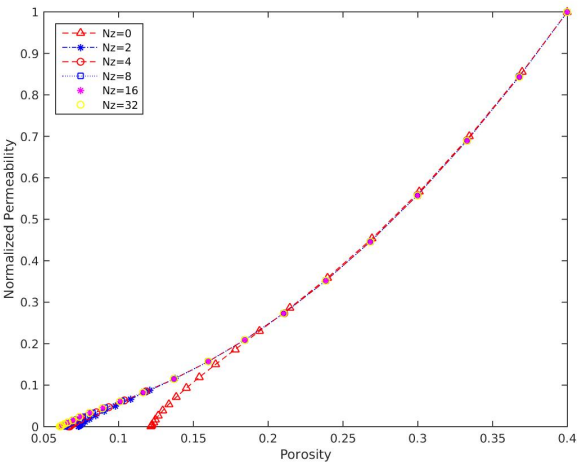

Figure 4.6: normalised permeability vs Porosity

4.3.2. CASE 2: DIFFERENT INLET CONCENTRATIONS, SAME RADII AND EQUAL N_z

Secondly we study the effects of the inlet concentration of nutrients on the biofilm growth in the cubic network. We performed three set of simulations in which we vary the inlet concentration of nutrients c_{in}. The values for the inlet concentration of nutrients are $c_{in} = 0.001$, $c_{in} = 0.01$ and $c_{in} = 0.1$.

In Figure 4.7 the normalised flux as a function of time is shown for the three different inlet concentrations used in this simulation, $c_{in} = 0.01$, $c_{in} = 0.1$, $c_{in} = 1$. It is shown that after 400 minutes the network is blocked due to biofilm growth for all the cases. However if the inlet concentration is $c_{in} = 0.01$ the curve that represents the relation between the normalised flux and time exhibits an inflection point. Figure 4.8 shows the fraction of biomass in the network S_b. For $c_{in} = 0.01$ S_b is about 0.1, for $c_{in} = 0.1$ S_b is about 0.3 and for $c_{in} = 1$ $S_b = 0.8$ approximately. It is shown that if the inlet concentration of nutrients is larger then the nutrients will be distributed over the network, including the regions near the outlet of the network. Therefore the depletion of nutrients will take longer and more biomass will grow through the network. This phenomenon is similar in the 2D case (see Figure 3.14. However for the 3D case lower initial concentration is needed to obtain a more uniform growth. This is because in a 3D network there are more paths in which the fluid with nutrients can flow, therefore the nutrients can reach the areas near the outlet even though the inlet concentration is low.

In Figure 4.9 the relation between the fraction of biomass and the normalised flux is shown for the three inlet concentrations used. In addition, the relation between the fraction of biomass and normalised flux for the uniform biofilm growth is shown. It is shown that for $c_{in} = 0.01$ and $c_{in} = 0.1$ the biofilm growth deviates from uniform growth fast, i.e. at a low fraction of biomass. On the other hand for $c_{in} = 1$ the biofilm growth stays longer in accordance with the uniform growth. The Damköhler number as a function of time is shown in Figure 4.10. For $c_{in} = 0.01$ the Damköhler number is initially around 10^2. This Damköhler number already corresponds to heterogeneous biofilm growth, see for example Figure 4.9 and Figure 4.10. For $c_{in} = 0.1$ the Damköhler number is initially less than 10^1. However after approximately 20 minutes the Damköhler number increases until 10^2 approximately. This means that the biofilm grows initially uniformly through the network; however after 20 minutes the biofilm starts to grow preferentially near the inlet of the network. Finally for $c_{in} = 1$ the Damköhler number is lower than 10^1 for the first 150 minutes. After that the Damköhler number increases dramatically to 10^2 approximately. During the first 150 minutes the biofilm grows uniformly through the network according to Figure 4.9, where we observe that the biofilm growth overlaps with the uniform growth. In Figure 4.11 the normalised flux as function of the porosity is shown for the inlet concentration of nutrients, $c_{in} = 0.01$, $c_{in} = 0.1$, $c_{in} = 1$.

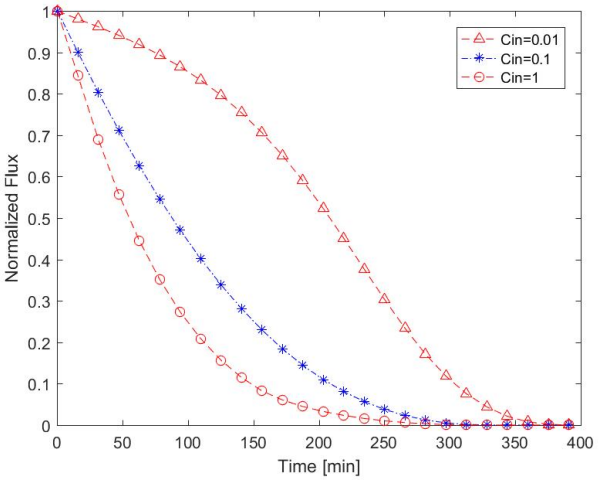

Figure 4.7: Different inlet concentrations Nz=32

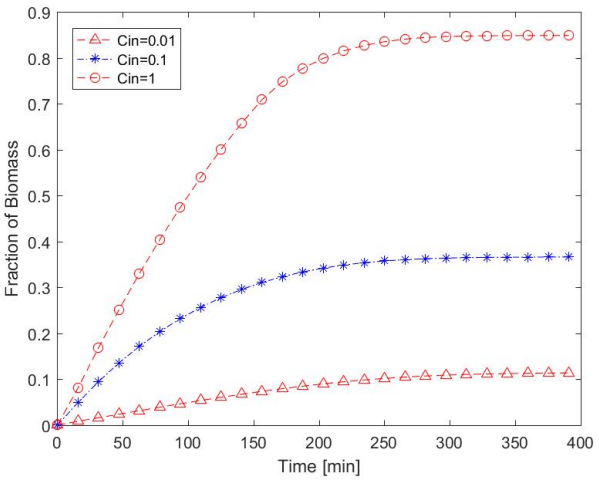

Figure 4.8: Different inlet concentrations Nz=32

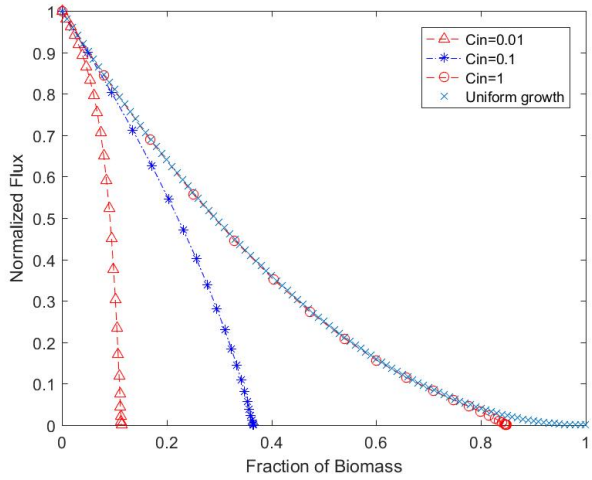

Figure 4.9: Different inlet concentrations Nz=32

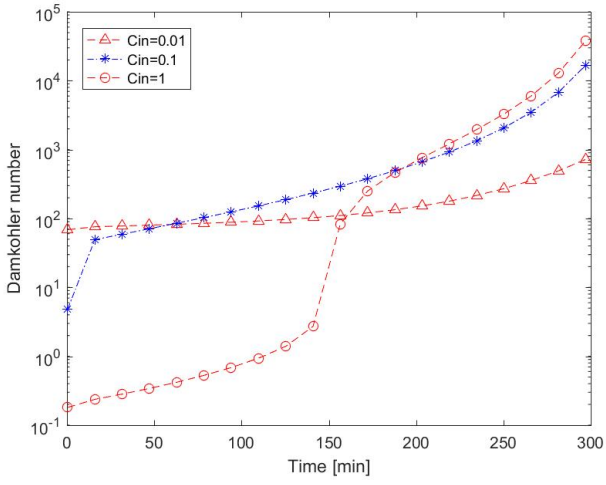

Figure 4.10: Different inlet concentrations Nz=32

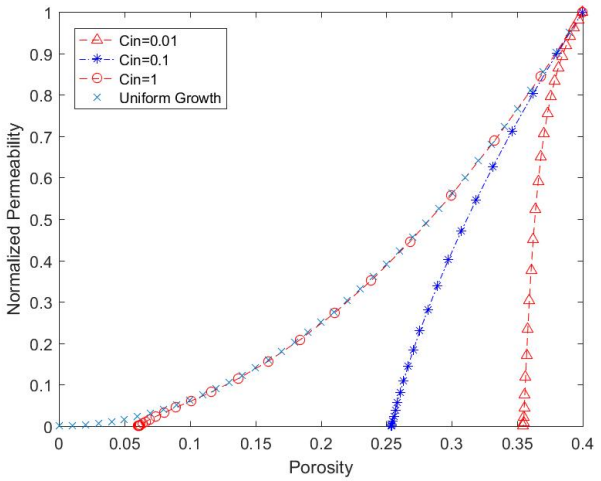

Figure 4.11: Different inlet concentrations Nz=32

4.3.3. CASE 3: LOG-NORMAL DISTRIBUTION FOR THE RADII DIFFERENT VARIANCE; A CONSTANT NUMBER OF NODES IN Z DIRECTION AND A CONSTANT INLET CONCENTRATION

In Figure 4.12 the normalised flux as a function of time is shown for the four variances σ: $\sigma = 0$, $\sigma = 1/2$, $\sigma = 1/4$, $\sigma = 1/8$. It is shown that after 250 min the network is blocked for variances $\sigma = 1/2$, $\sigma = 1/4$, $\sigma = 1/8$ due to biofilm growth. However for $\sigma = 0$ the blocking of the network occurs later: at 300 minutes approximately. Figure 4.13 shows the fraction of biomass in the network. We observe that if the variance tends to zero the curves tends to the case in which all the tubes are equal $\sigma = 0$.

In Figure 4.14 the relation between the fraction of biomass and the normalised flux is shown for the variances used. If the variance is $\sigma = 1/2$ the fraction of biomass needed to block the network is around 0.7, if the variance is $\sigma = 1/4$ the fraction of biomass needed is about 0.8. and if $\sigma = 1/8$ the fraction of biomass needed is about 0.82.

In Figure 4.15 the Damköhler number for the different variances is shown. We observe that there is a sudden increase of Damköhler number for the four cases. This increase occurs for different times. However the value of the Damköhler number when this sudden increase occurs is between $Da = 10^1$ and $Da = 10^3$) for all the cases.

4.4. DISCUSSION AND CONCLUSIONS

In this chapter we performed several numerical experiments in which we varied the number of nodes in z direction. In the first set we performed 6 simulations with a different number of nodes in the z direction: $z = 1$ (2D case), $z = 3$, $z = 5$, $z = 9$, $z = 17$, $z = 33$. We studied the dependence of the results on the number of nodes in the z direction to determine whether it is possible to describe the biofilm growth with a 2D network model, i.e. whether a 2D simulation is sufficient.

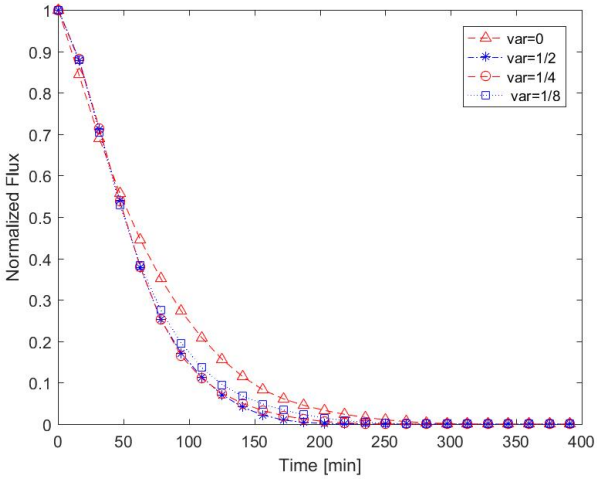

Figure 4.12: Different simulations

We obtained that for the $z = 1$ (2D case) the depletion of nutrients occurs faster. This implies that the biofilm growth deviates from uniform growth earlier in the 2D case than in the 3D case. The depletion occurs faster in 2D since in 3D there are more ways in which the water can flow, hence, the nutrients are able to travel further in a 3D network and depletion takes longer. The amount of biomass needed to block the network is larger for the 3D cases than for the 2D case. However, as the number of nodes in the z direction increases, the amount of biomass needed to block the network converges to a limit value.

Even though the depletion of nutrients occurs faster for the 2D case, the transition between uniform growth and preferential (or heterogeneous) growth occurs for the same values of the Damköhler number, which is between $Da = 10^1$ and $Da = 10^3$. Therefore we conclude that the criteria for uniform growth and therefore up-scalability in 3D are similar to the criteria used for the 2D network.

In addition the inlet concentration needed to obtain uniform growth is lower for the 3D case than for the 2D case. The lower inlet concentration of nutrients needed to obtain uniform biofilm growth in 3D is due to the lower percolation threshold. It is harder to block a part of the network which means that depletion sets in later. When the inlet concentration of nutrients decreases heterogeneous biofilm growth occurs at early stages. However this dependence on the inlet concentration is also incorporated in the Damköhler number; the transition from uniform growth to preferential growth takes place within the same Damköhler regime (i.e. between $Da = 10^1$ and $Da = 10^3$).

Finally we studied the effects of a log normal distribution for the radii on the permeability-porosity relation. We observed that as the variance tends to zero the fraction of biomass needed to block the network tends to the fraction of biomass needed when the radii are all equal. However if the variance of the distribution is larger then the amount of biomass needed to block the network is lower, because in the latter case only a few "big channels" are needed to block the network. But also in this case we ob-

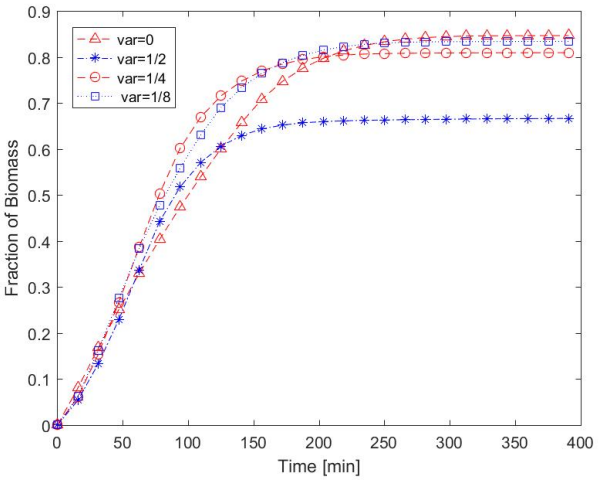

Figure 4.13: Different simulations

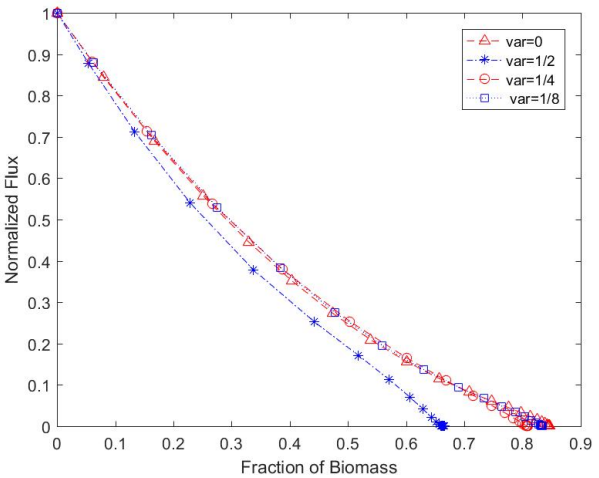

Figure 4.14: Different simulations

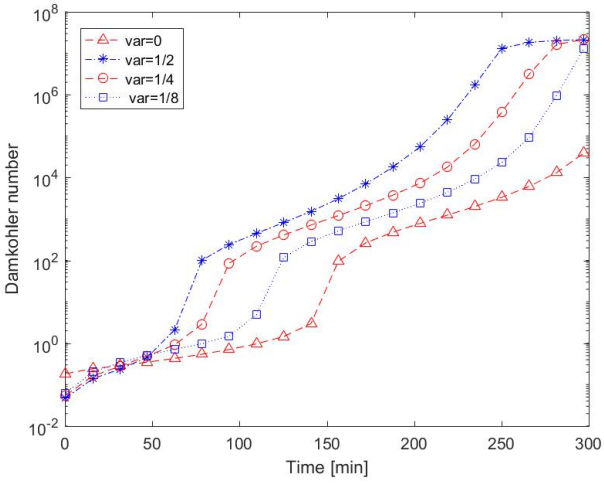

Figure 4.15: Different simulations

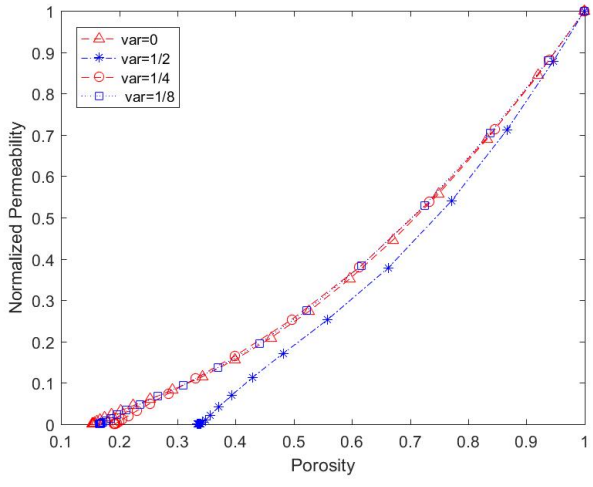

Figure 4.16: Different simulations

serve that the transition from uniform growth to preferential growth takes place within the same Damköhler regime (i.e. between $Da = 10^1$ and $Da = 10^3$).

REFERENCES

[1] C. Picioreanu, M. C. Van Loosdrecht, and J. J. Heijnen, *Mathematical modeling of biofilm structure with a hybrid differential-discrete cellular automaton approach,* Biotechnology and bioengineering **58**, 101 (1998).

[2] C.-Z. Qin and S. M. Hassanizadeh, *Pore-network modeling of solute transport and biofilm growth in porous media,* Transport in Porous Media **110**, 345 (2015).

[3] M. Thullner and P. Baveye, *Computational pore network modeling of the influence of biofilm permeability on bioclogging in porous media,* Biotechnology and Bioengineering **99**, 1337 (2008).

5

A NETWORK MODEL FOR THE KINETICS OF BIOCLOGGING FLOW DIVERSION FOR ENHANCED OIL RECOVERY

A micro-scale model that describes the sweep efficiency of a water-flood process when biofilm is growing in the porous media is useful to provide an insight of MEOR applicability at larger scales. The development of micro-scale models of flow diversion due to biomass accumulation is not available in the literature as far as we known. In this chapter we investigate the effects of biofilm growth on the direction of the water flow. For this purpose we assume that the porous medium has two regions with different permeabilities and we investigate the impact of biofilm growth on the flow rate through the low permeability region.

In section 5.1 we describe the MEOR process and some previous works of biofilm growth in porous media. In section 5.2 we explain the model used for the biofilm growth which differs from the previous biofilm growth model used in this thesis and the transport-diffusion equation. In this section we also describe the numerical approach used to solve the transport equation and the biofilm growth equations. In the following section 5.3 we present the results obtained for the effect of biofilm growth in permeability and porosity. In addition we present the results of the flow diversion when the network consists of two areas of different permeability. Finally in section 5.4 we mention some conclusions about the effects of biofilm growth on flow diversion of water.

5.1. INTRODUCTION

Microbial Enhanced Oil Recovery (MEOR) is a technique in which the growth of bacteria and the resulting by-products are used in order to increase residual oil production

in a tertiary oil recovery method. MEOR techniques involve the use of indigenous microorganisms or the injection of selected external bacteria into the reservoir to produce the desired by-products. Typically in MEOR techniques, bacterial population growth is supported by the injection of nutrients into the reservoir [1].

Microbes enhance oil displacement by different processes: interfacial tension reduction, rock wettability change and increment of the waterflood sweep efficiency caused by selective plugging [2]. Among these mechanisms, interfacial tension reduction and selective plugging are thought to have the greatest impact on recovery [1]. During selective plugging, bacteria grow and adhere, within a self produced matrix of extra cellular polymeric substances (EPS), to the walls of the pores of high permeability zones. The bacteria adhered and the self produced matrix is referred as biofilm. Biofilm growth leads to the plugging of the pores in high permeability zones, causing the diversion of the water-flood from the thief zones towards oil-rich areas.

The applicability of MEOR techniques to increase oil extraction has been shown in laboratory experiments [3–5] and field trials [5]. In laboratory experiments, it has been shown that biofilm accumulates in high permeability zones, diverting the water flood towards oil trapped zones [6]. Field trials have been implemented in order to verify the effectiveness of microbial processes predicted in laboratories. The Alton field in Australia showed that the net oil production increased 40% and it continued after 12 months of treatment [7]. A field study in Canada showed that selective plugging is one of the most promising processes in MEOR techniques [8]. The extent of success in oil recovery using MEOR techniques depends on several factors such as individual reservoir characteristics: lithology, porosity, permeability, temperature and oil composition. Additionally, microbial activity, bacterial composition and concentration of nutrients determine the performance of MEOR. Therefore, the prediction of the failure or success of the MEOR techniques is limited by the lack of measures in microbial activity [1]. However, it is possible to describe quantitatively the relationships between reservoir characteristics, microbes and operating conditions [9].

The development of mathematical and numerical models predicting the bacterial population growth, nutrients transport and in situ production of by-products is of vital importance to develop a proper field strategy [1]. Several numerical models have been developed to describe biofilm growth. There exist continuum Darcy models [10], bacterially-based models [11], Lattice Boltzmann based simulations [12, 13] and Pore Network Models (PNM) [14–17]. Frequently, in biofilm growth models, the porous media consists of three components: the grains, the biofilm which grows on the walls of the solid grains and the liquid in the pore space. The grains are assumed to be impermeable for the liquid and the nutrients, therefore hydrodynamic model equations are written only for the liquid and biofilm [12]. In the flow regimes that we are considering now, we also assume that the grains are non-deformable.

In PNMs, pores are considered as cylindrical interconnected tubes in which the water can flow. The dynamics of the problem is described by transport of nutrients through the network, bacterial population growth and biofilm development. Transport of nutrients is carried out within an aqueous phase and is described by a convection diffusion equation with a reaction term that considers the consumption of nutrients caused by bacterial population growth. Bacterial population will determine the development of

biofilm in the pores of the medium. This biofilm will grow and will change the radii of the pores, leading to a modification in the dynamics of the fluid that carries the nutrients through the network [14–17]. The geometric properties of the network such as connectivity, coordination number or coordination number distribution have an influence on the transport of solute and in multiphase flow in porous systems [18].

Among PNMs different approaches have been used to study the evolution of the fluid dynamics of the system and biofilm growth. Commonly, the biofilm is treated as an impermeable layer [15, 16, 19]. However, the assumption that nutrients can flow through the biofilm produces a better match with laboratory experiments [20]. Thullner et al. [20] considered that the flow in each of the tubes is described by a modified form of the Poiseuille flow where the flux through the biofilm and through the void space is taken into account. Considering that nutrients can also flow through the biofilm phase, Ezeuko et al. [14] used two different diffusion coefficients, one for diffusion through the water-water interface and another for the water-biofilm interface.

The Monod kinetics equation is usually used to describe the growth of bacteria in the pores [14, 16, 17, 20], this equation relates the growth rate of bacteria with the concentration of nutrients available in the network.

Even though the biofilm phase and the bacteria phase are two different phases, the distinction in PNM's between biofilm and bacteria has not been made explicit in the literature. In Thullner et al. [20] no distinction between biofilm and bacteria is taken into account while Ezeuko et al. [14] consider the biofilm as an attached phase of bacteria.

In this work, we model the growth of biofilm, the growth of the bacteria population and the transport of nutrients in a porous medium. As in the previous works of Thullner [20] and Ezeuko [14], we consider the biofilm phase as a permeable layer which means nutrients can travel through the biofilm phase due to advection. However, diffusion was considered only in the water phase. Note that we consider the bacteria and the biofilm separately. Additionally, we consider that the excess volume of biofilm can be spread to the neighbouring tubes. Finally, we study the possibility of flow diversion from thief zones to areas of low permeability by means of bioclogging. We model two regions with different permeabilities and we compute the flow out of the low permeability region, since this flow mimics the amount of oil that can be produced from the low permeability zone.

This chapter consists of four sections. In Section 5.2, in the Mathematical model subsection, we describe the physical, mathematical and biological considerations that are involved in the process of bioclogging in a porous medium. We illustrate how we model the porous medium, the injection of nutrients, the growth of bacteria, and the growth and development of biofilm. In Section 5.2, in the Numerical method subsection, the numerical method used is described and the computational steps are explained. In Section 5.3 the results and discussion are presented. Finally, in Section 5.4 the conclusions are drawn and the outlook to other problems are presented.

5.2. METHOD AND THEORY

5.2.1. MATHEMATICAL MODEL

We represent the porous medium as a 2D network composed of interconnected cylindrical tubes. The point where these tubes are connected is called a node of the network and is indexed as node n_i. The tube between the node n_i and n_j is indexed as the tube t_{ij}. A Rayleigh distribution for the radii was used. In addition, it is assumed that all the tubes have the same length l. The number of tubes connected in each node is four for interior nodes, three for boundary nodes and two for the nodes in the corner of the network (see Figure 2.1).

We assumed that the initial concentration of bacteria is necessary for the biofilm growth, therefore we consider that 4% of the tubes have an initial concentration of bacteria b_0. Initially nutrients are not present in the network, hence nutrients need to be injected through the network and transported within a fluid.

In this work we consider the biofilm as a permeable layer in which nutrients are able to be transported as well. Additionally, we consider a single concentration in each tube, hence no distinction between the concentration in the biofilm phase and the concentration in the water phase was made.

We define the thickness of the biofilm in the tube t_{ij} as $r_{b_{ij}}$, the radius of the tube available for water by $r_{w_{ij}}$ and the total radius of the tube by R_{ij} (see Figure 2.1).

The volumetric flow of the aqueous phase q_{ij} in the tube t_{ij} is described by a modified form of the Poiseuille equation [20],

$$q_{ij} = \frac{\pi}{8\mu l}[r_{w_{ij}}^4 + (R_{ij}^4 - r_{w_{ij}}^4)\beta^{-1}]\Delta p, \tag{5.1}$$

where Δp is the pressure drop between the neighbouring nodes n_i and n_j, μ is the viscosity of water that flows in the bulk, β is the ratio between the viscosity of water flowing through the biofilm and the viscosity of water flowing through the bulk and l is the length of the tube. According to [20] $\beta = 10^3$ is a good approximation for an impermeable biofilm.

Mass conservation is imposed in each of the nodes. For the node n_i we have

$$\sum_{j \in S_i} q_{ij} = 0, \tag{5.2}$$

where $S_i = \{j \mid n_j \text{ is adjacent to the node } n_i\}$ and further q_{ij} is the flux in the tubes connected to node n_i.

The transport of nutrients is described by an advection diffusion reaction equation. We denote the concentration of nutrients as C $[kg/m^3]$,

$$\frac{\partial C}{\partial t} = -\mathbf{u}\cdot\nabla C + D\nabla^2 C - \frac{\lambda_b^+}{Y}\frac{C}{E_{bs}+C}b, \tag{5.3}$$

where b is the biomass concentration, λ_b^+ is a microbial specific consumption rate, Y is the yield coefficient, E_{bs} is a saturation constant, D is the diffusion coefficient and $\mathbf{u}$ is the velocity which is related to the flux $\mathbf{q}$ by $\mathbf{u} = \mathbf{q}/A$, where A is the area of the cross section of the tube.

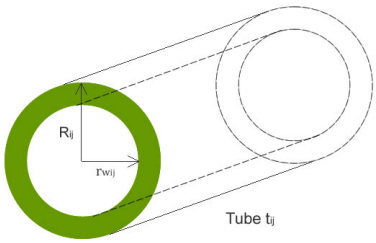

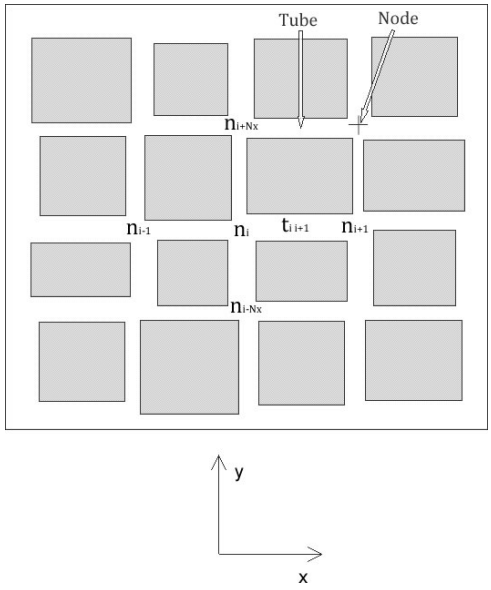

Figure 5.1: Pore Network and tubes

$$
\begin{array}{ccccc}
.. & .. & .. & .. & n_{N_x * N_y} \\
.. & .. & .. & .. & .. \\
.. & .. & n_{i+N_x} & .. & .. \\
.. & n_{i-1} & n_i & n_{i+1} & .. \\
.. & .. & n_{i-N_x} & .. & .. \\
n_{Nx+1} & .. & .. & .. & .. \\
n_1 & n_2 & .. & .. & n_{Nx}
\end{array}
$$

Figure 5.2: Order of the nodes in the network

The growth of the biomass concentration b $[kg/m^3]$ is given by

$$\frac{\partial b}{\partial t} = \frac{\lambda_b^+}{Y}\frac{C}{E_{bs}+C}b, \tag{5.4}$$

in which the growth rate is given by Monod Kinetics. In this equation λ_b^+ is a microbial specific growth rate, Y is the yield coefficient and E_{bs} is a saturation constant. We consider the biofilm as an adsorbed phase on the walls of the tubes. We describe the growth and development of the biofilm by its concentration Φ expressed as mass per pore volume unit.

The evolution of the concentration Φ is described by,

$$\frac{\partial \Phi}{\partial t} = \lambda_\Phi^+ \frac{C}{E_{\Phi_s}+C}\Phi - \lambda_\Phi^-\Phi, \text{ if } V_{bf} < V \tag{5.5}$$

$$\frac{\partial \Phi}{\partial t} = 0, \text{ if } V_{bf} \geq V \tag{5.6}$$

in this equation λ_Φ^+ is a microbial specific growth rate, $E_{\Phi s}$ is a saturation constant and λ_Φ^- is a decay rate for the biofilm due to shear stress, V_{bf} is the volume of biofilm and V is the total pore volume. If the volume of the biofilm is equal or larger than the volume of the tube, we consider that the biofilm can not grow anymore. The concentration of biofilm can be converted into volume of biofilm, assuming constant density of the biofilm and constant pore volume in each tube.

The volume of the biofilm $V_{bf_{ij}}$ in the tube t_{ij} is determined by

$$V_{bf_{ij}} = \frac{\Phi_{ij}}{\rho_{bf}}V_{ij}, \tag{5.7}$$

where Φ_{ij} is the concentration of biofilm, V the total pore volume and ρ_{bf} is the density of the biofilm.

In this model we take into account that biofilm can spread to the neighbouring tubes when an excess volume of biofilm is produced. For example, if for the tube t_{ij} we have that $V_{bf_{ij}}^t < V_{ij}$ equation (5.5) is used to compute the biofilm concentration Φ_{ij}^{t+1} at the next time step. The volume of biofilm at time $t+1$ for the tube t_{ij} can be computed using equation (6), if $V_{bf_{ij}}^{t+1} > V_{ij}$ and excess volume of biofilm is produced in the tube t_{ij},

$$V_{ex_{ij}} = V_{bf_{ij}} - V_{ij}. \tag{5.8}$$

The excess volume of biofilm is distributed to the neighbouring tubes according to the spreading potential, defined for each neighbouring tube t_{ij_k} as [14],

$$w_{ij_k} = \frac{q_{ij_k}C_{ij_k}}{\rho_{bf}V_{ij_k}}, \tag{5.9}$$

where q_{ij_k} is the volumetric flow, C_{ij_k} is the concentration of nutrients, V_{ij_k} is the total pore volume in the neighbouring tube t_{ij_k} and ρ_{bf} is the density of the biofilm. The biofilm is spread only to the downstream tubes. The volume excess given to the tube t_{ij_k} is defined as,

$$V_{ex_{ij_k}} = \frac{V_{ex_{ij}} w_{ij_k}}{\sum_{j_k} w_{ij_k}}, \tag{5.10}$$

the sum is over all the neighbouring downstream tubes.

The total concentration of biofilm $\Phi^{tot}_{ij_k}$ in the neighbouring tube that received the excess volume will be adjusted according to,

$$\Phi^{tot}_{ij_k} = \Phi_{ij_k} + \rho_{bf} \frac{V_{ex_{ij_k}}}{V_{ij_k}}. \tag{5.11}$$

in which the first term in the right hand side is the concentration computed using equation (5.5) and the second term is the concentration due to the spreading of the biofilm. The total volume of biofilm $V^{tot}_{bf_{ij_k}}$ in the neighbouring tubes is computed as,

$$V^{tot}_{bf_{ij_k}} = \frac{\Phi^{tot}_{ij_k}}{\rho_{bf}} V_{ij_k}. \tag{5.12}$$

Additionally, the concentration of the tube t_{ij} where the excess volume is produced is adjusted such that $V_{bf_{ij}} = V_{ij}$, therefore for the next time step equation (5.6) holds and no more biofilm grows in the tube t_{ij}. Following equation (5.5) and (5.6) spreading of the biofilm from the tube t_{ij} to the neighbouring tubes happens only once per tube.

The thickness of the biofilm can be computed from equation (5.12) and is coupled back to equation (5.1) and (5.3).

5.2.2. NUMERICAL METHOD

In this section we are going to outline the numerical procedure used in the model and the computational steps followed in this paper.

Substitution of equation (5.1) into (5.2) for each node n_i leads to a linear system for the pressure at the nodes, p_i, as unknowns. This system is solved assuming Dirichlet boundary conditions for the left and right boundary of the network and considering that there is no flow through the upper and lower boundary, therefore $\frac{\partial p}{\partial n} = 0$ is used in this part of the boundary.

After solving the nodal pressures p_i, we can substitute their values into equation (5.1) to obtain the flux in each tube of the network.

The solution to equation (5.3) is approximated by the use of the finite differences scheme. Then, for each node, n_i, the advection diffusion reaction equation can be written as,

$$\frac{\Delta C_i}{\Delta t} = \left[\frac{\Delta C_i}{\Delta t}\right]_{adv} + \left[\frac{\Delta C_i}{\Delta t}\right]_{diff} + \left[\frac{\Delta C_i}{\Delta t}\right]_{reaction}. \tag{5.13}$$

The advection part can be written as,

$$\left[\frac{\Delta C_i}{\Delta t}\right]_{adv} = \left[\frac{{C_i}^{t+1} - {C_i}^{t}}{\Delta t}\right]_{adv} = \sum_{j \in \Omega_i} \frac{{q_{ij}}^{t}}{V_{ij}} ({C_j}^{t+1} - {C_i}^{t+1}), \tag{5.14}$$

where $\Omega_i = \{j \mid q_{ij}$ is directed towards the node n_i and j is a neighbor of n_i connected through the tube $t_{ij}\}$ and V_{ij} is the total volume of the tube.

The diffusion of nutrients through the water phase can be written as,

$$\left[\frac{\Delta C_i}{\Delta t}\right]_{diff} = \left[\frac{{C_i}^{t+1} - {C_i}^{t}}{\Delta t}\right]_{diff} = \frac{D_w}{l^2}\sum_{j\in S_i}({C_i}^{t+1} - {C_j}^{t+1})\frac{A^t_{w_{ij}}}{A_{tot_{ij}}}, \tag{5.15}$$

where D_w is the diffusion coefficient of the water in the free space available for the bulk water. Further $A_{w_{ij}}$ is the area of the cross section of the bulk water in the tube t_{ij} and $A_{tot_{ij}}$ is the total area of cross section of the tube t_{ij}.

In this model, the reaction takes place in the tubes, therefore we describe the growth of bacteria b_{ij}, in the tube t_{ij}, as,

$$\frac{\Delta b_{ij}}{\Delta t} = \left[\frac{{b_{ij}}^{t+1} - {b_{ij}}^{t}}{\Delta t}\right] = \frac{\lambda^+_b}{Y}\left[\frac{{C_{ij}}^{t}}{E_{bs} + {C_{ij}}^{t}}\right]{b_{ij}}^{t+1}, \tag{5.16}$$

where $C_{ij} = \frac{C_i + C_j}{2}$ is the average concentration of the nodes n_i and n_j and represents the concentration in the tube t_{ij}.

However, in order to give an expression for the last term of equation (5.13) we need to know the concentration of bacteria in each node, b_i, then we average the concentration of bacteria of the tubes connected by the node n_i,

$$\frac{\sum_{j\in S_i} b_{ij}V_{ij}}{\sum_{j\in S_i} V_{ij}} = b_i, \tag{5.17}$$

Now the reaction term can be written as,

$$\left[\frac{\Delta C_i}{\Delta t}\right]_{reaction} = \left[\frac{{C_i}^{t+1} - {C_i}^{t}}{\Delta t}\right]_{reaction} = \frac{\lambda^+_b}{Y}\frac{C_i^{t+1}}{E_{B_s} + C_i^t}b_i^t. \tag{5.18}$$

The thickness of the biofilm is determined by the bacteria consumption as well as by the nutrients concentration. The change of biofilm concentration is given by

$$\frac{\Delta \Phi_{ij}}{\Delta t} = \left[\frac{{\Phi_{ij}}^{t+1} - {\Phi_{ij}}^{t}}{\Delta t}\right] = \lambda^+_\Phi\left[\frac{{C_{ij}}^{t}}{E_{\Phi s} + {C_{ij}}^{t}}\right]\Phi_{ij}^{t+1} - \lambda^-_\Phi\Phi_{ij}^{t+1}. \tag{5.19}$$

The computational procedure used in this work is as follows. Firstly, the external pressure is imposed in the left and right boundary of the network. Subsequently, the pressure in each node is computed from the linear system resulting from the mass conservation in each node. For solving this system, we consider Dirichlet boundary conditions in the left and right boundaries and homogeneous Neumann boundary condition for the upper and lower boundary. The pressures in each node are used to compute the flux in each tube by means of equation (5.2). After this step, we proceed to solve the transport diffusion equation for the nutrients and we compute the concentration of nutrients in each node as well as the concentration of bacteria and the concentration of biofilm in the tubes. Subsequently, the volume of the biofilm is computed using equation (5.7). If an excess volume is produced in one of the tubes, the biofilm will spread to

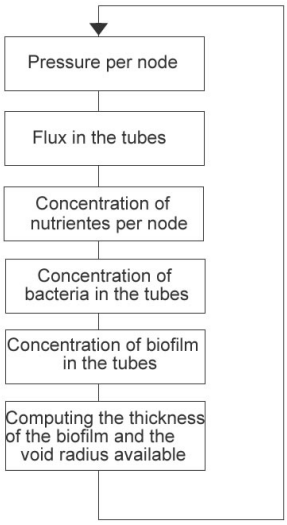

Figure 5.3: Flow chart for each time step

the neighbouring tubes. The volume of biofilm will be computed taking into account the spreading volume. The thickness of the biofilm and the radius of the void space available for water is updated and this process starts again at the next time step (See Figure 2.3).

5.3. RESULTS

First, we investigate the robustness of our results. The evolution of the concentration of nutrients through the network is studied without the presence of biofilm. We solve the advection-diffusion equation for the concentration of nutrients with our model using a mesh with 200 x 10 elements and assuming that all the tubes in the network have the same radius. Under these conditions for the size of the mesh and the uniform size of the radii in all the tubes, we can compare the results with a model based on Continuous Random Walk Theory (CRWT) and with an analytic solution in one dimension [21]. The analytic solution of the advection diffusion equation (equation (5.4) without reaction term) in 1-D is given by:

$$c(x,t) = \frac{C_{in}}{2}[erfc\Big(\frac{x-vt}{\sqrt{4Dt}}\Big) + erfc\Big(\frac{x+vt}{\sqrt{4Dt}}\Big)exp\Big(\frac{vx}{D}\Big)] \tag{5.20}$$

in which erfc is the complementary error function, v the velocity and D the diffusion coefficient.

Figure 5.4 shows the results for the concentration of nutrients in one of the tubes closest to the outlet of the network for our model, a model based on continuous time random walk (CTRW) and the analytic solution given by equation (19). We observe a good agreement between, the CTRW model, the analytic solution and our model.

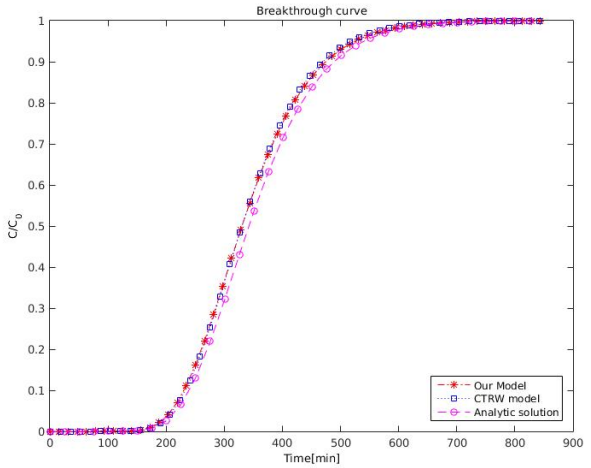

Figure 5.4: Comparison of the solution of the advection-diffusion equation of our model, CTRW and an analytic solution.

The next step was to study the effects of the growth of biofilm on the dynamics of the system. For this second set of simulations we used a mesh with 100 x 60 elements. A Rayleigh distribution for the radii of the tubes of the network was used.

Additionally, only 4% of the tubes were seeded with initial concentration of bacteria $b_0 = 1 \times 10^{-6}\ kg/m^3$ and initial concentration of biofilm $\phi_0 = 1 \times 10^{-6}\ kg/m^3$ in each of the tubes of the network. The complete set of parameters for this second set of simulations is listed in table 2.

Subsequently, we study the evolution of the flux over time. In Figure 5.5 the normalised flux is shown.

The normalised flux is defined as

$$Q_n = \frac{Q}{Q_0} \tag{5.21}$$

where Q is the flux and Q_0 is the initial flux. We observe a decrease of the normalised flux due to the accumulation of biomass in the network. The injection of nutrients through the network and the bacterial conversion of them leads to the clogging of the pores and consequently to the reduction of the normalised flux of the network.

In Figure 5.6 we observe the average concentration of nutrients in the network, C_{av}. This concentration is defined as,

$$C_{av} = \frac{\sum_{ij} C_{ij} V_{ij}}{\sum_{ij} V_{ij}}, \tag{5.22}$$

in which C_{ij} is the concentration in the tube t_{ij} and V_{ij} is the total volume of the tube t_{ij}. The sums are over all the tubes in the network. We observe that the injection of nutrients is very fast, after approximately 50 minutes the nutrients are distributed over

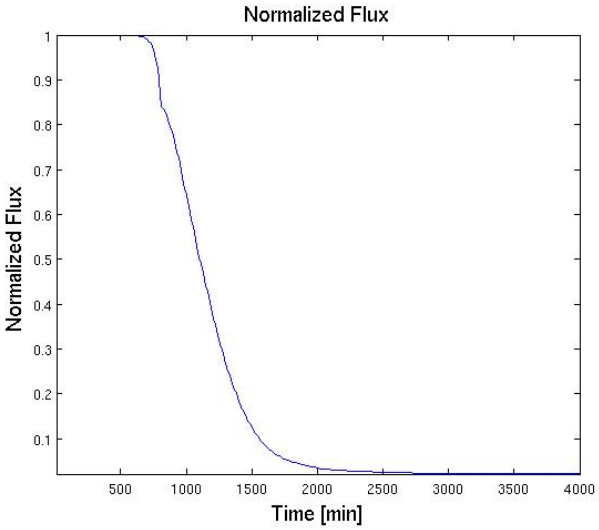

Figure 5.5: Evolution of the normalised flux through the network.

the whole network. The network is full of nutrients for approximately 700 min, hence the biofilm grow uniformly across the network. After 600 minutes we observe a decrease in the average concentration of nutrients in the network due to the consumption by bacteria and biofilm.

Next, we examine the evolution in time of the volume of biofilm in the network. In Figure 5.7 the fraction of volume of biofilm is shown. The fraction of volume of biofilm, V_{pbf}, is defined as,

$$V_{pbf} = \frac{\sum_{ij} V_{bf_{ij}}}{\sum_{ij} V_{ij}}, \tag{5.23}$$

where $V_{bf_{ij}}$ is the volume of biofilm in tube t_{ij} and V_{ij} is the total pore volume of the tube t_{ij}. After 3000 minutes, we observe that approximately 70% of the void space of the network is occupied by the volume of biofilm. Since the biofilm growth in the network is distributed uniformly over the network, there is no preferential growth of the biofilm at the inlet of the network and hence more biomass is necessary to reduce the flux through the network.

For this set of simulations we used 400 time steps, with the size of the time step $dt = 10\ [min]$.

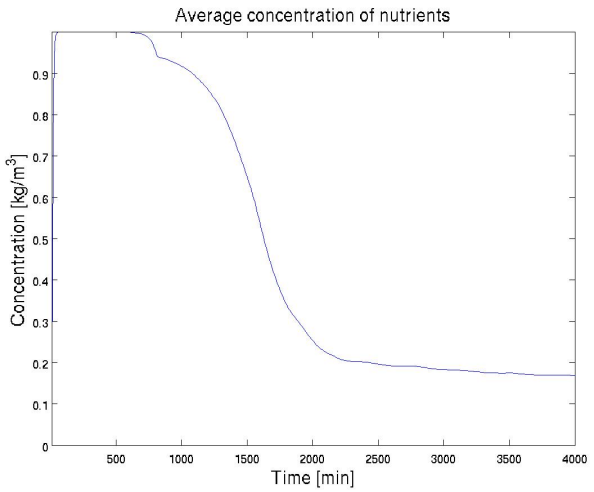

Figure 5.6: Average concentration of nutrients in the network

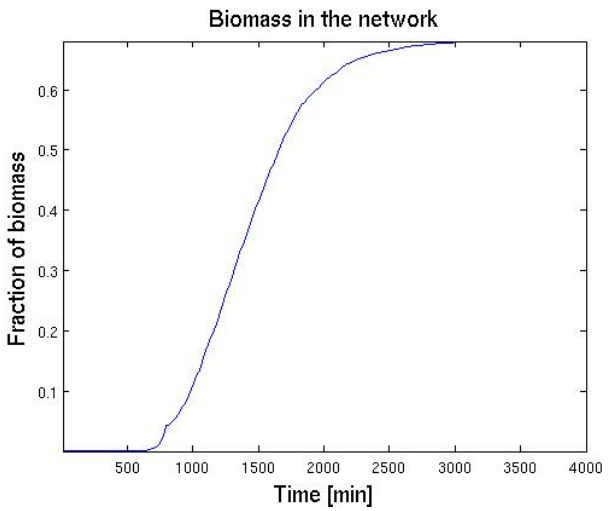

Figure 5.7: Evolution of the biomass in the network

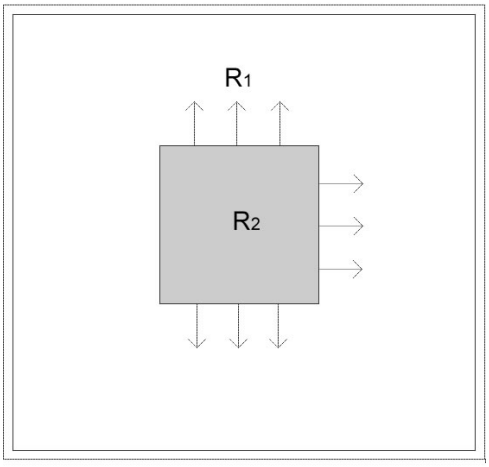

Figure 5.8: Low and high permeability regions, $r_{2_{mean}} < r_{1_{mean}}$

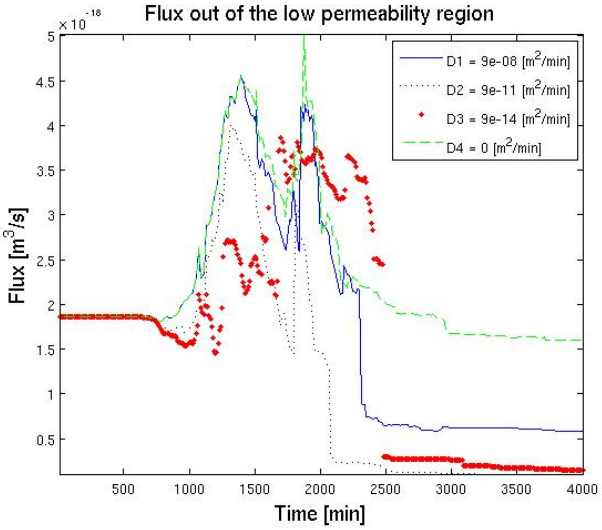

Figure 5.9: Flux measure out of the low permeability region, for different values of the diffusion coefficients in water, realisation 1

Volume through the low permeability region				
Diffusion Coefficient $[m^2/min]$	Time Interval [min]	Volume $[m^3]$ V_{low}	Volume without biofilm $[m^3]$	Increment [%]
9×10^{-8}	710 - 2480	4.69×10^{-15}	3.29×10^{-15}	27
9×10^{-11}	720 - 1940	3.01×10^{-15}	2.27×10^{-15}	32.5
9×10^{-14}	740 - 2310	4.68×10^{-15}	2.92×10^{-15}	60.2
0	740 - 2920	6.1×10^{-15}	4.06×10^{-15}	50.2

Table 5.1

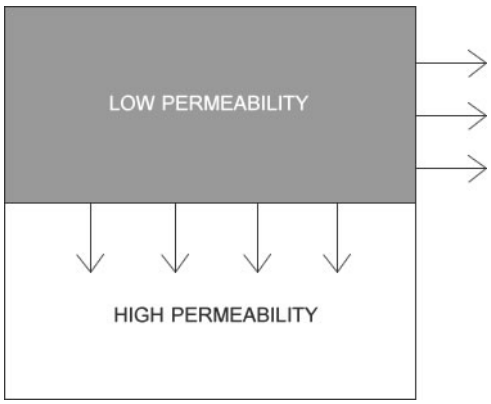

Figure 5.10: Low and high permeability regions, $r_{2_{mean}} < r_{1_{mean}}$

In order to study the possibility to redirect the flux of water to the low permeability regions, we simulate two areas of different permeability in the network. In both regions, a Rayleigh distribution is assumed for the radius but in the low permeability region, the mean radius is smaller than the mean radius of the high permeability region. Two sets of simulations with different geometries are performed. The first geometry is shown in Figure 5.8 and the second geometry is shown in Figure 5.10. As shown in Figure 5.8 the low permeability region is placed at the centre of the network. In the second geometry the low permeability region is placed parallel to the high permeability layer.

In Figure 5.9 the flux out of the low permeability region is shown for the first geometry and for different diffusion coefficients of the nutrients in the water. We observe that the flux out of the low permeability region increases for a period between 800 minutes and 2500 minutes approximately. However to have a better understanding of the effect of selective plugging in flow diverted to low permeability region, the volume of water out of the low permeability region is computed.

The volume out of the low permeability region is computed as follows,

$$V_{low} = \int_{t_0}^{t_f} Q_{low}\, dt. \tag{5.24}$$

The initial time limit t_0 was set as the time for which the normalised flux started to change and the final time limit was set as the last time for which the flux was above

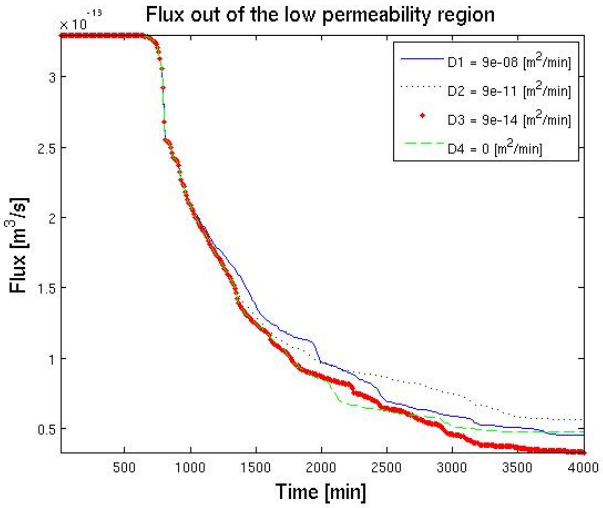

Figure 5.11: Flux measure out of the low permeability region, for different values of the diffusion coefficients in water, realisation 2

the initial value.

In order to compare the results with the case of the absence of biofilm, the volume out of low permeability region when no biofilm is present is computed within the same time limits.

In Table 1 the results for the volume of water out of the low permeability region for different diffusion coefficients with biofilm growth and without biofilm growth are shown. We observe that the volume of water flowing out of this region increases (compare to the case when no biofilm is present) for all the cases within a period which depends on the diffusion coefficient. We observe an increase between 27 % for a diffusion coefficient of 9×10^{-8} and 60% for a diffusion coefficient of 9×10^{-14} .

We observe that if the diffusion coefficient decreases then the increase in the volume of water is more significant. This is because when the diffusion coefficient decreases the transport of nutrients is dominated by the advection term, then nutrients are mainly located in the high permeability regions, which makes selective plugging more efficient.

In Figure 5.11 the results for the second geometry are shown. As we can see, for this geometry there is no increase in the flux through the low permeability region. Since the region of low permeability region is half of the network, when the bacteria starts growing in the high permeability region, there is a large tendency to plug the inlet of the high permeability region and hence the flux through the whole network (including the flux through the low permeability region) will decrease faster than in the first case.

Parameters for the simulations without growth of biofilm		
Name	Symbol	Value
Pore length	l	95×10^{-6} $[m]$
Network size in the x direction	L_x	0.019 $[m]$
Network size in the y direction	L_y	0.00095 $[m]$
Number of tubes in the network	N_a	4210
Mean pore radius	r_{mean}	3.5339×10^{-6} $[m]$ [14]
Global pressure gradient	ΔP	1.6 $[kPa/m]$
Viscosity of water	μ	$4.7 \times 10^{-}5$ $[Pa \cdot min]$
Density of water	ρ_w	1000 $[kg/m^3]$
Diffusion coefficient of water	D_w	3.9710×10^{-8} $[m^2/min]$ [22]
Inlet reservoir concentration	C_{in}	1 $[kg/m^3]$

Table 5.2

5

Parameters for the second series simulation		
Name	Symbol	Value
Mean pore radius	r_{mean}	12.2×10^{-6} $[m]$ [14]
Pore length	l	95×10^{-6} $[m]$
Global pressure gradient	ΔP	1.6 $[kPa/m]$
Viscosity of water	μ	0.001/60 $[Pa \cdot min]$
Density of water	ρ_w	1000 $[kg/m^3]$
Density of biofilm	ρ_{bf}	20 $[kg/m^3]$ [23]
Yield coefficient	Y	0.34 [24]
Biomass specific growth rate for bacteria	λ_b^+	$60 \times 1.1 \times 10^{-4}$ $[min^{-1}]$ [24]
Biomass specific decay rate for bacteria	λ_b^-	$60 \times 1.1 \times 10^{-6}$ $[min^{-1}]$ [14]
Half saturation constant for bacteria	E_{sb}	2 $[kg/m^3]$ [24]
Biomass specific growth rate for biofilm	λ_{bf}^+	$60 \times 1.1 \times 10^{-4}$ $[min^{-1}]$
Biomass specific decay rate for biofilm	λ_{bf}^-	$60 \times 1.1 \times 10^{-6}$ $[min^{-1}]$
Half saturation constant for biofilm	E_{sbf}	2 $[kg/m^3]$
Inlet reservoir concentration	C_{in}	1 $[kg/m^3]$
Initial biomass concentration	b_0	1×10^{-6} $[kg/m^3]$
Biofilm / bulk water viscosity ratio	β	10^3

Table 5.3

Parameters for the third series simulation		
Name	Symbol	Value
Mean pore radius 1	$r_{1_{mean}}$	$12.2 \text{ x } 10^{-6} m$ [14]
Mean pore radius 2	$r_{2_{mean}}$	$1.2 \text{ x } 10^{-7} m$

Table 5.4

5.4. CONCLUSIONS

In this work we studied the biofilm growth in porous media using a two dimensional pore network model. We assumed that the bacteria, necessary for the biofilm growth, were present in 4% of the tubes. The injection of nutrients for the bacteria population growth was described by an advection diffusion equation. Additionally, in our model we consider that the biofilm is able to spread to the neighbouring tubes according to a spreading potential which takes into account the direction of the flux, the velocity and the amount of nutrients available. We studied the hydrodynamic changes caused by biofilm growth using three different geometries for the pore network. In the first geometry a Raleigh distribution was used for the whole network. In the second geometry, we simulate two areas of different permeability, the area of low permeability was placed in the middle of the network. Finally, we used a layered geometry in which the low permeability region is placed parallel to the high permeability region. For the first case, a decrease in the normalised flux of 90% was observed when 70% of the void space in the network was occupied by biofilm.

In the second case, where two regions of different permeability were simulated, the model shows flow diversion to the low permeability region, and an increase of 60% of the flow volume was observed (compared to the flow out of the low permeability region without biofilm growth). This result might indicate an increase in the sweep efficiency in waterflood techniques, however a two phase flow model has to be developed additionally in order to adequately model the production of oil from heterogeneous reservoirs. However, after some time the flux through the low permeability region starts to decrease. Therefore, the injection of nutrients has to be stopped in order to prevent clogging of the low permeability regions. For the third case the total flux through the low permeability region does not increase, since there is more tendency to plug the inlet in the network. For the second and third geometry diffusion coefficient for water was varied. For the second geometry, it was observed that the flux through the low permeability region was larger when the diffusion coefficient was smaller. It could be of greatest interest to investigate the dependence of the sweep efficiency on other parameters such as the pressure drop in the network, the coefficient of bacterial growth or the concentration of nutrients in the network. Finally, the results obtained in this work can be used for a future up-scaling technique to the real reservoir scale in oil reservoir simulations.

We observed that the porosity does not change significantly, it does not depend on the permeability-porosity relation. The permeability is affected more, however the coupling of the velocity field back to the porosity change is not strong enough apparently to cause significant changes in the porosity field. But we expect changes if we increase the contribution of the velocity term in equation (1b), which is achieved by the increase of

the pressure difference.

REFERENCES

[1] R. Sen, *Biotechnology in petroleum recovery: the microbial eor,* Progress in energy and combustion Science **34**, 714 (2008).

[2] R. T. Armstrong and D. Wildenschild, *Investigating the pore-scale mechanisms of microbial enhanced oil recovery,* Journal of Petroleum Science and Engineering **94**, 155 (2012).

[3] K. Behlulgil, T. Mehmetoglu, and S. Donmez, *Application of microbial enhanced oil recovery technique to a turkish heavy oil,* Applied microbiology and biotechnology **36**, 833 (1992).

[4] M. M. Yakimov, M. M. Amro, M. Bock, K. Boseker, H. L. Fredrickson, D. G. Kessel, and K. N. Timmis, *The potential of bacillus licheniformis strains for in situ enhanced oil recovery,* Journal of Petroleum Science and Engineering **18**, 147 (1997).

[5] Q. Li, C. Kang, H. Wang, C. Liu, and C. Zhang, *Application of microbial enhanced oil recovery technique to daqing oilfield,* Biochemical Engineering Journal **11**, 197 (2002).

[6] R. A. Raiders, R. M. Knapp, and M. J. McInerney, *Microbial selective plugging and enhanced oil recovery,* Journal of industrial microbiology **4**, 215 (1989).

[7] A. Sheehy *et al.*, *Field studies of microbial eor,* in *SPE/DOE Enhanced Oil Recovery Symposium* (Society of Petroleum Engineers, 1990).

[8] T. Jack, L. Stehmeier, M. Islam, and F. Ferris, *Ch. f-6 microbial selective plugging to control water channeling,* in *Developments in Petroleum Science*, Vol. 31 (Elsevier, 1991) pp. 433–440.

[9] S. L. Bryant, T. P. Lockhart, *et al.*, *Reservoir engineering analysis of microbial enhanced oil recovery,* SPE Reservoir Evaluation & Engineering **5**, 365 (2002).

[10] W. Van Wijngaarden, F. Vermolen, G. Van Meurs, and C. Vuik, *A mathematical model and analytical solution for the fixation of bacteria in biogrout,* Transport in porous media **92**, 847 (2012).

[11] C. Picioreanu, J.-U. Kreft, and M. C. Van Loosdrecht, *Particle-based multidimensional multispecies biofilm model,* Applied and environmental microbiology **70**, 3024 (2004).

[12] T. Pintelon, D. Graf von der Schulenburg, and M. Johns, *Towards optimum permeability reduction in porous media using biofilm growth simulations,* Biotechnology and Bioengineering **103**, 767 (2009).

[13] D. G. von der Schulenburg, T. Pintelon, C. Picioreanu, M. Van Loosdrecht, and M. Johns, *Three-dimensional simulations of biofilm growth in porous media,* AIChE Journal **55**, 494 (2009).

[14] C. Ezeuko, A. Sen, A. Grigoryan, and I. Gates, *Pore-network modeling of biofilm evolution in porous media,* Biotechnology and bioengineering **108**, 2413 (2011).

[15] M. Thullner, J. Zeyer, and W. Kinzelbach, *Influence of microbial growth on hydraulic properties of pore networks,* Transport in porous media **49**, 99 (2002).

[16] B. J. Suchomel, B. M. Chen, and M. B. Allen, *Macroscale properties of porous media from a network model of biofilm processes,* Transport in porous media **31**, 39 (1998).

[17] B. Chen-Charpentier, *Numerical simulation of biofilm growth in porous media,* Journal of computational and applied mathematics **103**, 55 (1999).

[18] A. Raoof and S. M. Hassanizadeh, *A new method for generating pore-network models of porous media,* Transport in porous media **81**, 391 (2010).

[19] D.-S. Kim and H. S. Fogler, *Biomass evolution in porous media and its effects on permeability under starvation conditions,* Biotechnology and Bioengineering **69**, 47 (2000).

[20] M. Thullner and P. Baveye, *Computational pore network modeling of the influence of biofilm permeability on bioclogging in porous media,* Biotechnology and Bioengineering **99**, 1337 (2008).

[21] A. W. Warrick, *Soil water dynamics* (Oxford University Press, 2003).

[22] J. Lawrence, G. Wolfaardt, and D. Korber, *Determination of diffusion coefficients in biofilms by confocal laser microscopy,* Applied and environmental microbiology **60**, 1166 (1994).

[23] K. S. Ro and J. Neethling, *Biofilm density for biological fluidized beds,* Research journal of the water pollution control federation , 815 (1991).

[24] R. Bakke, M. G. Trulear, J. Robinson, and W. G. Characklis, *Activity of pseudomonas aeruginosa in biofilms: steady state,* Biotechnology and bioengineering **26**, 1418 (1984).

6

THE POROSITY-PERMEABILITY RELATION FOR PORE-ELASTICITY PROBLEMS

6.1. INTRODUCTION

The porosity of a porous medium may change over time in some physical problems. For example if a fluid is injected at high flow rate in a porous medium, the grains that formed the porous medium will be pushed from the region near the inlet towards the region near the outlet. This displacement of the grains might cause a local change of the porosity (an increase near the inlet and a decrease near the outlet). This porosity change might cause a decrease or a blockage of the flow through the whole medium. This means that the permeability of the medium would be almost zero even though the global porosity is non zero. This phenomenon is not taken into account in usual porosity-permeability relations such as the Kozeny-Carman relation.

The problem mentioned above is studied on the scale of meters. In this chapter we will look into the problem of a much finer scale (in the order of centimetres). We will then translate these results to the meter scale.

We investigate two physical problems in which the blockage of the flow through a porous medium is observed even though the porosity is different from zero. This means that we will need to use a porosity-permeability relation that exhibits this feature. We use a porosity-permeability relation that was obtained when we allowed the biofilm to grow randomly in pore networks. We will call this kind of relation a random growth porosity-permeability relation.

Whenever the porosity coincides with the percolation threshold p_c for a particular network topology the flow through the network is completely blocked. Furthermore, our permeability-porosity relation exhibits a linear decrease from $(\phi_n = 1, K_n = 1)$ to $(\phi_n =$

$p_c, K_n = 0$), where ϕ_n is the normal porosity defined as $\phi_n = \phi/\phi_0$ with ϕ_0 the initial porosity of the network.

6.2. GOVERNING EQUATIONS

The model provided by Biot's theory of linear poroelasticity with single-phase flow [1] is used in this study to determine the local displacement of the grains of a porous medium and the fluid flow through the pores, assuming that the deformations are very small. The fluid-saturated porous medium has a linearly elastic solid matrix and is saturated by an incompressible Newtonian fluid. Let $\Omega \subset \mathbb{R}^2$ denote the computational domain with boundary Γ, and $\mathbf{x} = (x, y) \in \Omega$. Furthermore, t denotes time, belonging to a half-open time interval $I = (0, T]$, with $T > 0$. The initial boundary value problem for the consolidation process of an incompressible fluid flow in a deformable porous medium is stated as follows [2, 3]:

$$\text{equilibrium equations:} \quad -\nabla \cdot \boldsymbol{\sigma}' + \nabla p = \mathbf{0} \qquad \text{on } \Omega \times I; \tag{6.1a}$$

$$\text{continuity equation:} \quad \frac{\partial}{\partial t}(\nabla \cdot \mathbf{u}) + \nabla \cdot \mathbf{v} = 0 \qquad \text{on } \Omega \times I, \tag{6.1b}$$

where $\boldsymbol{\sigma}'$ and $\mathbf{v}$ are defined by the following equations

$$\text{Biot's constitutive equations:} \quad \boldsymbol{\sigma}' = \lambda(\nabla \cdot \mathbf{u})\mathbf{I} + \mu(\nabla \mathbf{u} + \nabla \mathbf{u}^T); \tag{6.2}$$

$$\text{Darcy's law:} \quad \mathbf{v} = -\frac{K}{\eta}\nabla p. \tag{6.3}$$

In the above relations, $\boldsymbol{\sigma}'$ denotes the effective stress tensor, p the pore pressure, $\mathbf{u}$ the displacement vector, $\mathbf{v}$ Darcy's velocity, λ and μ the Lamé coefficients; K the permeability of the porous medium and η the fluid viscosity. In addition, appropriate boundary and initial conditions are specified in Section 6.4.

6.2.1. THE POROSITY-PERMEABILITY RELATIONS

In order to investigate the interaction between the mechanical deformations and the fluid flow after injection of water into the inlet, we consider in this study the spatial dependency of the porosity and the permeability of the porous medium. The porosity ϕ is computed from the displacement vector using the porosity-dilatation relation (see [4])

$$\phi(\mathbf{x}, t) = 1 - \frac{1 - \phi_0}{\exp(\nabla \cdot \mathbf{u})}, \tag{6.4}$$

with ϕ_0 the initial porosity. Subsequently, the permeability can be determined using the Kozeny-Carman equation [5]

$$K(\mathbf{x}, t) = \frac{d_s^2}{180} \frac{\phi(\mathbf{x}, t)^3}{(1 - \phi(\mathbf{x}, t))^2}, \tag{6.5}$$

where d_s is the mean grain size of the soil.

The Kozeny-Carman relation assumes that the permeability becomes zero if and only if the porosity also becomes zero. A new approach for the relation between the porosity

and the permeability is inspired by the fluid flow into a network, where the fluid flows through the edges (channels) of the network. We describe this phenomenon as the random closing of pores. This means that we can use the permeability-porosity relations for random growth that we are going to obtain in this chapter. The poro-elasticity problem on the meter scale is solved in sub-domains of the order of square centimetres. Each cell of the square centimetre has its own porosity. This porosity is changed due to the fast injection of water. This injection causes some pores to close. In a square shaped network, the network-inspired relation will look like:

$$K(\mathbf{x},t) = \begin{cases} 0 & \phi_n < 0.4935 \\ (-0.9743 + 1.9743\phi_n)K_0 & \phi_n \geq 0.4935 \end{cases}, \tag{6.6}$$

where K_0 is the initial permeability computed using the Kozeny-Carman relation and ϕ_n is the normal porosity defined as $\phi_n = \phi/\phi_0$. The network-inspired relation takes into account the case that channels in the porous medium are blocked in such a way that there are no connected paths any more. In this case, the fluid will stop flowing and the permeability will be expected to become zero. While for a random topology, the network-inspired relation states:

$$K(\mathbf{x},t) = \begin{cases} 0 & \phi_n < p_c \\ \frac{\phi_n - p_c}{1-p_c} K_0 & \phi_n \geq p_c \end{cases}, \tag{6.7}$$

where the percolation threshold p_c, which represents the minimal porosity needed to have connection via voids or channels from one end to the other, depends on the topology of the network. In the coming section we will derive the permeability-porosity relation using a network model.

6.3. NETWORK COMPUTATION OF POROSITY-PERMEABILITY RELATIONS

In this section we investigate the random growth of biofilm in the network. We use three different networks in 2D: quadrangular, triangular and triangular unstructured and in 3D we study a cubic network.

In the random growth problem solving the equation for the transport of nutrients is not needed. The tubes in the network are assumed to be filled with biofilm completely or to be entirely empty. The tubes which are filled are chosen randomly; the number of tubes filled with biofilm goes from 1% to 100%. The normalised permeability for the network is computed for each percentage of the number of filled tubes. For each configuration, 500 sample simulations have been performed. This yields a relation between the porosity and the permeability of the network.

6.3.1. QUADRANGULAR NETWORK

First we describe the results obtained for the quadrangular network. In this case we use a network with $N_x = 100$ and $N_y = 60$. We compute the fraction of biomass S_b needed to

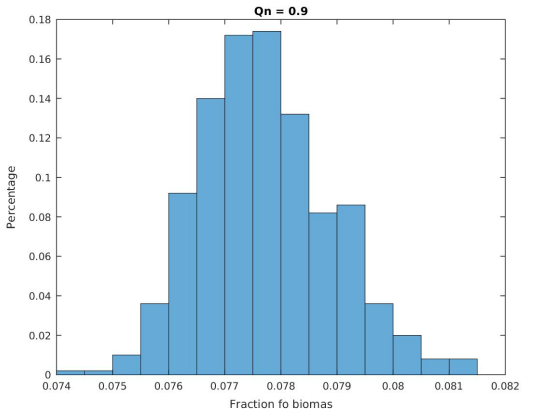

Figure 6.1: The histogram for a normalised permeability $0.85 < K_i < 0.95$ for a rectangular network. The fraction of biomass follows a distribution, with average around $S_b = 0.0777$ and standard deviation 0.0012

K_n	Average value of S_n	Standard deviation σ
$0.85 < K_n < 0.95$	0.0777	0.0012
$0.75 < K_n < 0.85$	0.1273	0.0014
$0.65 < K_n < 0.75$	0.1760	0.0016
$0.55 < K_n < 0.65$	0.2240	0.0018
$0.45 < K_n < 0.55$	0.2717	0.0019
$0.35 < K_n < 0.45$	0.3195	0.0022
$0.25 < K_n < 0.35$	0.3678	0.0023
$0.15 < K_n < 0.25$	0.4188	0.0026
$0.05 < K_n < 0.15$	0.4789	0.0037

Table 6.1: Average and standard deviations for the fraction of biomass S_n for the quadrangular network

obtain a normalised permeability K_n such that $K_i - 0.05 < K_n < K_i + 0.05$, where $K_i = 0.9$, $K_i = 0.8$, ... , $K_i = 0.1$. In Figure 6.1 to Figure 6.3 the histograms for $K_i = 0.9$, $K_i = 0.5$ and $K_i = 0.1$ are shown. The means and the standard deviations of the distributions of S_b depend on the normalised permeability K_n; see Table 6.1.

6.3.2. TRIANGULAR NETWORK

In this section we present the results obtained with a triangular network which is shown in Figure 6.4. The number of nodes in the x direction $N_x = 100$ and the number of nodes in y direction $N_y = 60$. The coordination number of the interior nodes is six or four (See Figure 6.4). We perform the same simulations as in the quadrangular network. In Figure 6.5 to Figure 6.7 the histograms for $K_i = 0.9$, $K_i = 0.5$ and $K_i = 0.1$ are shown. Since the number of tubes filled with biomass are chosen from one per cent to hundred per cent some fractions of biomass are not allowed in the network therefore some bins in the histograms are empty as seen in Figure 6.7. The means and the standard deviations of these distributions depend on the normalised permeability K_n; see Table 6.2.

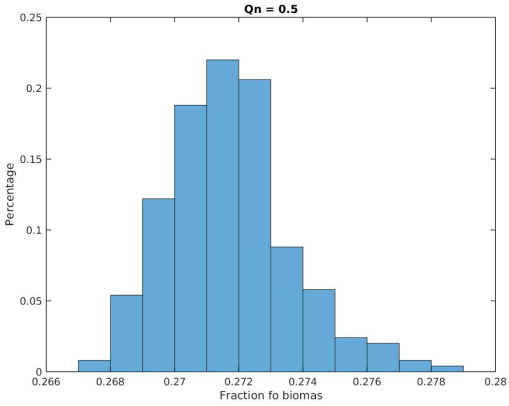

Figure 6.2: The histogram for a normalised permeability $0.45 < K_i < 0.55$ for a rectangular network. The fraction of biomass follows a distribution, with average around $S_b = 0.2717$ and standard deviation 0.0019

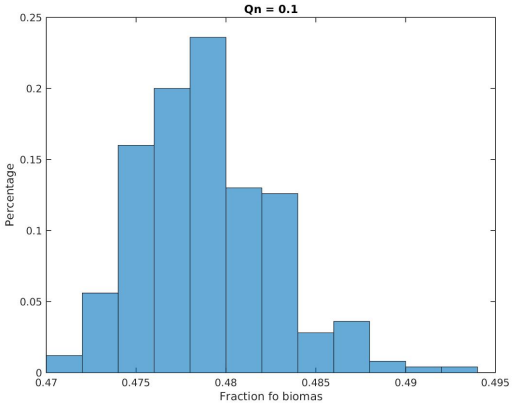

Figure 6.3: The histogram for a normalised permeability $0.05 < K_i < 0.15$ for a rectangular network. The fraction of biomass follows a distribution, with average around $S_b = 0.4789$ and standard deviation 0.0037

K_n	Average value of S_n	Standard deviation σ
$0.85 < K_n < 0.95$	0.1052	0.0103
$0.75 < K_n < 0.85$	0.1687	0.0104
$0.65 < K_n < 0.75$	0.2333	0.0111
$0.55 < K_n < 0.65$	0.2975	0.0108
$0.45 < K_n < 0.55$	0.3604	0.0105
$0.35 < K_n < 0.45$	0.4240	0.0102
$0.25 < K_n < 0.35$	0.4882	0.0099
$0.15 < K_n < 0.25$	0.5522	0.0086
$0.05 < K_n < 0.15$	0.6226	0.0077

Table 6.2: Average and standard deviations for the fraction of biomass S_n for the triangular network

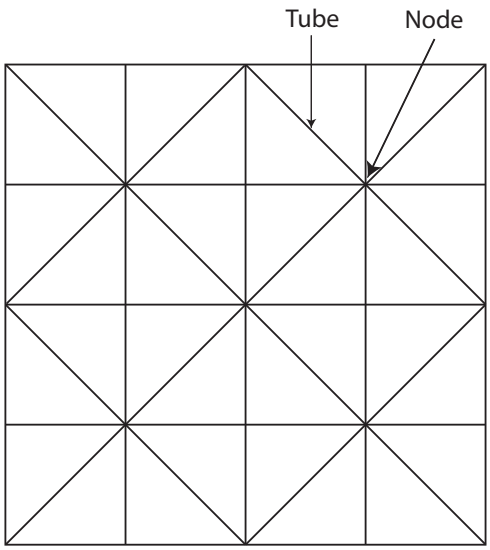

Figure 6.4: Triangular Network

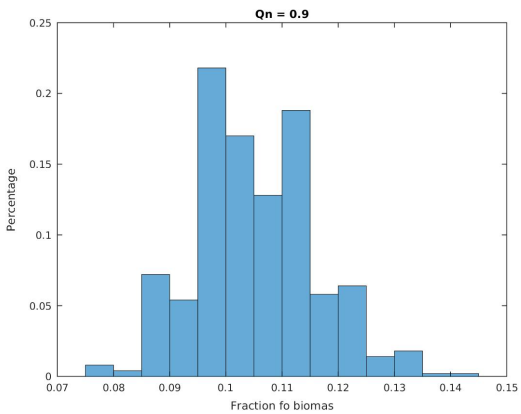

Figure 6.5: The histogram for a normalised permeability $0.85 < K_i < 0.95$ for a triangular network. The fraction of biomass follows a distribution, with average around $S_b = 0.1052$ and standard deviation 0.0103

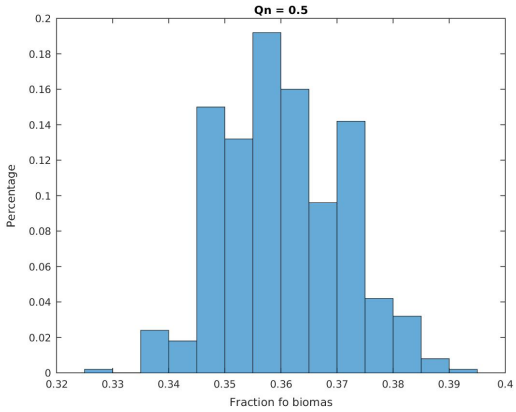

Figure 6.6: The histogram for a normalised permeability $0.45 < K_i < 0.55$ for a triangular network. The fraction of biomass follows a distribution, with average around $S_b = 0.3604$ and standard deviation 0.0105

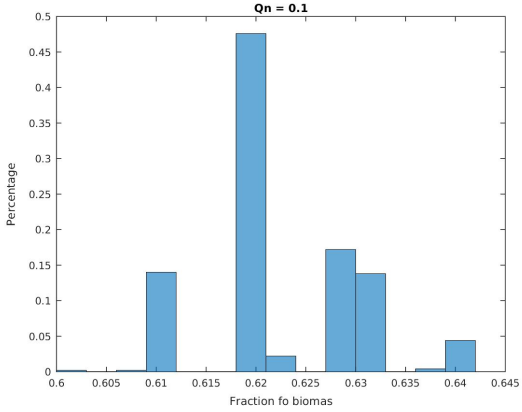

Figure 6.7: The histogram for a normalised permeability $0.05 < K_i < 0.15$ for a triangular network. The fraction of biomass follows a distribution, with average around $S_b = 0.6226$ and standard deviation 0.0077

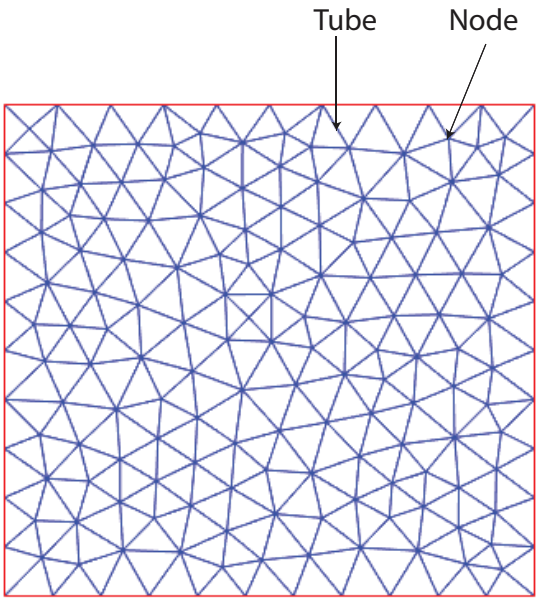

Figure 6.8: Unstructured triangular network

6.3.3. TRIANGULAR UNSTRUCTURED NETWORK

In this section we present the results obtained with a triangular unstructured network which is shown in Figure 6.8. The total number of nodes in this network is 6921. We perform the same simulations as in the quadrangular network. In Figure 6.9 to Figure 6.11 the histograms for these normalised permeabilities are shown. The means and the standard deviations depend on the normalised permeability K_n; see Table 6.3.

6.3.4. CUBIC NETWORK

In this section we present the results obtained with a cubic network in 3D which is shown in Figure 4.1. The number of nodes in the x direction $N_x = 25$ and the number of nodes in y direction is $N_y = 25$ and the number of nodes in the z direction is $N_z = 25$. The coordination number of the interior nodes is 6. We perform the same simulations as in the quadrangular network. In Figure 6.12 to Figure 6.14 the histograms for the histograms for $K_i = 0.9$, $K_i = 0.5$ and $K_i = 0.1$ are shown. Since the number of tubes filled with biomass is chosen from one per cent to hundred per cent some fractions of biomass are not allowed in the network and hence some empty bins are observed in these figures. The averages and the standard deviations depend on the normalised permeability K_n; see Table 6.4.

Finally we compare the results obtained for the relation between the permeability and the porosity for the quadrangular network, triangular network and triangular unstructured network. We observe that the permeability becomes zero at the porosities cor-

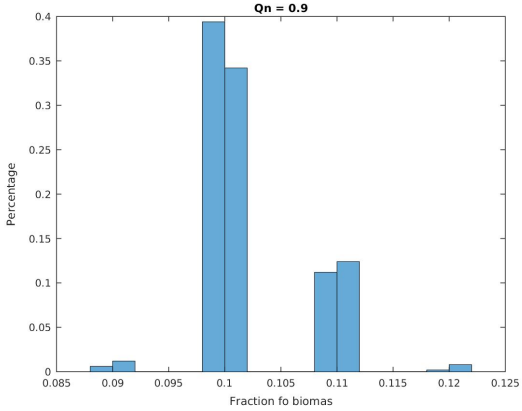

Figure 6.9: The histogram for a normalised permeability $0.85 < K_i < 0.95$ for a triangular unstructured network. The fraction of biomass follows a distribution, with average around $S_b = 0.1024$ and standard deviation 0.0049

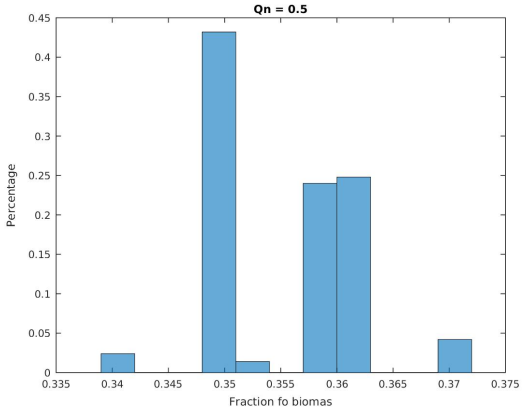

Figure 6.10: The histogram for a normalised permeability $0.45 < K_i < 0.55$ for a triangular unstructured network. The fraction of biomass follows a distribution, with average around $S_b = 0.3555$ and standard deviation 0.0062

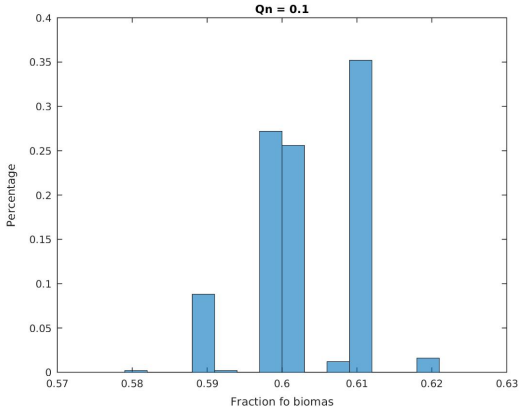

Figure 6.11: The histogram for a normalised permeability $0.05 < K_i < 0.15$for a triangular unstructured network. The fraction of biomass follows a distribution, with average around $S_b = 0.6030$ and standard deviation 0.0066

K_n	Average value of S_n	Standard deviation σ
$0.85 < K_n < 0.95$	0.1024	0.0049
$0.75 < K_n < 0.85$	0.1667	0.0059
$0.65 < K_n < 0.75$	0.2308	0.0061
$0.55 < K_n < 0.65$	0.2938	0.0063
$0.45 < K_n < 0.55$	0.3555	0.0062
$0.35 < K_n < 0.45$	0.4168	0.0063
$0.25 < K_n < 0.35$	0.4773	0.0059
$0.15 < K_n < 0.25$	0.5385	0.0062
$0.05 < K_n < 0.15$	0.6030	0.0066

Table 6.3: Average and standard deviations for the fraction of biomass S_n for the unstructured triangular network

K_n	Average value of S_n	Standard deviation σ
$0.85 < K_n < 0.95$	0.1011	0.0023
$0.75 < K_n < 0.85$	0.1671	0.0026
$0.65 < K_n < 0.75$	0.2326	0.0027
$0.55 < K_n < 0.65$	0.2984	0.0028
$0.45 < K_n < 0.55$	0.3639	0.0029
$0.35 < K_n < 0.45$	0.4300	0.0027
$0.25 < K_n < 0.35$	0.4978	0.0029
$0.15 < K_n < 0.25$	0.5700	0.0026
$0.05 < K_n < 0.15$	0.6558	0.0029

Table 6.4: Average and standard deviations for the fraction of biomass S_n for the cubic network

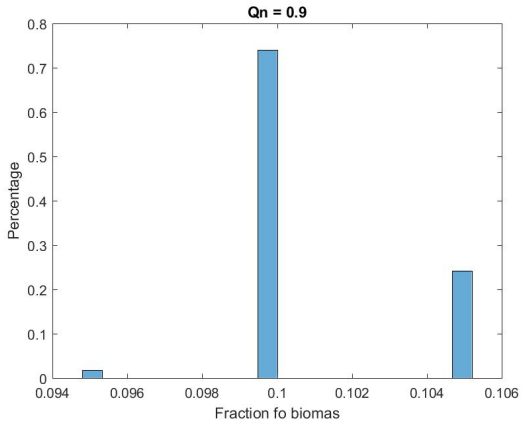

Figure 6.12: The histogram for a normalised permeability $0.85 < K_i < 0.95$ for a cubic network. The fraction of biomass average is around $S_b = 0.1052$ and standard deviation 0.0103

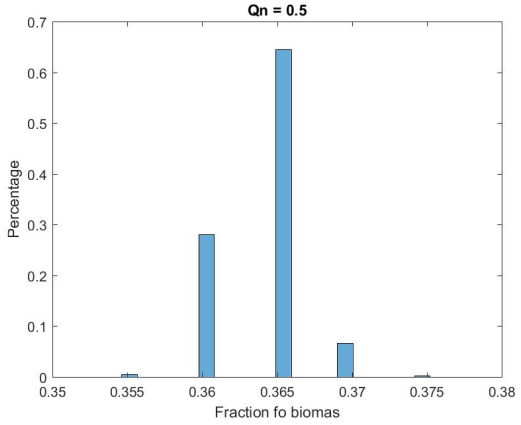

Figure 6.13: The histogram for a normalised permeability $0.45 < K_i < 0.55$ for a cubic network. The fraction of biomass average is around $S_b = 0.3555$ and standard deviation 0.0062

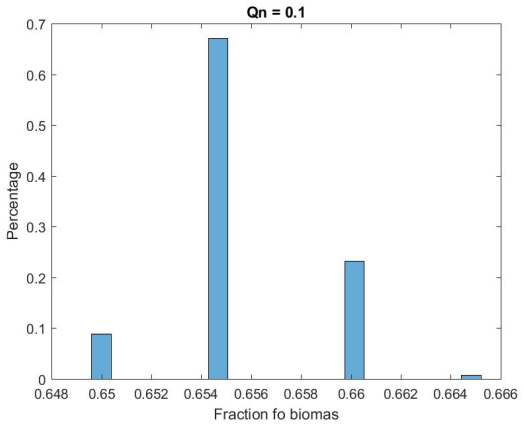

Figure 6.14: The histogram for a normalised permeability $0.05 < K_i < 0.15$ for a cubic network. The fraction of biomass average is around $S_b = 0.6030$ and standard deviation 0.0066

Network	p_c	K_n
Quadrangular	0.4935	1.6×10^{-3}
Triangular unstructured	0.3438	1×10^{-3}
Triangular structured	0.3232	1.6×10^{-3}
3D Cubic	0.2621	1.2×10^{-3}

Table 6.5: Percolation threshold for different network topologies

responding to the different percolation thresholds. We also observe that the relation between permeability and porosity exhibits an almost linear decrease for all four networks. Hence the slope of these lines depends on the network topology via the percolation threshold.

The different percolation thresholds for different topologies yield different values for the slope of the lines. In general the exact configuration or topology of the porous medium is not known explicitly. This means that we use an average slope with a certain uncertainty. We can both quantify the slope and the uncertainty by our numerical results. In Table 6.5 the percolation threshold for the different network topologies used in this chapter is shown. In addition the normalised permeability for these values of porosity is shown.

6.4. PROBLEM FORMULATION

The following numerical experiments are designed to study the different relations for the porosity and the permeability.

6.4.1. PROBLEM WITH HIGH PUMP PRESSURE

In this numerical experiment, the infiltration of a fluid through a filter into a 2D area is shown in Figure 6.16. During the infiltration a high pump pressure is used to inject water into the porous medium.

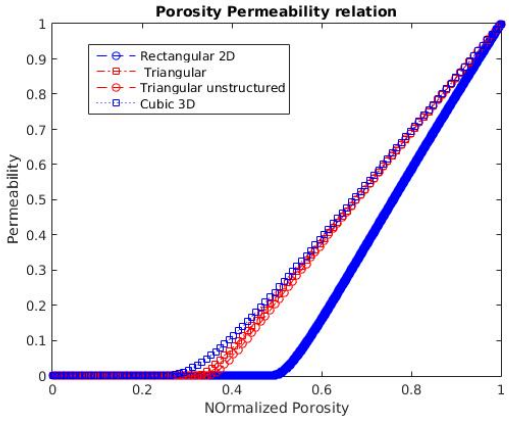

Figure 6.15: Permeability vs Porosity

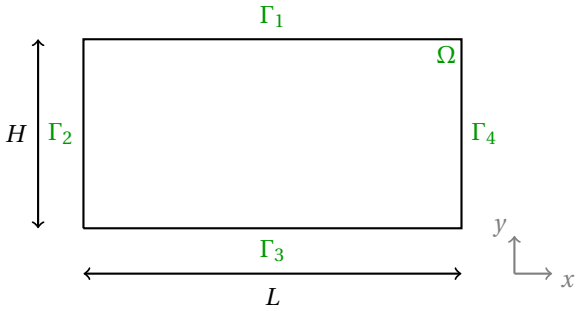

Figure 6.16: Sketch of the setup for the 2D problem with high pump pressure.

The computational domain Ω is a two-dimensional surface with Cartesian coordinates $\mathbf{x} = (x, y)$, as depicted in Figure 6.16. In order to solve this problem, Biot's consolidation model, as described in Section 6.2, is applied on the computational domain Ω with width L and height H. The fluid is injected into the soil through a filter placed on the boundary segment Γ_2. More precisely, the boundary conditions for this problem are given as follows:

$$\frac{K}{\eta}\nabla p \cdot \mathbf{n} = 0 \quad \text{on} \quad \mathbf{x} \in \Gamma_1 \cup \Gamma_3; \tag{6.8a}$$

$$p = p_{pump} \quad \text{on} \quad \mathbf{x} \in \Gamma_2; \tag{6.8b}$$

$$p = 0 \quad \text{on} \quad \mathbf{x} \in \Gamma_4; \tag{6.8c}$$

$$(\boldsymbol{\sigma}'\mathbf{n}) \cdot \mathbf{t} = 0 \quad \text{on} \quad \mathbf{x} \in \Gamma_1 \cup \Gamma_3 \cup \Gamma_4; \tag{6.8d}$$

$$\mathbf{u} \cdot \mathbf{n} = 0 \quad \text{on} \quad \mathbf{x} \in \Gamma_1 \cup \Gamma_3 \cup \Gamma_4; \tag{6.8e}$$

$$\boldsymbol{\sigma}'\mathbf{n} = \mathbf{0} \quad \text{on} \quad \mathbf{x} \in \Gamma_2, \tag{6.8f}$$

where $\mathbf{t}$ is the unit tangent vector at the boundary, $\mathbf{n}$ the outward unit normal vector and

p_{pump} is a prescribed high pump pressure due to the injection of the fluid. Figure 6.16 shows the definition of the boundary segments. Initially, the following condition is fulfilled:

$$\mathbf{u}(\mathbf{x},0) = 0 \quad \text{for} \quad \mathbf{x} \in \Omega. \tag{6.9}$$

6.4.2. SQUEEZE PROBLEM

The infiltration of a fluid through a filter into a 2D area is shown in Figure 6.17. In this numerical experiment, the porous medium is squeezed by applying a vertical load on the middle of the top and bottom edges of the domain.

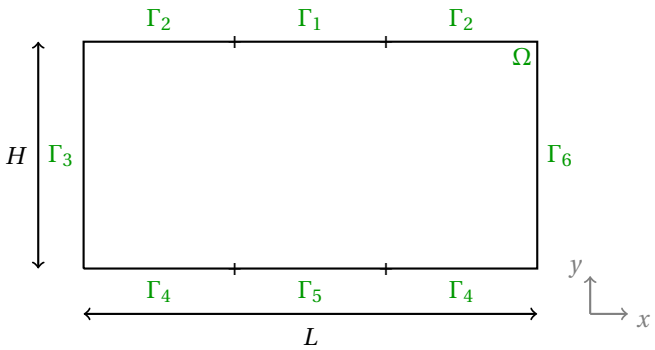

Figure 6.17: Sketch of the setup for the 2D problem.

This problem is solved using Biot's consolidation model, that is applied on the computational domain Ω with width L and height H. The fluid is injected into the soil through a filter placed on the boundary segment Γ_3. More precisely, the boundary conditions for this problem are given as follows:

$$\frac{K}{\eta}\nabla p \cdot \mathbf{n} = 0 \quad \text{on} \quad \mathbf{x} \in \Gamma_1 \cup \Gamma_2 \cup \Gamma_4 \cup \Gamma_5; \tag{6.10a}$$

$$p = p_{pump} \quad \text{on} \quad \mathbf{x} \in \Gamma_3; \tag{6.10b}$$

$$p = 0 \quad \text{on} \quad \mathbf{x} \in \Gamma_6; \tag{6.10c}$$

$$\boldsymbol{\sigma}'\mathbf{n} = (0, -\sigma_0')^T \quad \text{on} \quad \mathbf{x} \in \Gamma_1; \tag{6.10d}$$

$$\boldsymbol{\sigma}'\mathbf{n} = \mathbf{0} \quad \text{on} \quad \mathbf{x} \in \Gamma_2 \cup \Gamma_3 \cup \Gamma_4; \tag{6.10e}$$

$$\boldsymbol{\sigma}'\mathbf{n} = (0, \sigma_0')^T \quad \text{on} \quad \mathbf{x} \in \Gamma_5; \tag{6.10f}$$

$$\mathbf{u} = \mathbf{0} \quad \text{on} \quad \mathbf{x} \in \Gamma_6, \tag{6.10g}$$

where $\mathbf{t}$ is the unit tangent vector at the boundary, $\mathbf{n}$ the outward unit normal vector, p_{pump} is a prescribed pump pressure due to the injection of the fluid and σ_0' is the intensity of a uniform vertical load. Figure 6.17 shows the definition of the boundary segments. Initially, the following condition is fulfilled:

$$\mathbf{u}(\mathbf{x},0) = 0 \quad \text{for} \quad \mathbf{x} \in \Omega. \tag{6.11}$$

6.5. NUMERICAL RESULTS FOR THE UPSCALED PROBLEM

The Galerkin finite element method, with triangular Taylor-Hood elements [6, 7], is adopted to solve the discretised quasi-two-dimensional problem (6.1). The displacements are spatially approximated by quadratic basis functions, whereas a continuous piecewise linear approximation is used for the pressure field. For the time integration, the backward Euler method is applied. The numerical investigations are carried out using the matrix-based software package MATLAB (version R2015a).

The computational domain is a rectangular surface with width $L = 2.0\,\text{m}$ and height $H = 1.0\,\text{m}$. The domain is discretised using a regular triangular grid, with $\Delta x = \Delta y = 0.02$. In addition, values for some model parameters have been chosen based on literature (see Table 6.6).

Table 6.6: An overview of the values of the model parameters.

Property	Symbol	Value	Unit
Young's modulus	E	$35 \cdot 10^6$	Pa
Poisson's ratio	ν	0.3	-
Fluid viscosity	η	$1.307 \cdot 10^{-3}$	$\text{Pa} \cdot \text{s}$
Initial porosity	ϕ_0	0.4	-
Mean grain size	d_s	$0.2 \cdot 10^{-3}$	m
Pump pressure	p_{pump}	$50 \cdot 10^5$ / $5 \cdot 10^5$	Pa
Uniform load	σ_0'	$3 \cdot 10^6$	N/m^2

Furthermore, the Lamé coefficients λ and μ are related to Young's modulus E and Poisson's ratio ν by [2]

$$\lambda = \frac{\nu E}{(1+\nu)(1-2\nu)}, \quad \mu = \frac{E}{2(1+\nu)}. \tag{6.12}$$

The impact of the porosity-permeability relation on the water flow is defined in this study as the impact on the time average of the volume flow rate $\overline{Q}_{out}$ at a distance L from the injection filter. In the generations of the simulation results, the time step size is chosen to be $\Delta t = 0.5$.

6.5.1. NUMERICAL RESULTS FOR THE PROBLEM WITH HIGH PUMP PRESSURE

In order to obtain some insight into the impact of a high pump pressure on the water flow, we present an overview of the simulation results in Figures 6.18 - 6.20. In these simulations, water is injected into the soil at a constant pump pressure of 50.0 bar. The simulated pressure, fluid velocity, permeability and porosity profiles that have been obtained using the Kozeny-Carman relation are provided in Figure 6.18, while the simulated results that have been obtained using the network-inspired relation with $p_c = 0.3232$, corresponding with a triangular structured network, are provided in Figure 6.19. In Figure 6.20, the simulated results that have been obtained using the network-inspired relation with $p_c = 0.4935$, corresponding with a quadrangular network, are depicted.

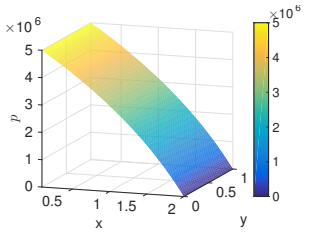

(a) Numerical solution for the pressure.

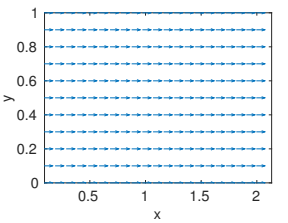

(b) Numerical solution for the fluid velocity.

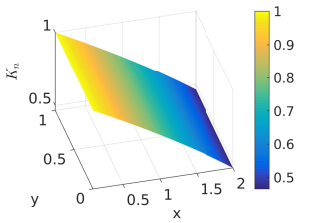

(c) Numerical solution for the permeability.

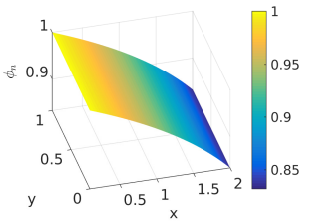

(d) Numerical solution for the porosity.

Figure 6.18: Numerical solutions for the pressure, the fluid velocity, the permeability and the porosity, at time $t = 300$ using a constant time step size $\Delta t = 0.5$, obtained using the Kozeny-Carman relation.

As shown in Figure 6.18a, the water pressure has a larger curvature in the direction of the pressure gradient, than the pressure profiles in Figures 6.19a and 6.20a, that are almost linear. In all three cases, the injected water flows in the horizontal direction through the domain from the inlet to the outlet. Furthermore, the magnitude of the velocity $|v|$ in the inlet is larger than in the outlet. This change in $|v|$ can be explained by the permeability profiles shown in Figures 6.18c-6.20c. In these figures we observe that the permeability decreases almost linearly from the inlet to the outlet. In addition, the permeability obtained using Kozeny-Carman exhibits a larger decrease than the permeabilities obtained with the network-inspired model. The normalised permeability using Kozeny-Carman decreases from 1 to 0.4659, while the permeabilities for the network-inspired relation decrease from 1 to 0.7519 and from 1 to 0.6684 for the triangular structured and the quadrangular network respectively. This behaviour is clarified by Figure 6.15 and Figures 6.18d-6.20d. Due to the boundary condition (6.8e) and the fact that the values in the displacement vector are small near the outlet, the porosities in all three cases are almost the same in the outlet and they are equal to 0.8321. In Figure 6.15, we see that for this value of the porosity, the normalised permeability is the lowest in Kozeny-Carman relation and the highest in the network-inspired relation derived from the triangular structured network. This explains the difference in decrease in the permeability profiles.

In Figure 6.21 the time average of the volumetric flow rate $\overline{Q}_{out}$ is depicted for different values of the percolation threshold. As expected from Figure 6.15, for low percolation thresholds the network-inspired relation results in higher flow rates than Kozeny-

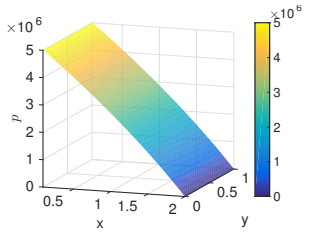

(a) Numerical solution for the pressure.

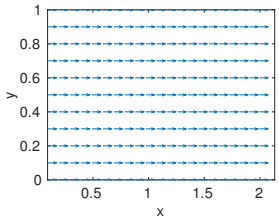

(b) Numerical solution for the fluid velocity.

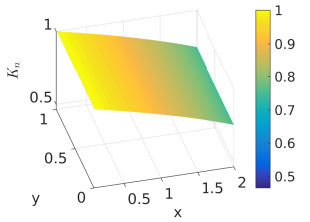

(c) Numerical solution for the permeability.

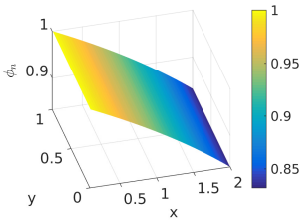

(d) Numerical solution for the porosity.

Figure 6.19: Numerical solutions for the pressure, the fluid velocity, the permeability and the porosity, at time $t = 300$ using a constant time step size $\Delta t = 0.5$, obtained using the network-inspired relation with $p_c = 0.3232$.

Carman relation. Furthermore, the flow rate changes significantly as a function of the percolation thresholds. Hence the water flow depends on the topology of the network.

The negative values of $\overline{Q}_{out}$ for the network-inspired relation for large percolation thresholds are caused by numerical instabilities. To demonstrate this, the problem is solved for a coarser grid as shown in Figure 6.22. In this figure we observe spurious oscillations for the network-inspired relation for percolation thresholds larger than 0.85 approximately.

6.5.2. NUMERICAL RESULTS FOR THE SQUEEZE PROBLEM

The impact of the imposed vertical load on boundary segments Γ_1 and Γ_5 is shown in Figures 6.23 - 6.25, using the Kozeny-Carman relation and the network-inspired relation respectively. In these simulations, water is injected into the porous medium at a constant pump pressure equal to 5.0 bar. The simulated pressure, fluid velocity, permeability and porosity profiles that are obtained using the Kozeny-Carman relation are provided in Figure 6.23, while the simulated results that are obtained using the network-inspired relation with $p_c = 0.3232$, corresponding with a triangular structured network, are provided in Figure 6.24. In Figure 6.25, the simulated results that are obtained using the network-inspired relation with $p_c = 0.4935$, corresponding with a quadrangular network, are depicted.

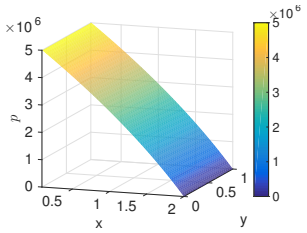

(a) Numerical solution for the pressure.

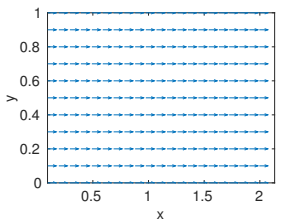

(b) Numerical solution for the fluid velocity.

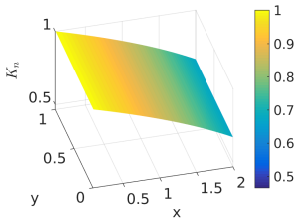

(c) Numerical solution for the permeability.

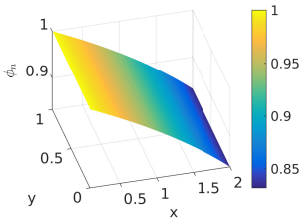

(d) Numerical solution for the porosity.

Figure 6.20: Numerical solutions for the pressure, the fluid velocity, the permeability and the porosity, at time $t = 300$ using a constant time step size $\Delta t = 0.5$, obtained using the network-inspired relation with $p_c = 0.4935$.

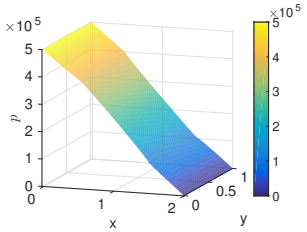

(a) Numerical solution for the pressure.

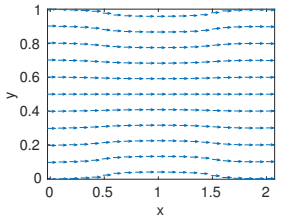

(b) Numerical solution for the fluid velocity.

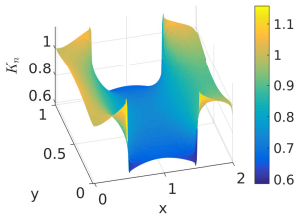

(c) Numerical solution for the permeability.

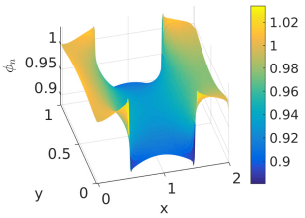

(d) Numerical solution for the porosity.

Figure 6.23: Numerical solutions for the pressure, the fluid velocity, the permeability and the porosity, at time $t = 300$ using a constant time step size $\Delta t = 0.5$, obtained using the Kozeny-Carman relation.

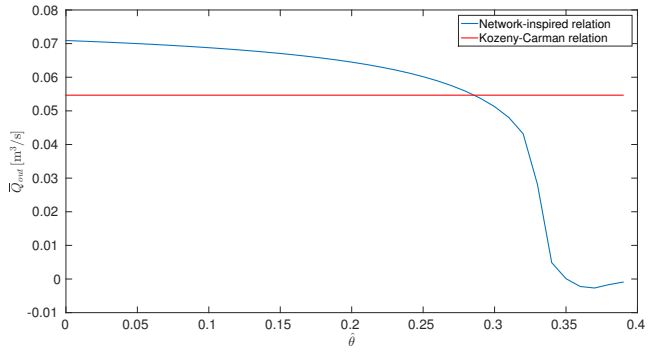

Figure 6.21: The time average of the volume flow rate $\overline{Q}_{out}$ as a function of the percolation threshold p_c

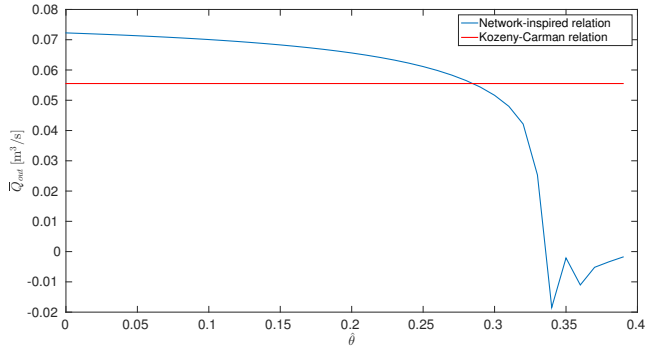

Figure 6.22: The time average of the volume flow rate $\overline{Q}_{out}$ as a function of the percolation threshold p_c

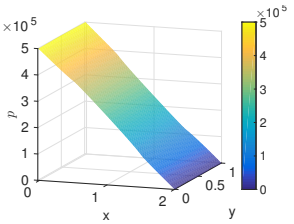

(a) Numerical solution for the pressure.

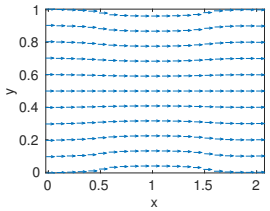

(b) Numerical solution for the fluid velocity.

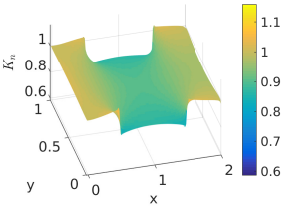

(c) Numerical solution for the permeability.

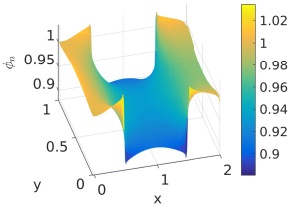

(d) Numerical solution for the porosity.

Figure 6.24: Numerical solutions for the pressure, the fluid velocity, the permeability and the porosity, at time $t = 300$ using a constant time step size $\Delta t = 0.5$, obtained using the network-inspired relation with $p_c = 0.3232$.

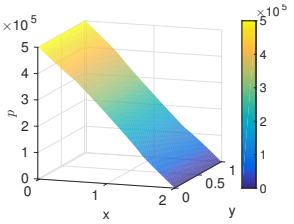

(a) Numerical solution for the pressure.

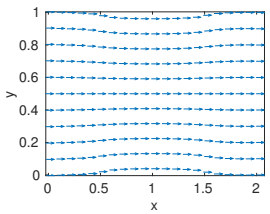

(b) Numerical solution for the fluid velocity.

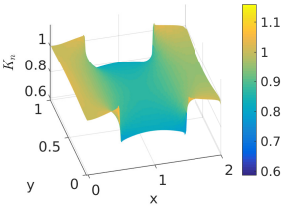

(c) Numerical solution for the permeability.

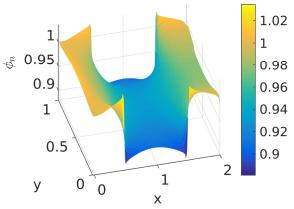

(d) Numerical solution for the porosity.

Figure 6.25: Numerical solutions for the pressure, the fluid velocity, the permeability and the porosity, at time $t = 300$ using a constant time step size $\Delta t = 0.5$, obtained using the network-inspired relation with $p_c = 0.4935$.

In Figure 6.23a there is an obvious transition between the stress free region and the region with the imposed load, while in Figures 6.24a and 6.25a the transition between these regions is smoother. In Figures 6.23b-6.25b, the impact of the imposed vertical load on the computational domain is shown. The velocity magnitude is low near the boundary segments where the vertical load is applied and high in the middle near the symmetry axis $y = H/2$. In the outlet, the velocity magnitude is the highest near the upper and lower boundary segments and decreases towards the symmetry axis. In all three cases, the fluid flows mainly in the horizontal direction. In the region where the load is imposed, the domain is squeezed, resulting in a larger density of the grains. This leads to a lower porosity in this region, with minimum values 0.8809, 0.8811 and 0.8810 for the Kozeny-Carman relation, the triangular structured network-inspired relation and the quadrangular network-inspired relation respectively. The change in the boundary condition for the stress tensor in the upper and lower boundaries (6.10d)-(6.10f) causes numerical instabilities. As expected from Figure 6.15 and the minimum values for the porosities, the decrease in permeability by the Kozeny-Carman relation, as shown in Figure 6.23c, is larger than the decrease in the porosities obtained using the network-inspired relation, Figures 6.24c and 6.25c.
In Figure 6.26 the time average of the volumetric flow rate $\overline{Q}_{out}$ is depicted for different values of the percolation threshold. Similarly to the high pump pressure problem, the flow rates for low percolation thresholds obtained using the network-inspired relation are higher than the flow rates obtained using the Kozeny-Carman relation. In addition, we observe that the flow rate depends significantly on the percolation threshold and hence on the topology of the network for large percolation thresholds.

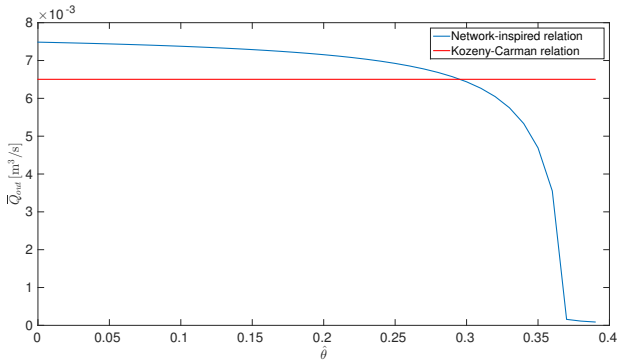

Figure 6.26: The time average of the volume flow rate $\overline{Q}_{out}$ as a function of the percolation threshold p_c for the squeeze problem

6.6. CONCLUSIONS

In this chapter, the network-inspired porosity-permeability relation obtained via the random biofilm growth model, is applied on two poroelasticity problems. This numerical experiment is designed in order to analyze the applicability of this microscopic relation on the macro-scale. Furthermore, we compare the results obtained with the network-inspired relation to the Kozeny-Carman relation which is often used for these physical

problems. In the first problem a high pump pressure is imposed in the inlet of a porous medium package. This high pressure forces the grains to move towards the outlet. In the second problem the package is squeezed by applying a load on the middle of the top and bottom edges of the domain. The purpose of considering these poroelasticity problems is to create a large density of the grains in the computational domain which results in a decrease of the porosity. In these problems Biot's model for poroelasticity is used to determine the water pressure and the displacements of the grains that are needed to compute the porosity. From the porosity the permeability is determined either by the network-inspired relations or by the Kozeny-Carman relation. Depending on the topology, three different percolation thresholds, corresponding with a quadrangular network ($p_c = 0.4935$), triangular structured network ($p_c = 0.3232$) and triangular unstructured network ($p_c = 0.3438$), are distinguished. However, since the topology of macro-scale porous media is not known, computations are performed with percolation thresholds in the interval $[0, 0.9]$ to investigate the influence of the percolation thresholds (and hence the topology of the medium) on the flow velocity displacements and porosity. First, the problems are solved with the Kozeny-Carman relation, the network-inspired relation based on the triangular structured network and the relation based on the quadrangular network. From the numerical results we conclude that the permeability obtained using the Kozeny-Carman relation exhibits a larger decrease than the permeabilities obtained with the network-inspired relations, which is clarified by Figure 6.15. In contrast, the porosity profile is not affected significantly by the selected porosity-permeability relation. Second, the time average of the volumetric flow rate was computed for percolation thresholds in the interval $[0, 0.9]$. For low percolation thresholds the network-inspired relation results in higher flow rates than the Kozeny-Carman relation, as expected from Figure 6.15. In addition, it is shown that the flow rate changes significantly as a function of the percolation thresholds which means that the water flow depends on the topology of the network. For large percolation thresholds spurious oscillations appeared due to numerical instabilities, the results for these percolation thresholds could be improved by using a finer grid.

For the studied problems and the set of parameters chosen, we noticed that the applied porosity-permeability relations result in small changes in the porosity while a major change is realised in the permeability profiles. A possible explanation for this behaviour can be that the relation, between the velocity field and the change of the displacements in time as stated in Equation (6.1b), is not strong enough to lead to significant changes in the porosity profile.

REFERENCES

[1] M. A. Biot, *General theory of three-dimensional consolidation,* Journal of applied physics **12**, 155 (1941).

[2] G. Aguilar, F. Gaspar, F. Lisbona, and C. Rodrigo, *Numerical stabilization of biot's consolidation model by a perturbation on the flow equation,* International journal for numerical methods in engineering **75**, 1282 (2008).

[3] H. F. Wang, *Theory of linear poroelasticity with applications to geomechanics and hydrogeology* (Princeton University Press, 2017).

[4] T.-L. Tsai, K.-C. Chang, and L.-H. Huang, *Body force effect on consolidation of porous elastic media due to pumping,* Journal of the Chinese Institute of Engineers **29**, 75 (2006).

[5] S.-J. Wang and K.-C. Hsu, *Dynamics of deformation and water flow in heterogeneous porous media and its impact on soil properties,* Hydrological Processes: An International Journal **23**, 3569 (2009).

[6] M. Rahrah and F. Vermolen, *Monte carlo assessment of the impact of oscillatory and pulsating boundary conditions on the flow through porous media,* Transport in Porous Media **123**, 125 (2018).

[7] I. A. Segal, *Finite element methods for the incompressible Navier-Stokes equations* (2012).

7

CONCLUSION

In this work, we presented a new model of biofilm growth that takes into account that the nutrients do not entirely penetrate the biofilm because the consumption is faster than the diffusion of nutrients within the biofilm. Additionally we incorporate a continuous spreading of biofilm from one tube to the neighbouring ones which results into spreading of biofilm through the whole network. The goal of this thesis is to give a description of biofilm growth at the micro-scale in order to study its effects on the porous medium characteristics and thereby on enhanced oil recovery. In particular we studied the changes in porosity and permeability due to the accumulation of biofilm. Furthermore, we related these changes in porosity and permeability to the flow diversion of water to low permeability regions. Finally we derived a relation between porosity and permeability that can be used as an alternative to the Kozeny-Carman relation.

Our numerical simulations showed that the nutrients are present in the whole network just after the beginning of the process. The presence of the nutrients causes the growth and the spreading of the biofilm over the whole network. Subsequently biofilm grows uniformly through the whole network for a certain period of time. After this, depletion of nutrients is observed and preferential growth near the inlet of the network occurs until the flow through the network is blocked. We compared our model to the uniform biofilm growth model and to a random biofilm growth model which blocks the tubes in the network randomly. We obtained that our model shows a transition between uniform biofilm growth and heterogeneous biofilm growth. We conclude that is possible to avoid the clogging near the inlet of the network, so that high permeability regions are partially blocked. Therefore biofilm accumulation in porous media can be beneficial for MEOR, especially during the uniform biofilm growth stage.

We studied the conditions needed to upscale our microscopic model to larger scales. We investigated the influence of the number of nodes per unit area, the size of the domain of computation and the inlet concentration on the permeability-porosity relation. The simulations show that there is a transition between homogeneous and heterogeneous biofilm growth. We used the Damköhler number to determine whether upscaling is possible. We obtain that the transition occurs between $Da = 10^1$ to $Da = 10^3$ ap-

proximately for all the cases studied. If the Damköhler number stays under $Da = 10^1$ during the whole process of biofilm growth then there is uniform growth and upscaling is possible. On the other hand if the Damköhler is larger than $Da = 10^3$, then the biofilm grows heterogeneously and upscaling is not possible. Our simulations revealed that upscaling is not possible if the inlet concentration is not large enough. In these cases the permeability-porosity relation depends on the number of nodes per unit area and on the size of the domain of computation.

We extended our 2D model to a 3D biofilm growth model. In this case we used a cubic 3D network. The influence of the number of nodes in the $z-$ direction was studied. In addition we incorporated a log-normal distribution for the radii of the tubes in the network. Further we derived a criterion for upscalability using this model and we compared it to the criterion obtained using the 2D network model. We concluded that there are two possibilities; heterogeneous growth and homogeneous biofilm growth. In the case of heterogeneous growth the amount of biomass needed to block the network, $\tilde{S_b}$ increases as the number of nodes in the $z-$ direction increases. However, $\tilde{S_b}$ converges to $\tilde{S_b^*} = 0.85$ as the number of nodes in the $z-$ direction tends to infinity. The amount of biomass needed to block the network increases with the number of nodes in the $z-$ direction because then there are more paths available for water flow. Therefore it takes a larger fraction of biomass to block the network. We observe that the transition between homogeneous and heterogeneous growth occurs between $Da = 10^1$ to $Da = 10^3$ which is approximately the same range as in the 2D model. Furthermore, the influence of the statistical parameters of the log-normal distribution for the radius on biofilm growth was studied. We obtained that $\tilde{S_b}$ decreases if the variance of the distribution increases. However, also in this case the transition between homogeneous and heterogeneous growth occurs within the same Damöhler number regime as in Chapter 3.

We used a 2D network model to study the influence of biofilm growth on the flow diversion of water. For this reason we divided the domain of computation into two regions with different permeabilities. The region with the lower permeability was placed in the centre of the domain of computation. Since we are interested in the production of oil from low permeability regions we computed the outflow of water from the low permeability region. We obtained that during the biofilm growth process the outflow from the low permeability region increased by around 60 per cent during about 30 per cent of the total simulation time. However, in the final stage the flux of water through the whole network, and hence also from the low permeability region, decreases as a result of biofilm accumulation. Therefore it is suggested that the injection of the nutrients has to be stopped in order to avoid blocking of the network. The increase of the outflow through the low permeability region may indicate successful flow diversion which is characterised by an increase of the efficiency of the waterflood.

The network-inspired porosity-permeability relation obtained via the random biofilm growth model was used to describe two poroelasticity problems. This new porosity-permeability relation depends on the percolation threshold and hence on the topology of the network. We obtained the porosity-permeability relation for three different networks in 2D (a rectangular network,a triangular network and a triangular unstructured network) and cubic network in 3D. The results obtained using the porosity-permeability relation for the 3 different networks were compared to the results obtained

via the Kozeny-Carman relation. From the numerical results we conclude that the permeability decreases larger using the Kozeny-Carman relation than the permeability obtained via the network models. On the other hand, the porosity is not affected significantly by the selected porosity-permeability relation. Probably this behaviour is because the relation between the velocity and the displacement field is not strong enough to lead significant changes in the porosity profile. In addition the average volumetric flow was computed for percolation thresholds from 0 to 0.9. For low percolation thresholds the network-inspired relation results in higher flow rates then the Kozeny-Carman relation.
In this thesis we presented a new biofilm growth model that describes some phenomena that have not been dealt with in literature; like the likelihood of a non-homogeneous distribution of nutrients within the biofilm and the spreading of biomass to the neighbouring tubes. Since we consider a 2D rectangular pore network model consisting of cylindrical tubes with the same radii, this model could be too simplified to describe a real reservoir field. Interesting further research is to find the representative elementary volume in order to upscale these results to the macroscale. In addition, future plans entail the study of the effects of biofilm growth in porosity and permeability in more complex topologies in 2D and 3D.
In addition it might be interesting to verify the relation between porosity and permeability, $K \sim \phi^2$, in laboratory scale and obtain an appropriate Damköhler number regime for uniform growth. Forthcoming research might be the extension of this model to two phase flow for studying the possibility of flow diversion for MEOR. Finally, this model can be used in other problems like pore-elasticity.

ACKNOWLEDGEMENTS

First of all, I want to thank Prof. Kees Vuik for giving me the opportunity to start this journey called PhD in Holland.
During this trip, I met many people who were important for the development of this dissertation. I have to mention my daily supervisor and promotor. Fred, thank you very much for all your support and your advice, not only in the scientific field but also on daily life issues. I'm very grateful to my co-promotor. Bernard thank you for all your dedication, compromise and for all the ideas that enrich this project. I would like to express my gratitude the committee members for accepting the invitation to the defense: Prof. F.A. Radu, Prof.S. M. Hassanizadeh, Prof. J. Bruining and Prof. P.L.J. Zitha.
Additionally, I want to acknowledge Menel for a nice collaboration and for a nice work together, which resulted in chapter 6 of this dissertation, a conference paper and a paper sent to a journal.
I want to thank the Mexican Institute of Petroleum (IMP) for financially support this research. I want to thank Dr. Erik Luna for his support and for giving me the opportunity to come back to Delft for the defence. In addition, I want to acknowledge Dr. Leonid Sheremetov for keeping track of the development of my PhD Program on behalf of the IMP and for his comments about this thesis.
I want to thank all my colleagues, friends and staff members of the Numerical Analysis department for creating a nice and friendly working environment. In geographical order, from nearest neighbours to furthest neighbours. I want to thank my office mates, Jiao and Shuaiqiang for showing me the Chinese generosity and kindness. Anne thanks for sharing so many interesting data about the Netherlands, I felt more integrated to NL when you arrived. I want to thank Lisa for inspiring me to think in a long term plan to try to stay in the Netherlands. I want to express my gratitude to Reinaldo for all the beers we drank together. Thanks to captain Baljaa for organising the football team of the department: The Krylov Tigers. I want to thank Behrouz for all the small talks we had during our encounters in the coffee machine and in the corridor.
I want to thank the colleagues of the third floor for providing cakes whenever it was needed: Roel, Owen, Johan, Mousa, Marieke, Prajatka, Vandana, Merel, Gaby, Mo, Alice. I would like to express my gratitude to Berna, Matthias, Martin, Neil, Domenico, Kees Ossterlee and Valia.
I want to thank Deborah Dongor for her help in administrative matters. I thank Kees Lemmens for his support in any Linux related issues.
I thank my friend Rock and his lovely family (Bibi, Fanny y Rodrigo) for providing me with a good company away from home. Special thanks to Bibi for feeding us with delicious Mexican food that made me feel closer to home.
I want to thank "Franka B." for helping me with the translation of the summary.
I want to thank Andrea "boo" for being the representation of my Mexican friends in Europe. Merci beaucoup for all your support in the difficult part of this era.

Finalmente, quiero agradecer a mis padres por ser siempre el mejor ejemplo que he tenido y por brindarme todo lo necesario para tener una vida feliz. Sin todo su cariño y apoyo esto no hubiera sido posible. Agradezco tambien a mi hermana Pau y a Dani, porque a pesar de la distancia siempre estuvieron ahí para ayudarme cuando yo lo requería.
Fin

Curriculum Vitæ

Luis Antonio Lopez Peña

Luis Antonio was born in Mexico City, Mexico, on February 24 1987. He studied his Bachelor in Physics at the Universidad Nacional Autónoma de México (UNAM) where he finished in 2010. During the last years of his studies he was teaching assistant in the course of Thermodynamics.
In 2013 he obtained his Master degree with honours in Materials Science and Engineering from UNAM. After finishing his Master studies he started a research project where he led a team in the laboratory of Optical Micro-manipulation at Physics Institute of UNAM. As a result of this research one journal paper and two conference papers were published.
In 2014 he was awarded a grant to realise his PhD project in the Netherlands. He started his PhD in Applied Mathematics under the supervision of Dr.Ir. Fred Vermolen and Dr. Bernard Meulenbroek in the department of Numerical Analysis at Delft University of Technology. His research topic is modelling biofilm growth for Microbial Enhanced oil recovery.
Luis has published conference papers and journal papers as a result of his research. He had the opportunity of presenting his work in national and International conferences, such as Burgers Symposium in Lunteren, the Annual SIAM Conference in Pittsburgh, PA, USA and Interpore conference in New Orleans, LA, USA.
Luis is currently a researcher in the Mexican Institute of Petroleum (IMP) in Mexico City.

List of Publications

1. **Lopez-Peña, L. A., Meulenbroek, B., and Vermolen, F. J.**,*Conditions for upscalability of bioclogging in pore network models*, Computational Geosciences (2018)

2. **Lopez-Peña, L. A., Meulenbroek, B., and Vermolen, F. J.**,*A network model for the biofilm growth in porous media and its effects on permeability and porosity*, Computing and Visualization in Science (2018) (Accepted)

3. **Lopez-Peña, L. A., Meulenbroek, B., and Vermolen, F. J.**, *A Network Model for the Kinetics of Bioclogged Flow Diversion for Enhanced Oil Recovery.* Proc. ECMOR XIV-15th European Conference on the Mathematics of Oil Recovery. (2016).

4. **Rahrah M., Vermolen F.J., Lopez-Pena L.A. and Meulenbroek B.** ,*A poroelasticity model using a network-inspired porosity-permeability relation.* Proc. The 20th European Conference on Mathematics for Industry, 18-22 June 2018, Budapest, Hungary

5. **Rahrah M., Lopez-Pena L.A., Vermolen F.J. and Meulenbroek B.** ,*Network-inspired versus Kozeny-Carman based permeability-porosity relations applied to Biot's poroelasticity model*, (Submitted)

6. **Salazar-Romero, M.Y., Ayala, Y.A., Brambila, E., Lopez-Peña, L.A., Sciberras, L., Minzoni, A.A., Terborg, R.A., Torres, J.P. and Volke-Sepúlveda, K.,** ,*Steering and switching of soliton-like beams via interaction in a nanocolloid with positive polarizability*, Optics letters, 42(13), 2487-2490. (2017)

7. **Lopez-Peña, L. A., Salazar-Romero, Y., Terborg, R. A., Hernández-Cordero, J., Torres, J. P., and Volke-Sepúlveda, K.**, *Waveguides in colloidal nanosuspensions*, Proc. SPIE 9164, Optical Trapping and Optical Micromanipulation XI, 916429 (16 September 2014).

8. **Lopez-Peña, L. A., Brambila-Tamayo, E. C., Velasco-Gutiérrez, C. R., Terborg, R. A., Torres, J. P., and Volke-Sepúlveda, K.** , *Beam-splitting waveguides induced in nanocolloids.* , Proc. SPIE 9164, Optical Trapping and Optical Micromanipulation XI, 916439 (16 September 2014).